DISPLACEMENT OF OIL FROM HYDRAULIC LINES

by

OLE IVAR ULVEN

THESIS

for the degree of

MASTER OF SCIENCE

(Master i Anvendt matematikk og mekanikk)

Faculty of Mathematics and Natural Sciences
University of Oslo

May 2010

Det matematisk- naturvitenskapelige fakultet
Universitetet i Oslo

Acknowledgements

First of all, I would like to thank Professor Ruben Schulkes for his supervision and helpful comments. Without his aid, it would not have been possible for me to write this thesis.

In addition, I would like to express my appreciation to Professor Arnold F. Bertelsen for his help on getting started using FLUENT, and for always being willing to help.

Finally, thanks to everyone in Realistforeningen for helping me maintain a social life while writing this thesis. My life as a student would have been a lot less weird without you.

> Mechanics is the paradise of the mathematical sciences, because by means of it one comes to the fruits of mathematics.
>
> —*Leonardo da Vinci*

Contents

Chapter 1

Introduction

Remote operation of valves in offshore operations is managed hydraulicly using so-called umbilicals. The flow lines containing the hydraulic fluid may be many kilometers in length, they are typically 1/2" in diameter and contain viscous oil. When umbilicals are de-commissioned, water is pumped into the hydraulic line in order to displace the hydraulic fluid. It is this displacement process that will be the topic of this master's thesis.

Since the hydraulic line is long, it would require a very large pressure at the inlet to make the flow fast enough to become turbulent. Thus, it is reasonable to assume that the displacement process can be described by the laminar motion of two immiscible fluids, where the original fluid occupying the pipe is much more viscous than the replacing fluid. Earlier works have shown that the less viscous fluid tends to form a core in the center of the pipe, while some of the more viscous fluid is left as a layer at the wall. The volume fraction of the most viscous fluid left in the pipe after the initial displacement with the less viscous fluid is traditionally denoted m. In a pipe with circular cross section of radius R, given that the radius of the core of less viscous fluid is denoted h, the volume fraction m in a pipe length L can be found using the equation

$$m = \frac{\pi R^2 L - \pi h^2 L}{\pi R^2 L} = 1 - \frac{h^2}{R^2} = 1 - H^2 \tag{1.1}$$

where we have introduced the dimensionless interface height $H = \frac{h}{R}$.

It is expected that the thickness of the film of oil left in the pipe will be reduced as time goes by, but the asymptotic behaviour of the drainage rate of this viscous film appears not to have been studied at all. The drainage rate determines how long time it takes to remove a certain fraction of oil from the hydraulic line, so this is of main interest in describing the displacement process.

Most of the articles related to the displacement process found in the literature treats the case of an inviscid gas displacing a viscous liquid. Fairbrother and Stubbs[9] found through experiments in which they varied the

molecular viscosity of the displaced fluid μ_2, the axial velocity of the front of the core of less viscous fluid U_{front} and the the coefficient of surface tension of the interface σ the empirical relation

$$m = \left(\frac{\mu_2 U_{front}}{\sigma}\right)^{\frac{1}{2}} \tag{1.2}$$

The dimensionless number $\frac{\mu_2 U_{front}}{\sigma}$ is known as the capillary number, Ca. Fairbrother and Stubbs did not obtain a value of the capillary number higher than $Ca = 0.014$, but Taylor[19] extended the range of validity of equation (1.2) to $0 < Ca < 0.09$. Bretherton[4] later showed that for $Ca < 0.003$ a more accurate relation could be given by

$$m = 1.29\,(3Ca)^{\frac{2}{3}} \tag{1.3}$$

Schwartz et al[16] found that the Bretherton result was actually more accurate only for relatively short bubbles, with length up to approximately ten tube diameters, and reported experimental results close to the Fairbrother and Stubbs equation (1.2) for longer bubbles. For capillary numbers above 0.09 it seems no analytical relations have been found, but Taylor observed that for higher capillary numbers m was lower than predicted by equation (1.2), and he stated that the relation (1.2) would actually be meaningless for capillary numbers higher than unity, as that would predict m larger than unity, which is a geometrical impossibility. At $Ca = 1.9$, the maximum value obtained experimentally by Taylor, he found that m had reached the value 0.55, and he stated that the trend of the curve indicated that m was approaching an asymptotic value somewhat above 0.55. Cox[5] later confirmed this, and found that the asymptotic value was 0.6, using experiments with Ca above 10.

Giavedoni and Saita[10] studied the problem numerically, using a finite element approach. They reported good agreement with the Bretherton theory for low capillary numbers, the Fairbrother and Stubbs relation for $0.003 < Ca < 0.09$ and the results found by Taylor for large capillary numbers.

Published work related to the liquid-liquid displacement problem is rather scarce. One of the few is the work by Goldsmith and Mason[11], in which they found experimentally that m was increased when the viscosity of the displacing fluid was increased. Soares et al[17] used a finite element method to study the problem with different viscosity ratios $\mu = \frac{\mu_2}{\mu_1}$, where index $1, 2$ refers to the displacing and displaced liquid, respectively. Their results were in agreement with what Goldsmith and Mason found, and they also found that a viscosity ratio as low as 20 was high enough to reproduce the limiting case of gas-liquid displacement.

If the situation is reversed, with the most viscous fluid in the core, we get what is known as a core annular flow. This type of flow has important

applications in the oil industry, and therefore a large variety of articles exist in the literature. Many of them treat the concept of stability of core annular flows, as it is important in the applications to be able to predict transition to other flow regimes. The book by Joseph and Renardy[12] summarizes much of what is known on this topic, and Rodriguez and Bannwart[14] have done a thorough stability analysis using a one-dimensional model.

In this thesis, the main topic is the development of a one-dimensional hydraulic model able to describe the displacement process. Ultimately, we want a model that is able to predict how fast the fraction of oil in the hydraulic line is reduced. To support this work, we start by finding analytical results for a steady, fully developed flow. Then we use the commercial finite element solver FLUENT to simulate the flow, with the assumption of axisymmetry. A hydraulic model is developed, and stability of the equations is studied. We then solve the equations in the hydraulic model numerically, and try to validate the model by simulating flows with well established solutions, hereunder core annular flow. We also compare the results from the hydraulic model with results found using another model introduced by Beresnev and Deng[2]. Finally, we find results for how fast the layer of oil at the wall is washed out, and find an analytical approximation able to describe the drainage rate in some detail.

Chapter 2

Analysis

The topic of this chapter is to try to find an analytical description of the flow, subject to certain simplifications. Our starting point is the full Navier-Stokes equations. The geometry of the flow considered is given in figure 2.1.

2.1 Problem definition

As a basic assumption in this thesis, we assume that the flow is laminar, that the fluids are Newtonian and incompressible, and that there is no heat transfer, chemical reactions or other sources of momentum involved. In addition, it is a fair assumption that the continuum hypothesis is fulfilled. With these assumptions, the flow of oil and water can be described by the following version of Navier-Stokes equations:

- The mass conservation equation

$$\nabla \cdot \mathbf{v} = 0 \tag{2.1}$$

  where $\mathbf{v}$ is the velocity of the fluid.

- The momentum equation

$$\frac{\partial \mathbf{v}}{\partial t} + \mathbf{v} \cdot \nabla \mathbf{v} = -\frac{1}{\rho}\nabla p + \frac{1}{\rho}\nabla^2 \mathbf{v} + \mathbf{g} \tag{2.2}$$

  where p is the pressure, ρ is the density of the fluid, $\mathbf{g}$ is the gravity, μ is the molecular viscosity of the fluid and t is time.

These equations are valid in both phases, and we from here on introduce the subscript $k = 1, 2$ to denote values in water and oil, respectively. As boundary condition, we assume no slip at the wall. This condition can be expressed

$$\mathbf{v}_2|_{pipe\ wall} = 0 \tag{2.3}$$

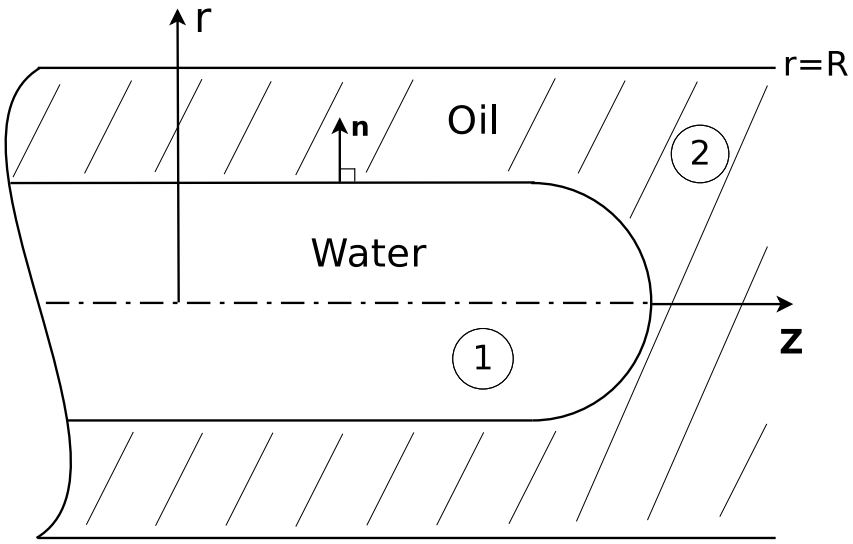

Figure 2.1: *Typical geometry of the flow.*

We assume that the fluids are immiscible, and thus that the interface is a material surface. Further, we neglect any gradients in surface tension. The jump condition for momentum then becomes

$$[\mathbf{T}] \cdot \mathbf{n} = 2\mathcal{C}\sigma\mathbf{n} \tag{2.4}$$

where square brackets denote the jump of a quantity across the interface, $\mathbf{n}$ is a unit normal vector at the interface as shown in figure 2.1, $\mathcal{C}$ is the surface curvature as viewed from phase 1 and $\mathbf{T}$ is the stress tensor, given by

$$\mathbf{T} = -p\mathbf{I} + \mu\left(\nabla\mathbf{v} + \nabla\mathbf{v}^T\right) \tag{2.5}$$

where $\mathbf{I}$ is the identity matrix. We now introduce the stress vector $\mathbf{t}_n$ defined by

$$\mathbf{t}_n = \mu\left(\nabla\mathbf{v} + \nabla\mathbf{v}^T\right) \cdot \mathbf{n} \tag{2.6}$$

The stress vector can be written as $\mathbf{t}_n = t_n\mathbf{n} + \mathbf{t}_t$, where t_n is the normal stress component and $\mathbf{t}_t$ the tangential stress vector. We can now separate the components which are normal and tangential to the interface and obtain

$$[p] - [t_n] = 2\sigma\mathcal{C} \tag{2.7}$$

$$[\mathbf{t}_t] = 0 \tag{2.8}$$

It is common to neglect normal stress, since large normal velocity gradients are uncommon near a liquid-liquid interface that would be deformed by fluid

motion. Relation (2.7) states that the pressure change across an interface with no normal stress must be given by

$$p_{1,interface} - p_{2,interface} = 2\sigma\mathcal{C} \tag{2.9}$$

Relation (2.8) gives that we must have continuity of shear stress across the interface. We must also have continuity of velocity at the interface, since we would otherwise have an infinite velocity gradient. This can be given by

$$\mathbf{v}_{1,interface} = \mathbf{v}_{2,interface} \tag{2.10}$$

Some dimensionless numbers are relevant for our problem. We have already met the capillary number Ca in chapter 1. For typical values of the factors in the capillary number, we have

$$Ca = \frac{\mu_2 U_{front}}{\sigma} \leq \mathcal{O}(1) \tag{2.11}$$

With low capillary numbers, surface tension forces dominates viscous forces. Other relevant dimensionless numbers are the Weber number We and the Reynolds number Re, defined by

$$We = \frac{\rho_1 U_{front}^2 R}{\sigma} \tag{2.12}$$

$$Re = \frac{\rho_1 U_{front} R}{\mu_1} \tag{2.13}$$

We can now notice that $Ca = \mu\frac{We}{Re}$, where we have introduced the viscosity ratio $\mu = \frac{\mu_2}{\mu_1}$. Since we for typical viscosities have $\mu = \mathcal{O}(10)$, we must have $\frac{We}{Re} = \mathcal{O}(10^{-1})$. A typical Reynolds number for this flow is $Re = \mathcal{O}(10^2)$, which shows that viscous forces dominates inertia. From this, we find $We \leq \mathcal{O}(10)$. This is a quite small Weber number, and since the Weber number gives the ratio of inertia to capillary forces, we see that the capillary forces are dominating in this case. Thus, capillary forces are dominating both viscous forces and inertia in the current problem.

The Bond number is given by

$$Bo = \frac{|\rho_1 - \rho_2| gR^2}{\sigma} \tag{2.14}$$

and gives the ratio of gravitational forces to capillary forces. For typical values, we find $Bo = \mathcal{O}(10)$, which is not an especially high Bond number. Thus, it is reasonable to assume that capillary forces are dominating gravitational forces, as well. The conclusion of this analysis is that the dynamics is in this case dominated by capillary forces. We therefore from here on neglect gravity, and assume a perfect axisymmetric flow.

2.2 The velocity profile

In this section, we assume that for a certain section of pipe length, the interface is located at the same radial position, denoted h. We also assume the flow to be fully developed and stationary. Given a stationary and fully developed flow, the volume flow of each fluid is constant. We denote the volume flow of water Q_1 and the volume flow of oil Q_2.

We now write the Navier-Stokes equations (2.1),(2.2) in cylindrical coordinates (r, θ, z) and introduce the velocity vector $\mathbf{v} = [v_r, v_\theta, v_z]$. When we neglect gravity and assume that the flow is axisymmetric, we can write the equations as a two-dimensional problem in the $r-z$-plane:

- The mass conservation equation

$$\frac{1}{r}\frac{\partial}{\partial r}\left(r v_{r,k}\right) + \frac{\partial}{\partial z}\left(v_{z,k}\right) = 0 \tag{2.15}$$

- The momentum equation

$$\frac{\partial v_{r,k}}{\partial t} + v_{r,k}\frac{\partial v_{r,k}}{\partial r} + v_{z,k}\frac{\partial v_{r,k}}{\partial z} = -\frac{1}{\rho_k}\frac{\partial p_k}{\partial r} + \nu_k\left(\nabla^2 v_{r,k} - \frac{v_{r,k}}{r^2}\right) \tag{2.16}$$

$$\frac{\partial v_{z,k}}{\partial t} + v_{r,k}\frac{\partial v_{z,k}}{\partial r} + v_{z,k}\frac{\partial v_{z,k}}{\partial z} = -\frac{1}{\rho_k}\frac{\partial p_k}{\partial z} + \nu_k\nabla^2 v_{z,k} \tag{2.17}$$

From the given conditions, we can conclude that the flow is purely axial ($\mathbf{v} = [0, 0, v_z]$). For a stationary flow, we have no time dependence $\left(\frac{\partial}{\partial t} = 0\right)$, and for a fully developed flow there is no dependence on z-coordinate for any other quantities than the pressure $\left(\frac{\partial}{\partial z} = 0\right)$. We still assume an axisymmetric flow, even though it would be possible to have the core of water centered around some other point than the axis of the pipe.

The θ-component of the momentum equation would with the current assumptions simplify to

$$\frac{1}{\rho_k r}\frac{\partial p_k}{\partial \theta} = 0 \tag{2.18}$$

which tells us that the pressure is independent of θ. This is necessary to find a simple analytical solution. In the same way, the equation for the r-component, equation (2.16), simplifies to

$$\frac{1}{\rho_k}\frac{\partial p_k}{\partial r} = 0 \tag{2.19}$$

and this tells us that the pressure is independent of r. We can conclude that the pressure is a function of z only.

The z-component of the momentum equation, equation (2.17), simplifies to

$$\frac{1}{r}\frac{d}{dr}\left(r\frac{dv_z}{dr}\right) = -\frac{\Theta}{\mu_k} \tag{2.20}$$

where we have defined the pressure gradient $\Theta = -\frac{\partial p_k}{\partial z}$. Since the curvature of the interface is constant with the current assumptions, we can conclude that the pressure gradients in the two phases are equal. The mass conservation equation (2.15) is trivially fulfilled in this case. The general solution to the momentum equation for phase k is given by

$$v_{z,k} = -\frac{\Theta}{4\mu_k}r^2 + C_{1,k}\ln r + C_{2,k} \tag{2.21}$$

for arbitrary constants $C_{1,k}$ and $C_{2,k}$. Since there is only one velocity component, we can leave out the subscript z to simplify notation. As introduced in section 2.1 we denote values in the least viscous phase (water) with subscript 1 and values in the most viscous phase (oil) with subscript 2.

To find a particular solution to our problem, we have to impose the boundary and interfacial conditions introduced in section 2.1. We start with the no slip-condition at the wall, equation (2.3). If we assume the pipe to have radius R, this condition can be written

$$v_2(R) = 0 \quad \Rightarrow \quad -\frac{\Theta}{4\mu_2}R^2 + C_{1,2}\ln R + C_{2,2} = 0 \tag{2.22}$$

At the interface between the phases, the velocity has to be continous according to condition (2.10), which gives

$$v_1(h) = v_2(h) \quad \Rightarrow \quad -\frac{\Theta}{4\mu_1}h^2 + C_{1,1}\ln h + C_{2,1} = -\frac{\Theta}{4\mu_2}h^2 + C_{1,2}\ln h + C_{2,2} \tag{2.23}$$

Viscous shear must also be continous at the interface, so with the simplifications introduced in this chapter, relation (2.8) imply

$$\mu_1\frac{dv_1}{dr}\Big|_{r=h} = \mu_2\frac{dv_2}{dr}\Big|_{r=h} \quad \Rightarrow \quad \mu_1\left(-\frac{\Theta h}{2\mu_1} + \frac{C_{1,1}}{h}\right) = \mu_2\left(-\frac{\Theta h}{2\mu_2} + \frac{C_{1,2}}{h}\right) \tag{2.24}$$

Finally, the velocity cannot be infinite at the center of the pipe, giving

$$|v_1(0)| < \infty \quad \Rightarrow \quad C_{1,1} = 0 \tag{2.25}$$

Using the four conditions (2.22)-(2.25) we find the particular solution

$$v_1 = \frac{\Theta}{4\mu_1}\left(h^2 - r^2\right) + \frac{\Theta}{4\mu_2}\left(R^2 - h^2\right) \tag{2.26}$$

$$v_2 = \frac{\Theta}{4\mu_2}\left(R^2 - r^2\right) \tag{2.27}$$

2.3 The hold-up equation

The term "hold-up" is used to describe the liquid level at equilibrium, and thereby the fraction of each liquid present in a certain cross section of the pipe. In the previous section, h denoted the liquid hold-up. The hold-up equation gives the liquid hold-up in terms of relevant physical parameters. Using the calculated velocity profiles from the previous section, one can easily find the hold-up equation for the present case.

First, we find the superficial velocity of each liquid. The superficial velocity is defined as the volume flow of each liquid divided by the total flow area:

$$U_{1,SL} = \frac{Q_1}{\pi R^2} \tag{2.28}$$

$$U_{2,SL} = \frac{Q_2}{\pi R^2} \tag{2.29}$$

Then we average the the fluid velocity of each phase over the area available to the phase:

$$\overline{v_1} = \frac{1}{\pi h^2}\int_0^{2\pi}\int_0^h v_1(r) r dr d\theta = \frac{\Theta}{4}\left(\frac{h^2}{2\mu_1} + \frac{R^2-h^2}{\mu_2}\right) \tag{2.30}$$

$$\overline{v_2} = \frac{1}{\pi\left(R^2-h^2\right)}\int_0^{2\pi}\int_h^R v_2(r) r dr d\theta = \frac{\Theta\left(R^2-h^2\right)}{8\mu_2} \tag{2.31}$$

The superficial and mean velocities are related through the expressions $\pi h^2 \overline{v_1} = \pi R^2 U_{1,SL}$ and $\pi\left(R^2-h^2\right)\overline{v_2} = \pi R^2 U_{2,SL}$. Using these two equations, we can eliminate the pressure gradient, and after some algebra we find the hold-up equation

$$\frac{U_{1,SL}}{U_{2,SL}} - \frac{h^4\left(\frac{\mu_2}{\mu_1}-2\right)+2R^2h^2}{\left(R^2-h^2\right)^2} = 0 \tag{2.32}$$

To investigate this expression further, it is convenient to introduce dimensionless variables. We define $U \equiv \frac{U_{1,SL}}{U_{2,SL}}$, $\mu \equiv \frac{\mu_2}{\mu_1}$ and $H \equiv \frac{h}{R}$. With these variables, we can rearrange equation (2.32) and get

$$U - \frac{H^4(\mu-2)+2H^2}{\left(1-H^2\right)^2} = 0 \tag{2.33}$$

Figure 2.2 shows H as a function of μ for different values of U. From the figure, it seems that H tends to zero in the limit where μ is very large, and that H tends to some value dependent on U when μ is very small. It can be shown analytically that this is the correct behaviour. The equation actually has an analytical solution, which can be given by

$$H = \pm\sqrt{\frac{U+1\pm\sqrt{1+\mu U}}{U+2-\mu}} \tag{2.34}$$

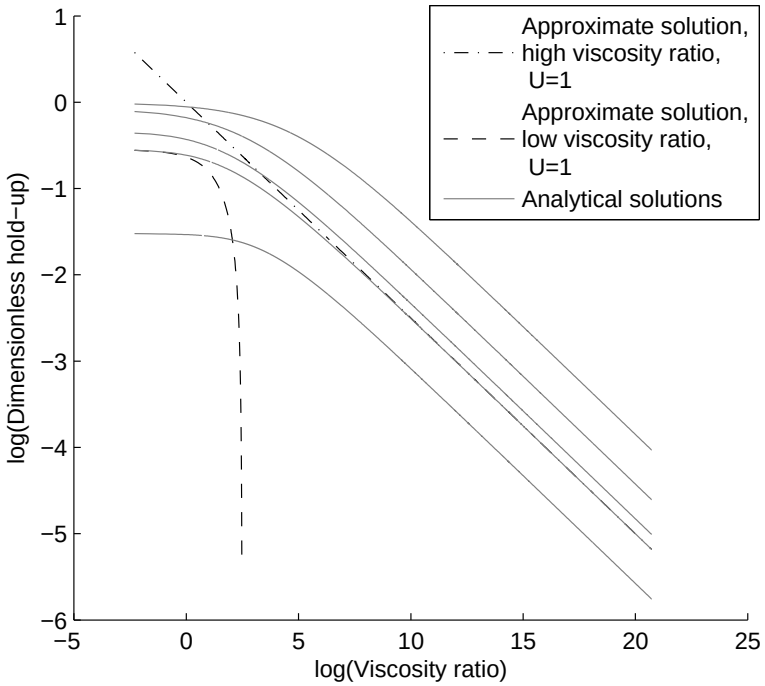

Figure 2.2: *Dimensionless liquid hold-up as function of viscosity ratio for different ratios of volume flow* $U = \frac{U_{1,SL}}{U_{2,SL}}$*, with approximations for small and large* μ*. The different curves with solid lines are, from top to bottom, for* $U = 100$*,* $U = 10$*,* $U = 2$*,* $U = 1$ *and* $U = 0.1$*.*

Since H is only defined in $[0, 1]$, it is easy to see that we can simplify the solution, and get

$$H = \sqrt{\frac{U + 1 - \sqrt{1 + \mu U}}{U + 2 - \mu}} \tag{2.35}$$

It is now interesting to check how this equation behaves in the limits of very small or very large μ. If we assume μ to be small, μU is also small. In that case we can expand the term $\sqrt{1 + \mu U}$ in the series

$$\sqrt{(1 + \mu U)} = 1 + \frac{1}{2}\mu U - \frac{1}{8}(\mu U)^2 + \dots \tag{2.36}$$

We can then write equation (2.35)

$$H = \sqrt{\frac{U + 1 - 1 - \frac{1}{2}\mu U + \mathcal{O}(\mu^2)}{(U + 2)\left(1 - \frac{\mu}{U+2}\right)}} \tag{2.37}$$

Then we expand the term in the denominator:

$$\left(1 - \frac{\mu}{U + 2}\right)^{-1} = 1 + \frac{\mu}{U + 2} + \left(\frac{\mu}{U + 2}\right)^2 + \dots \tag{2.38}$$

Inserting this, we find

$$\begin{aligned} H &= \sqrt{\frac{U - \frac{1}{2}\mu U}{U + 2}\left(1 + \frac{\mu}{U + 2} + \mathcal{O}(\mu^2)\right)} \\ &= \sqrt{\frac{U}{U + 2}}\sqrt{1 - \frac{1}{2}\mu U + \frac{\mu}{U + 2} + \mathcal{O}(\mu^2)} \end{aligned}$$

If we do another series expansion of the last square root, rearrange a little and throw away terms that are $\mathcal{O}(\mu^2)$, we find the equation

$$H = \sqrt{\frac{U}{U + 2}}\left(1 + \frac{1}{2}\mu\left(\frac{1}{U + 2} - \frac{U}{2}\right)\right) = \sqrt{\frac{U}{U + 2}} + \mathcal{O}(\mu) \tag{2.39}$$

We can notice that in the limit where $\mu = 0$ the equation simplifies further to $H = \sqrt{\frac{U}{U+2}}$, which is in agreement with the observation from figure 2.2.

In the same way, if we assume μ to be very large, we can rewrite equation (2.35)

$$H = \sqrt{\frac{\sqrt{\mu U\left(1 + \frac{1}{\mu U}\right)} - U - 1}{\mu\left(1 - \frac{U+2}{\mu}\right)}} \tag{2.40}$$

Now we can expand the terms $\sqrt{1+\frac{1}{\mu U}}$ and $\left(1-\frac{U+2}{\mu}\right)^{-1}$ and find

$$\begin{aligned}\sqrt{1+\frac{1}{\mu U}} &= 1+\frac{1}{2\mu U}-\frac{1}{8\left(\mu U\right)^2}+\ldots \\ \left(1-\frac{U+2}{\mu}\right)^{-1} &= 1+\frac{U+2}{\mu}+\left(\frac{U+2}{\mu}\right)^2+\ldots\end{aligned}$$

Inserting these expansions and rearranging a little, we find

$$\begin{aligned}H &= \frac{1}{\sqrt{\mu}}\sqrt{\sqrt{\mu U}-U-1+\mathcal{O}\left(\mu^{-\frac{1}{2}}\right)} \\ &= \frac{1}{\sqrt{\mu}}\left(\mu U\right)^{\frac{1}{4}}\sqrt{1-\frac{U+1}{\sqrt{\mu U}}+\mathcal{O}\left(\frac{1}{\mu}\right)}\end{aligned}$$

If we now expand the last square root, rearrange and throw away terms that are $\mathcal{O}\left(\mu^{-\frac{1}{2}}\right)$, we end up with the equation

$$H=\left(\frac{U}{\mu}\right)^{1/4}+\mathcal{O}\left(\mu^{-\frac{1}{2}}\right) \tag{2.41}$$

Again, we can notice that this is in agreement with what we observed in figure 2.2, H tends to zero as μ tends to infinity. A comparison of these two limiting results with the exact solution is also given in figure 2.2, and we can notice that the approximate solutions perform well in the limits where μ is either very small or very large.

We see that the solution behaves very differently for the two cases $\mu \to 0$ and $\mu \to \infty$. Namely, for $\mu \to 0$ interface height is a function of U only, while it is a function of both U and μ for $\mu \to \infty$. This can be explained by looking at the velocity profiles plotted for two different viscosity ratios given in figure 2.3. Both cases are for $U = 16$. We see that for a large viscosity ratio, the layer close to the wall moves quite slowly, and the higher the viscosity ratio is, the slower it will move. Since the volume flow of each phase is constant, as the layer close to the wall moves slower, it must get thicker. Thus, hold-up will be dependent on viscosity ratio for a large μ. The opposite is the case for low viscosity ratio. Since the core is now very viscous, it moves through the pipe more or less like a rigid body with a constant velocity in the entire cross section. As the core gets more viscous, it gets closer to a rigid body, but that can not affect the mean velocity of the core much as the velocity profile is already close to being plug-shaped. Mean velocity and hold-up are obviously intimately coupled, and thus, hold-up is independent of viscosity ratio when μ is small.

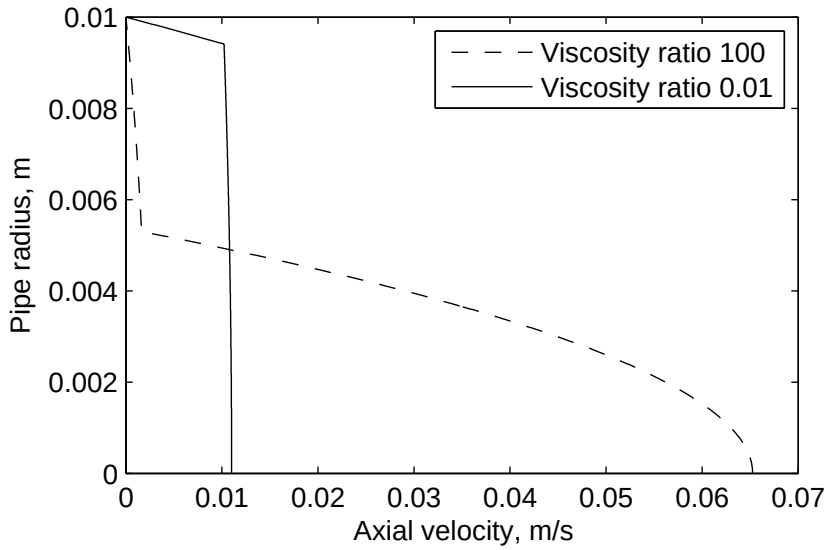

Figure 2.3: *Comparison of velocity profile for two different viscosity ratios.* $U = 16$.

Chapter 3

CFD simulations

The topic of this chapter is simulation of the initial displacement process using the solver FLUENT available from ANSYS, Inc. The results will be compared to previous results by Soares et al[17] and Giavedoni and Saita[10].

3.1 FLUENT

FLUENT is a computer program capable of modeling a large diversity of flows in complex geometries, also including heat transfer and chemical reactions. For the flow in the present problem, FLUENT offers various algorithms to solve the Navier-Stokes equations, given by equations (2.1) and (2.2) with the simplifications introduced in section 2.1.

The Volume of Fluid (VOF) model is used as a formulation of the two-phase system. VOF is able to model the dynamics of two or more immiscible fluids, and compute the location of the interface between the fluids. It is used when the interface location is of primary interest, as is the case in the present problem.

A new variable is defined in VOF, the volume fraction α_q for each phase q. In each cell, there are three possible conditions for α_q:

- $\alpha_q = 0$: The cell does not contain fluid q.
- $\alpha_q = 1$: The entire cell is filled with fluid q.
- $0 < \alpha_q < 1$: The cell is partially filled with fluid q, the rest of the cell is filled with one or more other fluids. That means this cell contains an interface between two or more liquids.

Based on the volume fractions, volume averaged fluid properties are computed for each cell. These averaged properties are then used in the Navier-Stokes equations. Thus, only a single set of Navier-Stokes equations is solved in the entire flow, and the fields for all variables and properties are shared by the phases, representing volume-averaged values.

The interface is tracked using the volume fraction equation. The volume fraction equation is a continuity equation for the volume fraction of a phase q, and assuming no mass transfer between the phases and no mass sources, it is given by:

$$\frac{1}{\rho_q}\left(\frac{\partial}{\partial t}\left(\alpha_q \rho_q\right) + \nabla \cdot \left(\alpha_q \rho_q \mathbf{v}_q\right)\right) = 0 \tag{3.1}$$

where ρ_q is the density of phase q and $\mathbf{v}_q$ is the fluid velocity in the cell. This equation is solved for every phase except the phase defined as the primary phase. The volume fraction of the primary phase is given by the constraint

$$\sum_{q=1}^{n} \alpha_q = 1 \tag{3.2}$$

where n is the number of phases. This equation can be solved either implicitly or explicitly.

The interface needs special attention. For some of the available algorithms for solving the volume fraction equation, the interface is treated in the exact same way as cells completely filled with a single fluid. This generally gives interfaces that are not especially sharp. The best results are found using the Geometric Reconstruction Scheme. In this approach, the volume fraction equation is solved explicitly for every cell completely filled with only one fluid, using standard interpolation to calculate face fluxes. Cells that contains more than one fluid, and thus are part of the interface, are treated by the Geometric Reconstruction Scheme in three steps using a piecewise-linear approach. In the first step, the position of the linear interface in each cell is computed, based on volume fraction and derivatives of volume fraction from the last time step. Secondly, the advected amount of fluid through each face of the cell is computed, using the representation of the interface from the previous step and velocity information obtained from solving Navier-Stokes equation this time step. In the third step, fluxes through all faces of the cell are balanced, thereby calculating a new volume fraction.

3.2 Grid, boundary condition, fluid properties and FLUENT parameters

A pipe section of 1 m length and 1 cm in radius is used in the computation. The equations then need to be solved in the domain $0 \leq r \leq 0.01$, $0 \leq z \leq 1$, a square. The pipe wall is defined as the upper boundary of the domain, and the axis of the pipe is defined as the lower boundary of the domain. The pipe inlet is defined to be at $z = 0$, and the outlet at $z = 1$.

Two different grids are tested, as shown in figure 3.1. Grid 1 has cells of varying dimension. The length of each cell along the axis of the pipe is

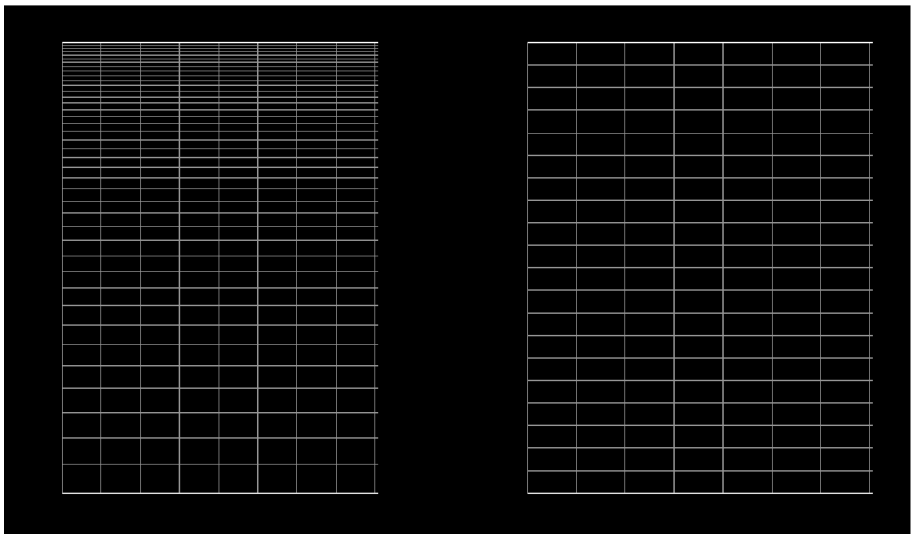

Figure 3.1: *Figure shows the inlet section of the two grids used in the computations. The left face of each grid is the inlet, the top face is a solid wall, and the bottom face is the axis of the pipe. Both grids are identical further downstream. The left grid will be referred to as grid 1, whereas the right grid will be referred to as grid 2.*

a constant, 0.8 mm. In the radial direction, the dimension changes from approximately 0.63 mm at the axis to approximately 0.063 mm at the wall. Totally, the grid has 1250x40 = 50000 cells. Grid 2 consists of cells of constant dimension 1 mm x 0.5 mm, totally 20000 cells. The varying cell dimension in grid 1 is intended to give a high resolution close to the wall, where the remaining oil layer is expected to be, making it possible to perform computations for relatively thin oil layers, and at the same time use a lower resolution close to the axis of the pipe to reduce computational time. In addition, FLUENT's user's guide states that the aspect ratio, which is defined as the length of the longest side of a cell divided by the length of the shortest side, should be kept below 5:1 in the bulk flow, away from walls, while it can be increased significantly in boundary layers. Grid 2 is intended to reduce computational effort, and check whether a grid with significantly lower resolution changes the computed flow noticeably.

The following is a summary of the boundary conditions used in the computations:

- The boundary condition for inflow is set to a constant velocity at the entire inlet. The inlet velocities considered are 0.01 m/s and 0.005 m/s.
- No slip is assumed at the wall.
- The outflow is assumed to be without normal gradients.

- Since the flow is supposed to be axisymmetric, the axis is supposed to be a symmetry line with no normal gradients and no normal velocity components.

As initial condition, it is assumed that the entire pipe is filled with oil with zero velocity.

Default FLUENT settings are used, but with some exceptions. Axisymmetric and unsteady solver is chosen, and PRESTO!, Second Order Upwind and Geo-Reconstruct are used as discretizations for pressure, momentum and volume fraction, respectively. PISO is used as pressure-velocity coupling.

For the fluids, we assume the following properties:

- Water has density $\rho_1 = 998.2\,\mathrm{kg/m^3}$ and viscosity $\mu_1 = 0.001003\,\mathrm{Pa \cdot s}$.
- The generic oil has density $\rho_2 = 800\,\mathrm{kg/m^3}$ and viscosity $\mu_2 = 0.02\,\mathrm{Pa \cdot s}$. The value for μ_2 is chosen to match the values for $\frac{\mu_2}{\mu_1}$ used by Soares et al.

3.3 Initial test

The flow is first modelled using grid 1. After a flow time of 6.57 s the situation shown in figure 3.2 is found. By measuring the interface thickness in FLUENT, we find the thickness to be 0.55 mm. This shows that the grid needs to be refined to achieve results with good enough precision. FLUENT is able to automatically adapt the grid to the solution at specified time intervals. Using this function, and refining the grid in areas with gradients in density, FLUENT can track the interface, and refine the grid only where necessary. The settings used in the menu "Gradient Adaption" are

- Allow both refining and coarsening of grid.
- Gradient method.
- Adapt to gradients in density for phase mixture.
- Maximum two refining steps in each cell.
- Refine threshold 0.1, coarsen threshold 0.01.
- Maximum number of cells 100000, to keep computational time down.
- Dynamic adaption, with adaption at every time step.

An example of the resulting grid after a flow time of 6.57 s is given in figure 3.4. As shown in figure 3.3 the interface now gets sharper, with a thickness of 0.12 mm. Since the interface still has a quite significant thickness, the mid-point of the interface thickness will in the following be considered the exact position of the interface.

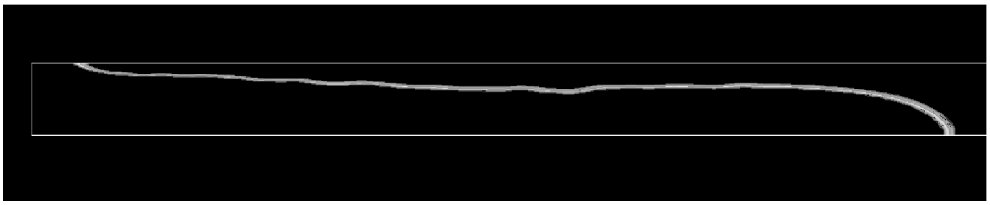

Figure 3.2: *Situation after 6.57* s*, using grid 1, inlet velocity 0.01* m/*s and surface tension coefficient 0.00025* N/*m*.

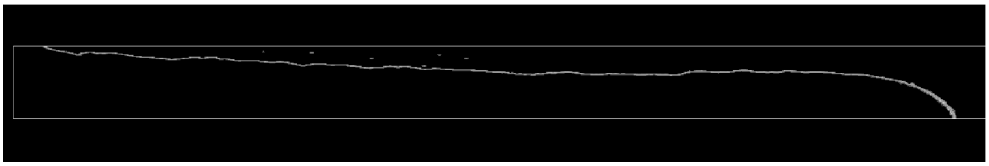

Figure 3.3: *Situation after 6.57* s*, using grid 1 with adaption, inlet velocity 0.01* m/*s and surface tension coefficient 0.00025* N/*m*.

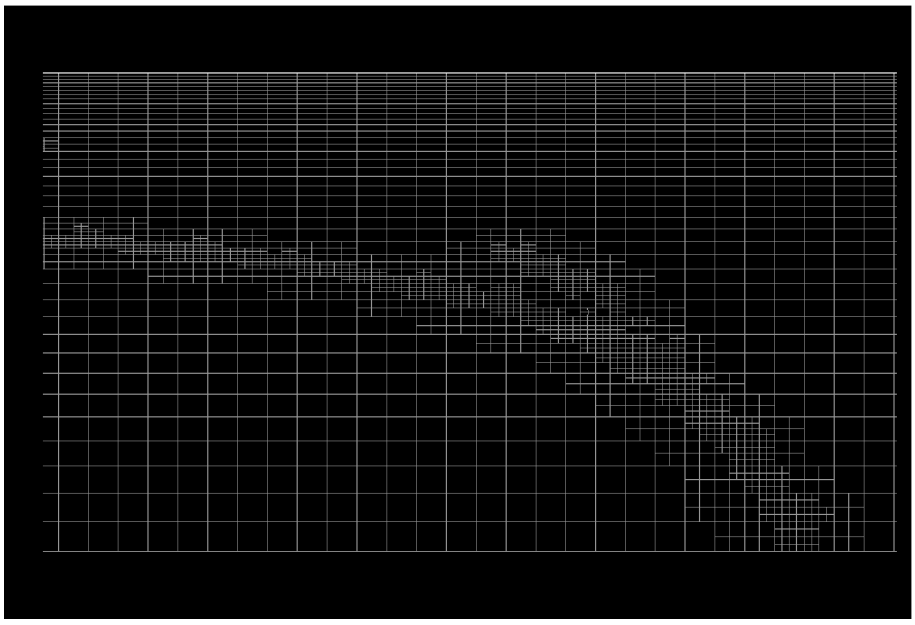

Figure 3.4: *Grid with adaption turned on, after 6.57* s*. The section of grid includes the nose of phase 1.*

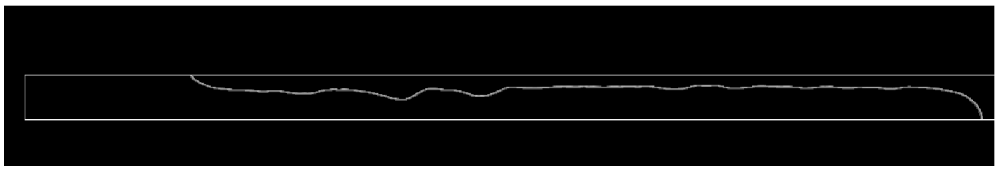

Figure 3.5: *A typical shape of the interface. In this case* $u_{inlet} = 0.01$ m/s *and* $\sigma = 0.0008$ N/m

3.4 Results

An example of a typical result of a computation is given in figure 3.5. We see that a core of water is formed, with a layer of oil close to the wall. Within a pipe diameter from the tip of the interface between the phases, a relatively stable interface is formed. Apart from this stable part, the rest of the interface is quite wavy, which makes it difficult to define the fraction of oil left on the wall. Therefore, in the following, the exact position of the interface is computed as the mean value of the position of the center of the interface sampled at regular intervals along the stable part. The length of the stable portion varies, and seems to be shorter for low capillary numbers than for higher capillary numbers. Close to the inlet, we can notice that oil seems to be completely displaced by water. This is discussed further in section 3.4.2.

We also have to determine the axial velocity of the tip of the interface, to be able to calculate the capillary number. The simplest solution is to find the local axial velocity of points along the tip of the interface, and compute an average of the values. The result should be expected to be close to the actual axial velocity of the tip. Another solution is to find the position of the tip of the interface at different time steps, and calculate how far the tip has actually moved during a known time. Doing this, we find a velocity that deviates significantly from what is found using the simplest method of finding local axial velocities. The second method is obviously the most accurate, as long as the difference in time between the two readings is quite large, so this method is used to determine the tip velocity in the following text.

3.4.1 Comparison of results using different grids

In section 3.3 we found that grid 1 gave reasonably good results when gradient adaption was applied. Now let us compare results from grid 1 with results from grid 2. Using the same system as in section 3.3, $\sigma = 0.00025$ N/m and $u_{inlet} = 0.01$ m/s, with the same setting for gradient adaption, we find after a flow time of 27.5 s the result given in figure 3.6 for grid 1. Solving the exact same system, with the same setting for gradient adaption, on grid 2, we find the result given in figure 3.7. The two figures show qualitatively the

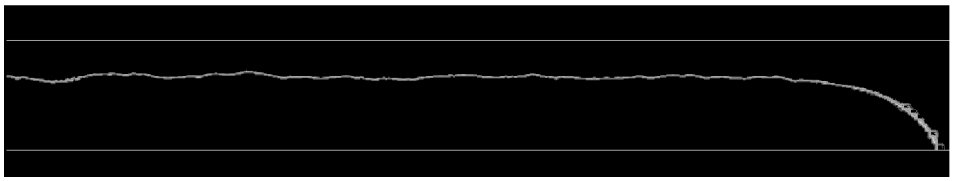

Figure 3.6: *Solution using grid 1 with adaption after 27.5* s, $u_{inlet} = 0.01$ m/s, $\sigma = 0.00025$ N/m.

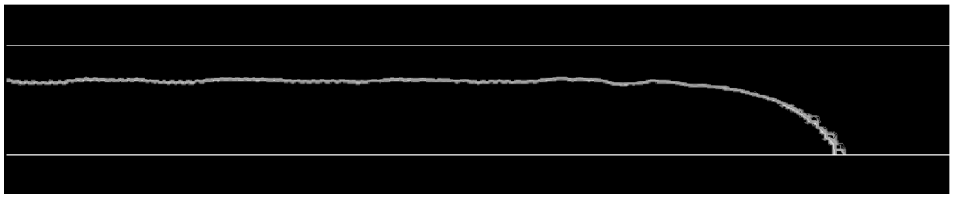

Figure 3.7: *Solution using grid 2 with adaption after 27.5* s, $u_{inlet} = 0.01$ m/s, $\sigma = 0.00025$ N/m.

same result. A comparison of key features read from the figures are given in table 3.1. From these values, we see that grid 2 gives roughly the same results as grid 1, except that grid 2 gives a less sharp interface. We seem to find grid-independent results, which gives some confidence to the solutions found. Although grid 1 gives a sharper interface, the advantage of performing faster computations on grid 2 makes grid 2 the preferred grid for the rest of the computations.

3.4.2 Moving contact line between fluids and wall

In figure 3.5 we see that close to the inlet of the pipe, oil has been completely displaced. The interface between the phases is then in contact with the pipe wall at a point. This point is usually referred to as a contact line. A moving

	Grid 1	Grid 2
m	0.5527	0.5434
Distance front of water has penetrated	0.564 m	0.553 m
Capillary number	1.624	1.688
Mean thickness of interface	0.12 mm	0.23 mm
Maximum time step	0.07 s	0.088 s
Approximate time consumption for one time step of maximum length, after a total flow time of 27.5 s	319 s	33 s

Table 3.1: *Comparison of results found using different grids.*

contact line is observed for the entire range of capillary numbers considered in this work.

A moving contact line seems to violate our assumption of no slip at the wall, a thin layer of oil should be left behind. But we know from a large diversity of everyday situations that moving contact lines are actually possible. A simple example is water spreading out over an initially dry surface, in this case the point where the interface between water and surrounding air touches the surface is obviously moving. Dussan and Davis[8] have shown that the intersection of the interface between two immiscible fluids and a solid is able to move without violating the assumption of no slip, if we assume the displacing fluid to perform a "rolling" motion onto the solid. They support this assumption with a few simple experiments, clearly showing that at least in simpler flows, a rolling motion occur. But with this explanation, the velocity becomes multi-valued at the contact line, and thus the fluid excerts an infinite force on the wall at the contact line, as long as the fluids are Newtonian. Dussan and Davis point out that the force singularity can be relieved by treating the fluids as non-Newtonian close to the contact line or to allow some slip close to the contact line.

Blake[3] gives a review of current approaches, and compares their successes and limitations. In addition to fluid dynamical approaches to avoid the force singularity, which he calls the hydrodynamic model, he also describes entirely different models based on molecular dynamics. He points out that both methods perform well in some cases, but have serious limitations in other cases. This, he argues, might indicate that both fluid dynamical and molecular mechanisms are at work. Although he mentions various models combining fluid dynamics and molecular dynamics, with reasonably good results, his conclusion is that there is still a lot that is unknown about the behaviour of contact lines.

According to Blake[3], the basics of the hydrodynamic model in most approaches can be explained using the details of the contact line as given in figure 3.8. At the microscopic level, the contact angle θ_m is usually assumed to be determined by short-range intermolecular forces, and it is commonly assumed that this angle is independent of the contact line velocity U, although Blake mentions that some dependence on the contact line velocity has been proposed. Thus, we can assume the microscopic contact angle to be dependent on wall material and the fluids involved, and not the flow itself. In the mesoscopic layer, viscous shear bends the interface until the interface reaches its static shape, at which point the macroscopic level starts. If we extrapolate the static interface to the surface, we find what is known as the dynamic contact angle, θ_D. This angle is the angle one is usually able to observe experimentally, and it is dependent on the velocity U, due to viscous bending of the interface at the mesoscopic level. Blake states that this dependence is usually monotonical, but that anomalies have been found. In its simplest form, he gives the relation between dynamic contact angle and

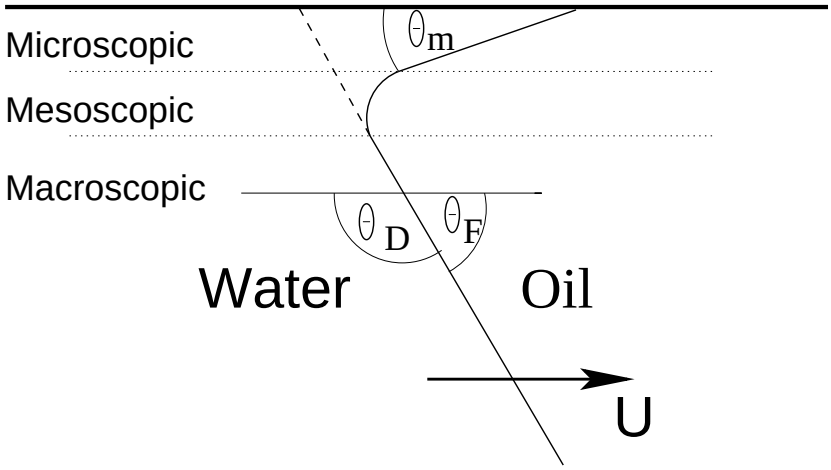

Figure 3.8: *Details of the contact line, with definition of contact angles. θ_D is the dynamic contact angle, θ_m the microscopic contact angle and θ_F the contact angle as it is defined in FLUENT. It should be noticed that although θ_m is shown as quite small, it could equally well be larger than 90 degrees.*

viscous bending as the equation

$$\chi(\theta_D) - \chi(\theta_m) = Ca_c \ln\left(\frac{L}{L_m}\right) \tag{3.3}$$

where χ is the integral

$$\chi(\theta) = \frac{1}{2}\int_0^{\theta}\left(\frac{\hat{\theta}}{\sin\hat{\theta}} - \cos\hat{\theta}\right)d\hat{\theta} \tag{3.4}$$

Ca_c is a capillary number describing the motion of the contact line, and L and L_m are typical dimensions of the macroscale and the microscale, respectively. Blake comments that this solution is only a first-order expansion in Ca_c, which means that Ca_c has to be small. The velocity of the contact line enters the equation through the capillary number, which Blake defined as $Ca_c = \frac{\mu U}{\sigma}$, where σ is the surface tension coefficient and μ the viscosity of the displacing fluid. It is assumed that the microscopic contact angle θ_m is equal to the static contact angle, which is the macroscopic contact angle observed when the contact line is not moving. We can notice that the function $\chi(\theta)$ is positive and monotonically increasing when θ is in the interval $[0, \pi]$, and that the right-hand side of equation (3.3) is essentially U multiplied by a constant. From this we see that increasing U leads to an increased dynamic contact angle θ_D. Replacing one of the fluids or the wall material, and thereby reducing or increasing θ_m, would lead to reduced or increased θ_D, respectively. It should be noticed that although this model has performed well in some situations with small Ca_c, it is not able to offer

a complete description of the contact line movement in every situation. In addition, it is not necessarily obvious which length scales to use, so as a predictive tool, the equation is not especially useful. But it offers some qualitative insight in the problem.

It should be noted that the model described here is for the limiting case of a viscous fluid displacing an inviscid fluid. Cox[6] has found solutions for liquid-liquid displacement where the viscosity ratio $\frac{\mu_2}{\mu_1}$ is included, and with higher order solutions in Ca_c. His results show that the behaviour of the system is qualitatively the same with low viscosity ratio as with high viscosity ratio, but that when θ_m and U is held constant, an increasing viscosity ratio leads to an increased dynamic contact angle.

Figure 3.9 shows the velocity of this contact line as a function of the surface tension coefficients that has been used in the computations. This figure indicates that the contact line moves with a velocity that is a linear function of the surface tension coefficient, and independent of inlet velocity. This result couples well with the predictions from equation (3.3). We have not changed any of the contact angles, and we have no means of changing the dimensions of the microscale and the macroscale. Thus, we should expect the local capillary number to be constant, and that is fulfilled if the velocity of the contact line is a linear function of the surface tension coefficient. The result is found using the default contact angle in FLUENT, $\theta_F = \frac{\pi}{2}$. In this case, the capillary number related to the contact line is $\mathcal{O}\left(10^{-3}\right)$, so the requirement for small capillary number for equation (3.3) to be valid is fulfilled.

FLUENT is not able to compute the dynamic contact angle, probably because no exact relation between velocity and θ_D is known, but it is possible to define the angle, and observe what impact different angles have on the velocity of the contact line. It should be noticed that the definition of the contact angle in FLUENT is the opposite to what we have used, as shown in figure 3.8. Interestingly, we find that increasing the angle from the default 90 degrees reduces the velocity of the contact line significantly. This is the same effect as we would have in equation (3.3) if θ_m is increased. It thus seems that FLUENT treats the defined contact angle as the microscopic contact angle.

If we go back to our comparison of grids from section 3.4.1 and check the velocity of the contact line, we find that using grid 1 the velocity is approximately 0.055 cm/s, while it for grid 2 is approximately 0.12 cm/s. The finer resolution of grid 1 gives a slower rear front. This indicates that the values we have in figure 3.9 are too high, and that the actual velocity of the contact line is lower than what we have found. It seems reasonable to expect the velocity to be affected by non-physical numerical errors. Obviously, the VOF method has a limited resolution, and it can be expected to run into problems when the interface is close to the wall compared to the height of a cell. The thin film of oil that should be left at the wall close to the contact

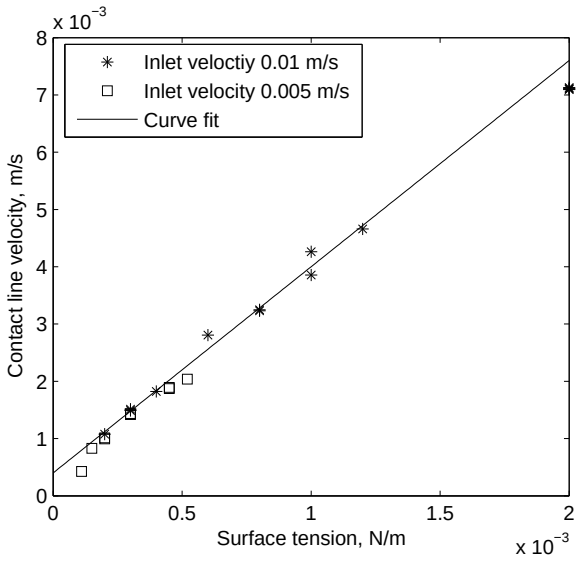

Figure 3.9: *Velocity of moving contact line as function of surface tension coefficient.*

line would not give an especially high volume fraction of oil for the cell closest to the wall when the film is thin enough. Because of this, VOF could be expected to treat the cell closest to the wall as being completely filled with the less viscous, thereby incorrectly predicting a complete displacement. This would tend to increase the velocity of the intersection. The minimum thickness of the oil film would be further limited by surface tension, since the curvature of the interface is limited by surface tension. An example of this curvature dependence is given in figure 3.10, we see that the curvature is highest for the case with lowest surface tension.

Obviously, we have observed a lack of numerical accuracy in this case, since the two grids give significantly different result. We have also seen that the behaviour of the contact line is dependent on contact angle, with some agreement with previously reported results. But we have no detailed knowledge of what microscopic contact angle we should expect, and amongst others Dussan[7] mentions that the behaviour of the contact line is dependent on surface roughness, which we have not taken into account at all. Dependence on other quantities as well, e.g. viscosity ratio or Reynolds number, can not be ruled out. The hydrodynamic theory, with equation (3.3), is able to describe some systems, but we have no guarantee it can be used with good results in our case. All in all, it seems that too little is known about the

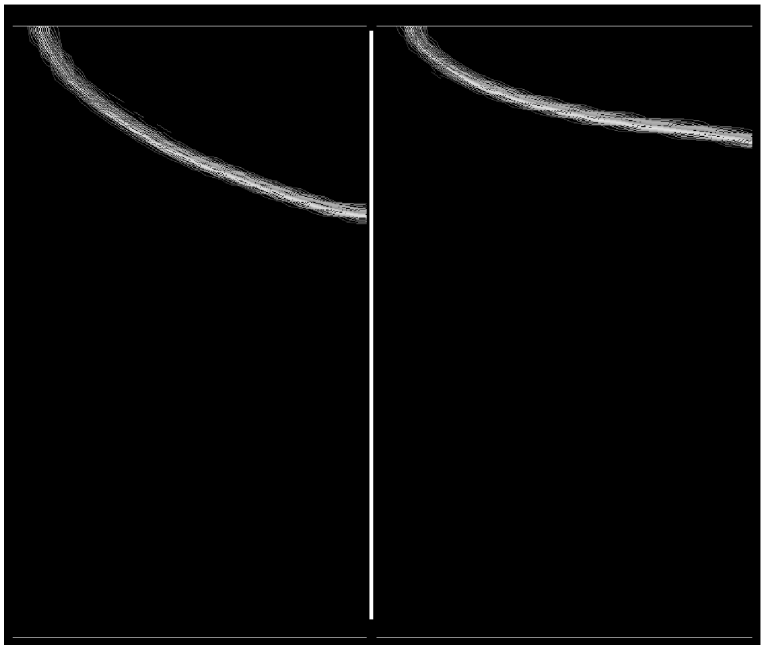

Figure 3.10: *Shape of moving rear front for different values of surface tension coefficient, the left hand side is for* $\sigma = 0.0012$ N/m*, the right hand side for* $\sigma = 0.0002$ N/m

physics behind the movement of contact lines to come to any conclusions.

3.4.3 Recirculation and bypass flow

For different capillary numbers and different interface heights, the front moves with different velocity. If the flow is laminar, then far downstream from the front the flow is a fully developed Poiseuille flow, where the velocity at the center of the pipe is constant and only dependent on the net volume flow in the pipe. Simple mass conservation arguments imply that there must exist at least two distinctly different types of flow ahead of the front, in phase 2. This behaviour was first predicted by Taylor[19], who realized that the flow had to change character when the fraction of mass left at the wall, m, was equal to 0.5. He superimposed a velocity $-U$ on the flow, where U is the velocity of the front. Thus, he changed to a lagrangian view, where the front is stationary. If we now introduce the control volume defined in figure 3.11, it is easy to argue that there must exist different flow patterns. Since the front is now considered stationary, there is no flow through the boundary along the front. Also, since we have assumed an axisymmetric flow, there can be no flow through the boundary along the axis. If the front moves faster than the liquid ahead of the flow, we must in the lagrangian view have that liquid downstream of the flow moves toward the front. Thus, there must be

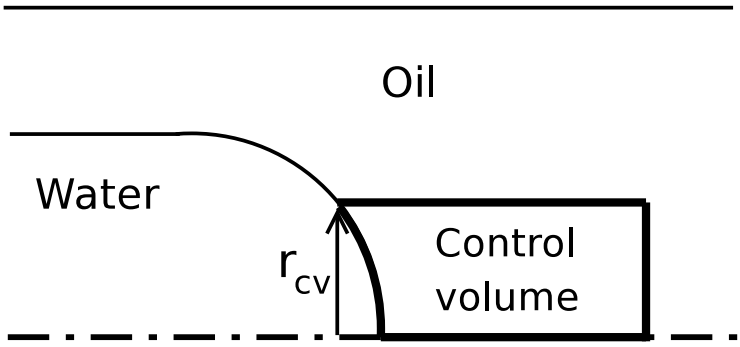

Figure 3.11: *Control volume defined to argue why different flow regimes must exist.*

an inflow through the downstream boundary, which gives that there must be a net outflow through the boundary at $r = r_{cv}$. In the opposite case, where the front moves slower than fluid ahead of the flow, the same kind of argument gives that there has to be a net inflow through the boundary at $r = r_{cv}$. The first kind of flow is usually referred to as a bypass flow, whereas the second is referred to as a recirculation flow. Looking at figure 3.12, the origin of this notation is quite obvious.

Taylor proposed a flow pattern for high m, figure 3.12a, and two different streamline patterns that illustrated the two simplest types of flow for low m, 3.12b,c, but he was not able to decide which of the patterns for low m were the correct one, if any. Giavedoni and Saita[10] later found the same type of flow through numerical experiments, and actually confirmed the guesses Taylor made, as they found all three types of flow that Taylor proposed. The pattern in figure 3.12a were, as predicted by Taylor, the correct one for $m > 0.5$. For low m, the pattern in figure 3.12c dominated. As a transition between these two patterns, the one shown in figure 3.12b was observed. Giavedoni and Saita found the transition to take place at a capillary number $Ca \approx 0.7$. Soares et al[17] observed that the transition took place at higher Ca when the viscosity ratio μ was reduced, but did not comment this observation further.

Soares and Thompson[18] made a thorough investigation of the problem, and showed analytically that the critical value for m at which the transition had to take place could be given by

$$m_c = \frac{1}{2\left(1 - \frac{1}{\mu}\right)} \tag{3.5}$$

With $m > m_c$, bypass flow was observed. Reducing m below m_c, one of the two recirculation regimes was observed, however, the results by Soares and Thompson were not able to predict which recirculation type. For very large μ, as in the system used by Taylor[19] and Giavedoni and Saita[10], the

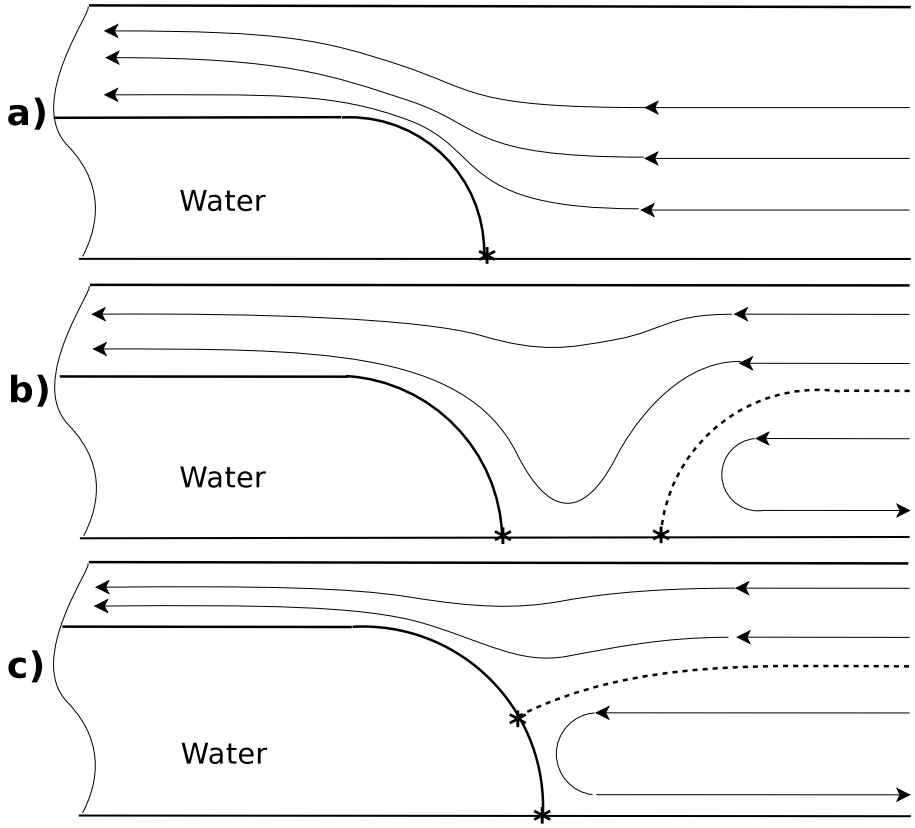

Figure 3.12: *The flow patterns predicted by Taylor. a) shows a bypass flow, typical for high capillary numbers, b) and c) show two types of recirculation, typical for low capillary numbers. The dotted lines in the recirculating flow patterns show boundaries of the recirculation, liquid outside these boundaries are flowing like in the bypass case. Stagnation points are marked by asterisks (*). The off-center stagnation point in c) is actually a stagnation ring due to axisymmetry.*

critical value $m_c = 0.5$ is reproduced. In the relation found by Soares and Thompson, we see that there is a problem with $\mu < 2$. For $\mu < 2$ equation (3.5) predicts m_c above unity, and this is obviously impossible. Numerical experiments performed by Soares and Thompson show that with $\mu \leq 2$, the flow will always be a recirculation flow.

The relation for m_c found by Soares and Thompson[18] can actually be reproduced quite easily using the hold-up equation (2.33). Rewriting a bit, we can find

$$\overline{u}_1 = \frac{Q\left(H^2\left(\mu - 2\right) + 2\right)}{A\left(H^4\left(\mu - 1\right) + 1\right)} \tag{3.6}$$

where $\overline{u}_1$ denotes the mean velocity in phase 1. Assuming a fully developed flow, this velocity is equal to the velocity of the front itself. If the front itself moved faster or slower than the mean velocity of the fluid behind, the interface would go down or up, and hence, the flow would not be fully developed. It is well known that the maximum velocity in a fully developed Poiseuille flow is given by $u_{max} = 2\frac{Q}{A}$, and we thus know the maximum velocity downstream of the front. Thus, we will have bypass flow if $\overline{u}_1 > u_{max}$, which gives

$$\frac{H^2\left(\mu - 2\right) + 2}{H^4\left(\mu - 1\right) + 1} > 2 \tag{3.7}$$

Rearranging and assuming $H \neq 0$, which is not an interesting solution, we get

$$H^2 < \frac{\mu - 2}{2\left(\mu - 1\right)} \tag{3.8}$$

Since by definition $m = 1 - H^2$, the inequality can be written

$$m > \frac{1}{2\left(1 - \frac{1}{\mu}\right)} \tag{3.9}$$

which is exactly the same relation as found by Soares and Thompson. This should not come as a surprise, as Soares and Thompson made the same assumptions of fully developed flow far upstream and far downstream from the front as we did here.

Unfortunately, FLUENT seems not to be able to superimpose a velocity on the solution, so plots of lagrangian streamlines from the solution found by FLUENT is not available. But if we plot vectors of radial velocity, a change from bypass flow to recirculation flow is clearly observed.

Amongst others, Soares and Thompson also describes a secondary recirculation that takes place in phase 1 close to the front when the flow is in the full recirculation mode shown in figure 3.12c. The grid used in FLUENT is too coarse to capture this secondary recirculation with any accuracy, but it is likely that it is this recirculation that makes it difficult to define the front velocity as a mean value of local velocities close to the front.

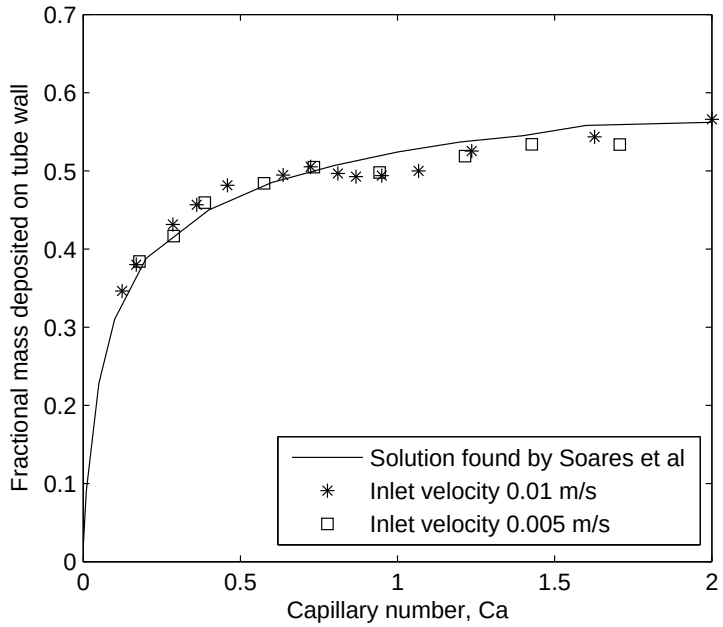

Figure 3.13: *Comparison with solution found by Soares et al.*

3.4.4 Comparison with results found by Soares et al

By performing the same computations for different values of surface tension coefficient, and hence different capillary numbers, values for m are found for different capillary numbers. When these values for m are plotted together with results found by Soares et al[17], we find the results given in figure 3.13.

First, we can notice that the results seem to be independent of inlet velocity, and only depend on capillary number. For both inlet velocities, we see that the results deviate in the same way from the results found by Soares. In the region with low capillary number, this work gives a higher fraction of oil left on the wall than the value found by Soares. For higher capillary numbers, we find a lower fraction of oil left on the wall compared to the computations by Soares.

The change seem to occur at a capillary number of approximately 0.7, and with m quite close to 0.5. This is close to the point where we would expect the transition from recirculation flow to bypass flow, as discussed in section 3.4.3. Actually, all the points in the interval $[0.7, 1.1]$ that fall below the results reported by Soares have a fraction of oil left at the wall that is just below the critical value for m computed from equation (3.5), $m_c \approx 0.52$. This

might well show that our grid is too coarse to give any good description of the complex flow ahead of the front, and thus, that we can not expect to get any good predictions for when the transition occur. Since the fraction of mass left at the wall is intimately coupled to the transition between recirculation flow and bypass flow through equation (3.5), this could explain the deviation.

In addition, the change seems to occur when the velocity of the contact line discussed in section 3.4.2 is approximately 20% of the inlet velocity, this trend is observed for both inlet velocities considered. As we saw in section 3.4.2, the contact line velocity depends on the contact angle. If we reduce the contact angle from the default 90 degrees to 0.01 degrees, the velocity of the contact line is reduced significantly. For $Ca \approx 1.0$ this increases the value of m, and we get a result closer to what is found by Soares. For $Ca \approx 0.36$ no significant change is observed, although m is somewhat reduced, making the result closer to what is found by Soares. Since, as discussed in section 3.4.2, the behaviour of the contact line is probably not correctly predicted, this could be the reason for the observed discrepancy between the results found here and the results found by Soares.

3.4.5 Comparison with analytical results

In section 2.2 we found analytical results for the shape of the velocity profile. In figure 3.14 the analytical result is compared with the numerical result for $Ca \approx 1.24$. The numerical velocity profile is found in a section of the pipe where the interface is stable. In the analytical result, we have used the interface height h that is found from the numerical solution. As we see from the figure, the analytical solution is quite close to the numerical one. This gives some confidence to the assumptions made in chapter 2, although it should be noted that the numerical solution seems to suggest that the pressure gradient Θ is actually not a constant, but fluctuates a little.

3.5 Stability and accuracy

During the computations, it has been observed that large values for the surface tension coefficient tends to destabilize the solution. To keep the solution stable, the length of the time step Δt needs to be reduced when the surface tension is increased. The maximum length of the time step is plotted versus surface tension coefficient in figure 3.15. We can notice that the requirement for the length of the time step seems to be independent of the inlet velocity, and a simple curve fit suggests $\Delta t \approx \frac{2}{\sigma} \cdot 10^{-5}$ s as a maximum length for the time step. With a longer time step, short wave length capillary waves appear at the interface, as shown in figure 3.16. The waves grow quickly, and the entire solution deteriorates fast. Computation with a refined mesh also suggests that Δt has a first-order dependence on the dimension of the smallest cell in the grid.

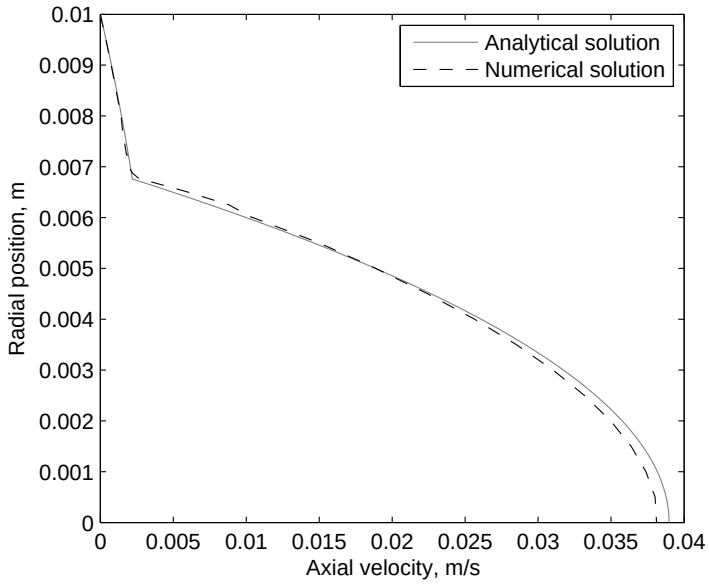

Figure 3.14: *Comparison of analytical velocity profile with velocity profile found numerically.* $Ca \approx 1.24$.

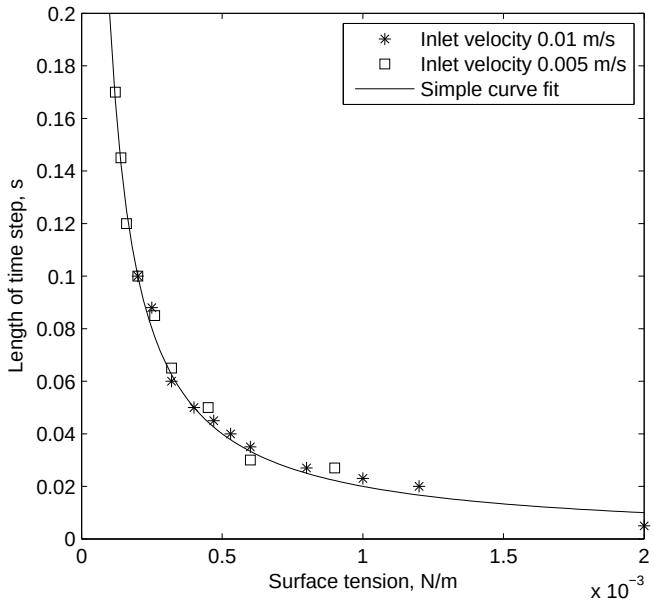

Figure 3.15: *Maximum length of timestep,* Δt, *plotted as a function of surface tension coefficient. We see that this stability requirement is independent of inlet velocity. The curve fitted function is* $\Delta t = \frac{2}{\sigma} \cdot 10^{-5}$.

Numerical experiments suggest therefore that $\Delta t_{max} \sim \frac{\Delta z}{\sigma}$. This condition can be justified as follows. Let us assume that the reason for the instability is the balancing of viscous shear forces versus surface tension. Viscous shear can be represented by

$$\tau_s \sim \mu \frac{\partial \mathbf{v}}{\partial r} \sim \mu \frac{U}{L} \tag{3.10}$$

where U is a typical velocity scale and L is a typical length scale. Surface tension can be represented by

$$\tau_\sigma \sim \mathcal{C}\sigma \sim \frac{\sigma}{L} \tag{3.11}$$

where $\mathcal{C}$ is the surface curvature. Setting these two equations approximately proportional to each other, we find

$$\frac{\sigma}{L} \sim \mu \frac{U}{L} \tag{3.12}$$

The velocity U can be represented by a length scale divided by a time scale, and since the velocity is mainly in the z-direction, we choose $U \sim \frac{\Delta z}{\Delta t}$. Inserting that into the equation and rearranging, we find

$$\Delta t \sim \frac{\mu}{\sigma} \Delta z \tag{3.13}$$

If this is the correct forces to balance, we can assume the stability requrement to be of the form

$$\Delta t < \alpha \frac{\mu}{\sigma} \Delta z \tag{3.14}$$

where α is some unknown constant. It is not obvious which value for μ is the correct to use, μ_1 or μ_2. A few simple experiments showing stability dependence on both μ_1 and μ_2 suggest $\mu = \mu_1 + \mu_2$. With gradient adaption turned on, as described in section 3.3, the smallest value for Δz is $2.5 \cdot 10^{-4}$. Inserting the values for μ and Δz, we see that if $\alpha = 3.8$ we reproduce approximately the equation for the curve-fit in figure 3.15.

In the limit of no surface tension, the expression for the curve fit seems to allow an infinitly long time step. This is clearly not possible, simple tests suggests a time step $\Delta t < 0.4$ s for inlet velocity 0.01 m/s. The stability requirement in this case is not investigated further, since it is of little interest in the present problem.

It should also be expected that the accuracy of the solution is dependent on the length of the time step. A priori it would be expected that a shorter time step leads to a more accurate solution. This is investigated using three different time step lengths for solving the same system. First, it is solved using a time step close to the stability requirement described above. Then, it is solved using a time step one-third of the one above, and finally one-tenth

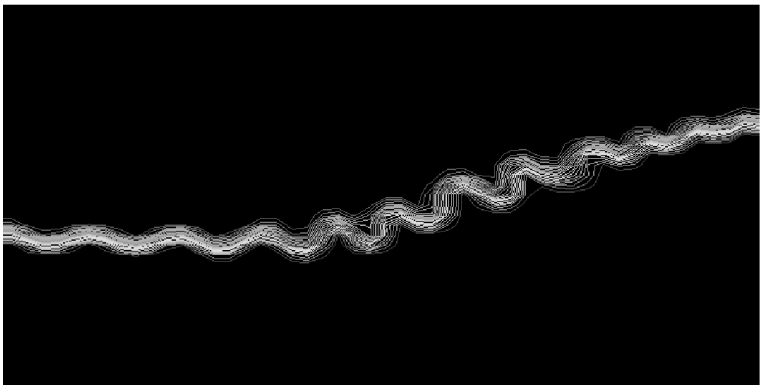

Figure 3.16: *Detailed view of a section of the interface for a typical instable flow. The wave length of the waves are approximately four cell lengths.*

	1	1/3	1/10
m	0.4414	0.5266	0.5277
Capillary number	0.276	0.306	0.306

Table 3.2: *Comparison of results found using different time step lengths,* $\sigma = 0.00132$ N/m*, inlet velocity* 0.01 m/s*. Maximum* Δt *is found to be* 0.03 s.

of the stability limit. As shown in table (3.2), the solution seems to converge for shorter time steps. Assuming that the results from Soares[17] are correct, we should get a value for m of approximately 0.4 for this system, which tells us that the system seems to converge to a solution further away from the solution found by Soares.

The shape of the interface for the different time step lengths are given in figure 3.17. We see that the interfaces are quite similar, but that the interfaces are more stable for the smallest time steps. For the shortest time step, the height of the interface does not vary more than 0.01 mm over the first stable part of the interface, close to 15 cm. It is surprising to find such a stable interface. We can also notice the sudden changes in interface height for the two shortest time steps, intuitively we would expect the changes in interface height to happen more gradually, like the situation for the longest time step.

As mentioned in section 3.4.3 a recirculation should be formed ahead of the front of water below some borderline value for the capillary number. In figure 3.18 and 3.19 contours of axial and radial velocity for the three different time steps are given for a capillary number $Ca \approx 0.3$, showing the section of the pipe where the front of water is. We see that only for the longest time step there is both a zone with higher axial velocity and a zone with negative

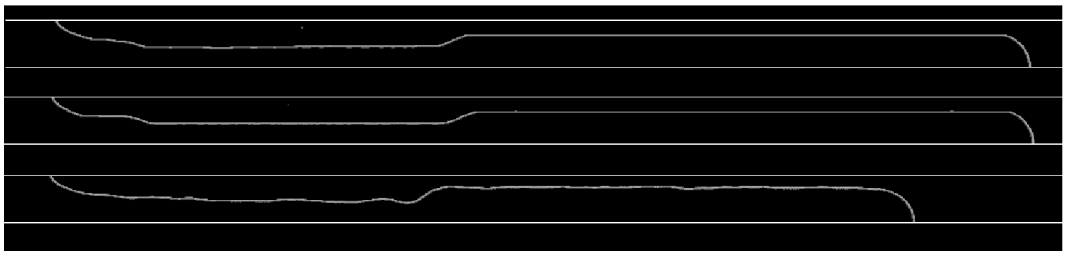

Figure 3.17: *Shape of interface for different length of time steps, from top to bottom* 0.003 s, 0.01 s *and* 0.03 s. $\sigma = 0.00132$ N/m. *The situation is achieved after a flow time of* 20 s.

radial velocity ahead of the water front. Both these properties should be expected in a flow with recirculation. If we redo the experiment with a capillary number approximately 1.4, we do not observe any recirculation at all, independent of the length of the time step. According to the discussion in section 3.4.3 no recirculation should be expected, either.

Although we expect the solution to be most accurate for low values of Δt, we have the following observations to support using the longest possible time step:

- We find a value for m closer to the one found by Soares et al.
- The shorter time steps seems to give too stable interfaces.
- The abrupt changes in interface height predicted by the shorter time steps seems unphysical.
- We find the recirculation described in section 3.4.3 only for the longest time step.

Because of these observations, the solution is assumed to be most accurate using a time step length close to the stability limit. No reason for this behaviour is known.

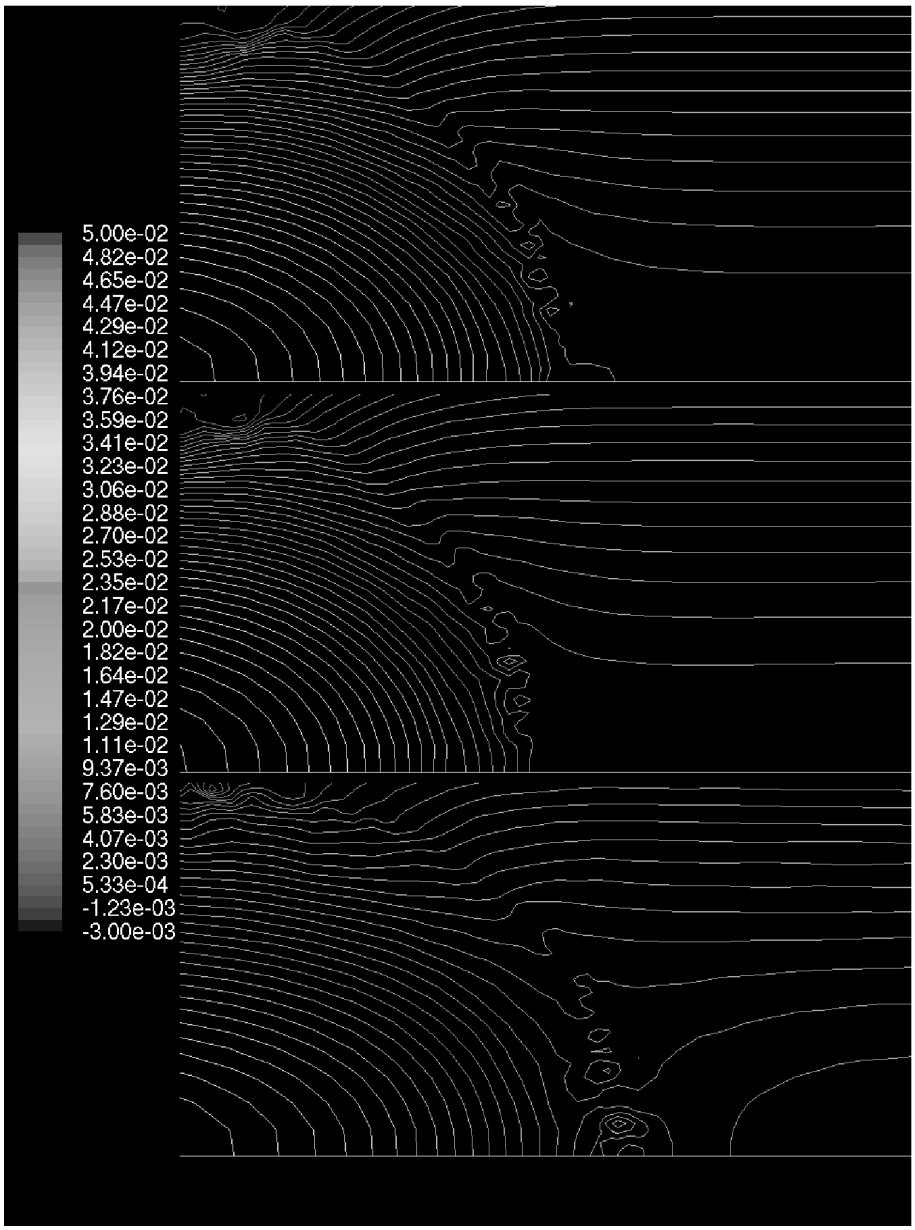

Figure 3.18: *Contours of axial velocity for different time step lengths, showing the front of the water phase. From top to bottom the plots show one-tenth of the stability limit, one-third of the stability limit and approximately the stability limit. The velocity is highest in the lower left corner of each contour plot, and lowest close to the top of each plot. One should notice that, in the case of the longest time step, there is a small area with low velocity right in front of the water front, further downstream we find a zone with higher velocity. The capillary number is approximately* 0.3.

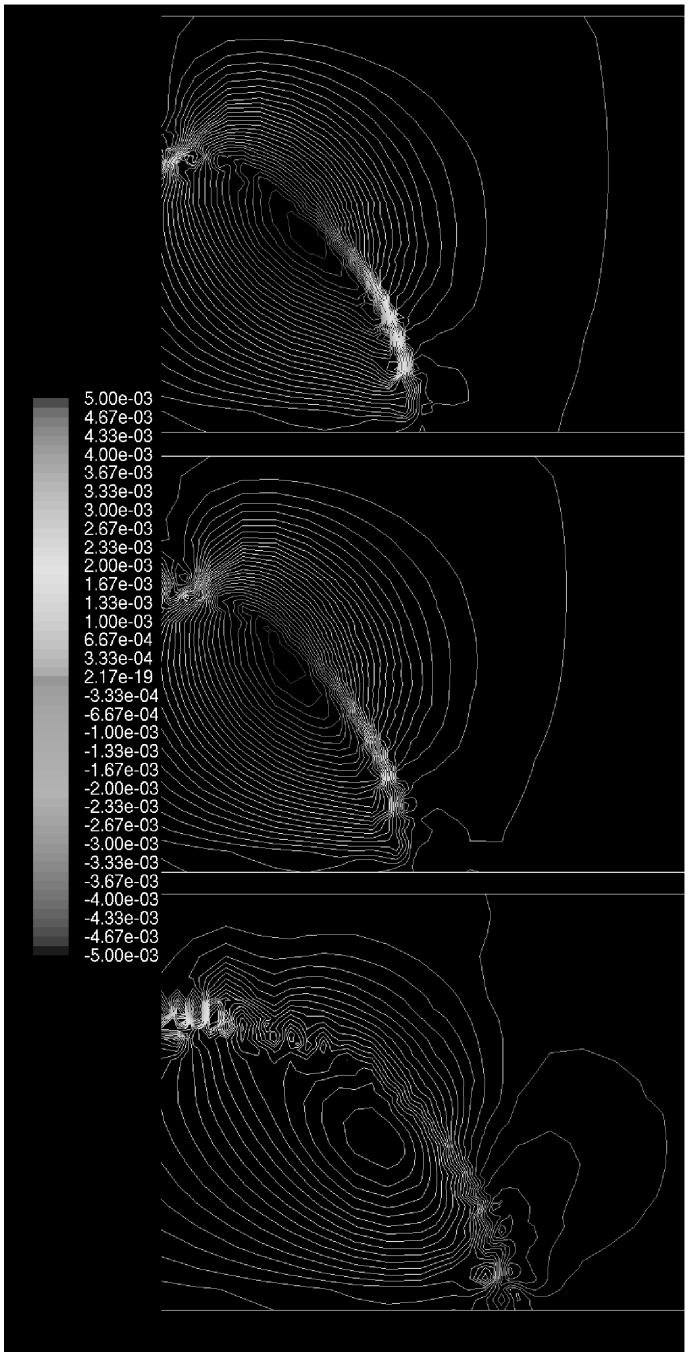

Figure 3.19: *Contours of radial velocity for different time step lengths, showing the front of the water phase. From top to bottom the plots show one-tenth of the stability limit, one-third of the stability limit and approximately the stability limit. The radial velocity is highest in the center of the plotted contours. One should notice the zone with negative velocity ahead of the water front in the case of the longest time step, there is no negative velocity at all in the two cases with shorter time steps. The capillary number is approximately* 0.3.

Chapter 4

Hydraulic model

In a hydraulic model, we use one-dimensional equations to describe the flow. These equations are found by averaging the three dimensional equations over the cross sectional area of the pipe. In this process, detailed information of the velocity profile is removed, and thereby information that is actually necessary to solve the equations is removed. For instance, knowledge of the velocity profile is needed to find exact expressions for shear stresses. Thus, shear stresses will have to be modelled somehow. In doing this, we obviously loose some accuracy. We also loose the ability to describe properties of the flow with typical dimension smaller than the pipe diameter, as these structures are removed by the averaging process.

For our case, with laminar flow and where gravity can be neglected, the one-dimensional equations can according to Schulkes[15] be given by the mass conservation equations

$$\frac{\partial}{\partial t}\left(A_k \rho_k\right) + \frac{\partial}{\partial z}\left(A_k \rho_k u_k\right) = 0 \tag{4.1}$$

with $k = \{1, 2\}$, corresponding to water and oil, respectively, and the momentum equations

$$\begin{aligned} \frac{\partial}{\partial t}\left(A_1 \rho_1 u_1\right) &+ \frac{\partial}{\partial z}\left(c_1 A_1 \rho_1 u_1^2\right) \\ &= -A_1 \frac{\partial p_{1I}}{\partial z} + 2\frac{\partial}{\partial z}\left(A_1 \mu_1 \frac{\partial u_1}{\partial z}\right) - \tau_{1I} s_I \end{aligned} \tag{4.2}$$

$$\begin{aligned} \frac{\partial}{\partial t}\left(A_2 \rho_2 u_2\right) &+ \frac{\partial}{\partial z}\left(c_2 A_2 \rho_2 u_2^2\right) \\ &= -A_2 \frac{\partial p_{2I}}{\partial z} + 2\frac{\partial}{\partial z}\left(A_2 \mu_2 \frac{\partial u_2}{\partial z}\right) - \tau_w s_w + \tau_{2I} s_I \end{aligned} \tag{4.3}$$

In addition, the jump conditions describing the change in pressure and shear stress across the interface can be given by

$$p_{1I} - p_{2I} = 2\sigma\mathcal{C} \tag{4.4}$$

$$\tau_{1I} = \tau_{2I} \tag{4.5}$$

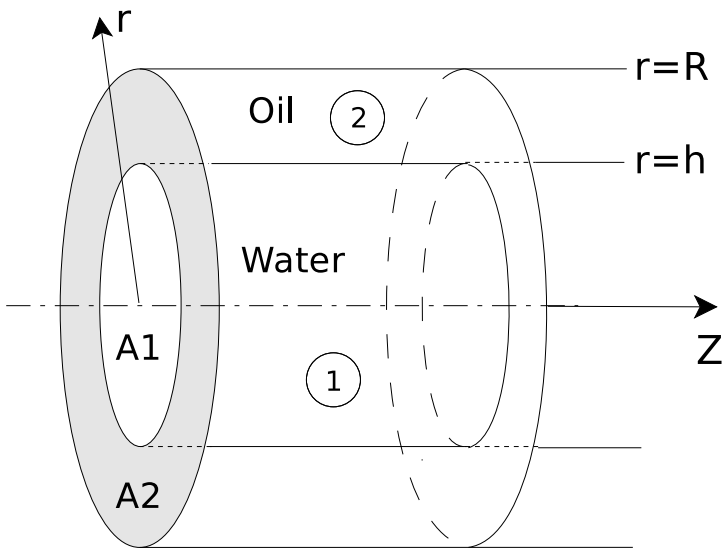

Figure 4.1: *Geometry for the hydraulic model.*

In the equations, A_k denotes cross sectional area occupied by phase k, ρ_k the density of phase k, c_k is known as the profile parameter of phase k, p_{kI} denotes the interfacial pressure in phase k, μ_k molecular viscosity of phase k, τ_w wall shear stress, defined only for the oil phase, τ_{kI} interfacial shear stress on phase k, s_I is the length of the interface between the phases, and u_k is the mean velocity of phase k. s_w is the circumferential length of the wall wetted by the oil phase, equal to the circumference of the pipe, since water is assumed not to be in contact with the wall. $\mathcal{C}$ denotes the mean curvature of the interface, which is defined by

$$\mathcal{C} = \frac{1}{2}\left(\frac{1}{R_1} + \frac{1}{R_2}\right) = \frac{1}{2}\nabla \cdot \mathbf{n} \tag{4.6}$$

where R_1 and R_2 are the principal radii of of curvature of the interface, and $\mathbf{n}$ is a unit normal vector at the interface. If we calculate the divergence $\nabla \cdot \mathbf{n}$ we find that the mean curvature can be given as

$$\mathcal{C} = \frac{1}{2}\left(\frac{1}{h\sqrt{1+\left(\frac{\partial h}{\partial z}\right)^2}} - \frac{\frac{\partial^2 h}{\partial z^2}}{\left(1+\left(\frac{\partial h}{\partial z}\right)^2\right)^{\frac{3}{2}}}\right) \tag{4.7}$$

The profile parameter c_k enters the equations because the average of a product is not the same as the product of averages, and for our case it is defined by $c_k = \frac{1}{Au_k^2}\int_A \left(v_k(r)\right)^2 dA$, where $v_k(r)$ is the axial velocity at radial position r. Since we do not have any information regarding the velocity

profile, we assume that the veloctiy profile is as defined in equation (2.26). Strictly speaking, this velocity profile is valid only for a stationary, fully developed flow, but unfortunately we do not have any other velocity profile to use. Integrating this profile, we can find an expression for c_1 to be

$$c_1 = \frac{\frac{1}{3}\mu A_1^2 + \mu A_2 A + A_2^2}{\frac{1}{4}\mu A_1^2 + \mu A_2 A + A_2^2} \tag{4.8}$$

where, again, we have introduced $\mu = \frac{\mu_2}{\mu_1}$. Obviously, we must demand $0 \leq A_1, A_2 \leq A$ and $A_1 + A_2 = A$ in this equation. We then quite easily see that the minimum value of c_1 is 1 when $A_1 = 0$, and that c_1 increases monotonically to the maximum value of $\frac{4}{3}$ when $A_1 = A$. It will become obvious that c_2 is actually not needed, so this term is not discussed further.

The wall shear stress and interfacial shear stress need to be modelled somehow. It is common to assume that wall shear stress is given by

$$\tau_w = \frac{1}{8}\rho_2 u_2^2 f_2 \tag{4.9}$$

where f_2 is an unknown friction factor. For laminar flow, this friction factor is often given as $f_2 = \frac{32}{Re_2}$, where Re_2 is the Reynolds number in the oil phase, defined as $Re_2 = \frac{\rho_2 u_2 (R-h)}{\mu_2}$. R and h are the radius of the pipe and the radius of the central core of water, respectively, as introduced in section 2.1 and 2.2. Due to the jump condition for shear stress, we can define $\tau_{1I} = \tau_{2I} \equiv \tau_I$. The interfacial shear stress is then in the same way given as

$$\tau_I = \frac{1}{8}\rho_1 (u_1 - u_2) |u_1 - u_2| f_I \tag{4.10}$$

with the friction factor given by $f_I = \theta \frac{64}{Re_1}$, where the Reynolds number is defined as $Re_1 = \frac{\rho_1 u_1 2h}{\mu_1}$. θ is a constant that has to be decided.

4.1 Stationary, fully developed flow

If we assume the situation to be as we did in the analysis in chapter 2, with a stationary and fully developed flow, we can again conclude that we have no time dependence $\left(\frac{\partial}{\partial t} = 0\right)$ and that there is no dependence on z-coordinate for any other quantities than pressure $\left(\frac{\partial}{\partial z} = 0\right)$. In addition, since the entire pipe wall is wetted by oil, $s_w = 2\pi R$, and $s_I = 2\pi h$, due to the axisymmetric situation. With the simplifications, the mass conservation equations are trivially fulfilled, and the momentum equations simplify to

$$0 = -A_1 \frac{\partial p_{1I}}{\partial z} - 2\tau_I \pi h \tag{4.11}$$

$$0 = -A_2 \frac{\partial p_{2I}}{\partial z} - 2\tau_w \pi R + 2\tau_I \pi h \tag{4.12}$$

Due to the jump condition for pressure, the two pressure gradients have to be equal. Eliminating the pressure gradient between the two momentum equations, we can find the hold-up equation

$$\tau_I h \left(\frac{1}{A_1} + \frac{1}{A_2} \right) = \frac{\tau_w R}{A_2} \tag{4.13}$$

If we now insert the expressions for shear stresses and friction factors, we end up with the equation

$$\frac{(u_1 - u_2)\,|u_1 - u_2|\theta}{u_1} \left(\frac{1}{A_1} + \frac{1}{A_2} \right) = \frac{\mu_2}{\mu_1} \frac{u_2 R}{A_2(R-h)} \tag{4.14}$$

To get any further, it is now necessary to assume $u_1 - u_2 > 0$. This can be justified by looking at the velocity profile presented in figure 3.14, the mean velocity in the central core must always be larger than the mean velocity in the annulus close to the wall. We now introduce the superficial velocities, as defined in chapter 2. The superficial and mean velocities are still related through the expressions $\pi h^2 u_1 = \pi R^2 U_{1,SL}$ and $\pi \left(R^2 - h^2\right) u_2 = \pi R^2 U_{2,SL}$. We also introduce dimensionless variables $H = \frac{h}{R}$, $\mu = \frac{\mu_2}{\mu_1}$ and $U = \frac{U_{1,SL}}{U_{2,SL}}$. With these changes, the assumption $u_1 - u_2 > 0$ can now be given by $\left(1 - H^2\right) U > H^2$. This relation will be useful later in this section. After some rearranging, we now get

$$-\mu H^5 + \left(\theta \left(U + 2 + \frac{1}{U} \right) - \mu \right) H^4 - 2\theta(U+1)H^2 + \theta U = 0 \tag{4.15}$$

We can notice that this equation is more complicated than the hold-up equation we found in chapter 2, we can not find analytical solutions any more. But we can make some simplifications, and find the behaviour of the equation in the limit of very large or small μ.

If $\mu = 0$ the equation simplifies, and we find

$$\theta \left(U + 2 + \frac{1}{U} \right) H^4 - 2\theta(U+1)H^2 + \theta U = 0 \tag{4.16}$$

The solution to this equation is $H = \sqrt{\frac{U}{U+1}}$, while we from the exact solution in chapter 2 found $H = \sqrt{\frac{U}{U+2}}$. The simplifications we have introduced in the hydraulic model have thus changed the behaviour of the solution in the limit of very small μ. If we now go back to the assumption that $\left(1 - H^2\right) U > H^2$, we see that we can rewrite this as $H < \sqrt{\frac{U}{U+1}}$, thus, we have assumed that H is smaller than in the limit where μ is zero. $H > \sqrt{\frac{U}{U+1}}$ corresponds to solutions where the mean velocity in the annulus close to the wall is larger than the mean velocity in the central core. Such solutions are deemed to be unstable, as interfacial shear would tend to accelerate phase 1.

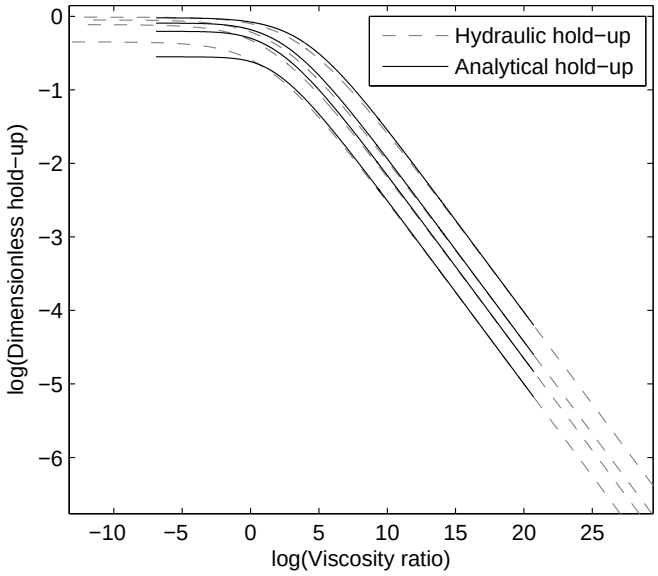

Figure 4.2: *Comparison of liquid hold-up as function of viscosity ratio for the exact analytical solution and the hydraulic solution. The analytical hold-up is shown with solid lines, and the hydraulic hold-up with dashed lines. The different pairs of solutions are, from top to bottom, for* $U = 50$*,* $U = 10$*,* $U = 4$ *and* $U = 1$*.*

When μ is very large, we expect H to be quite small. In that case, we can approximate equation (4.15) as

$$-\mu H^4 + \theta U = 0 \tag{4.17}$$

since the other terms are small. Rewriting, we find

$$H = \left(\frac{\theta U}{\mu}\right)^{\frac{1}{4}} \tag{4.18}$$

from which we see that $\theta = 1$ reproduces the behaviour of the exact equation in chapter 2 in the limit where μ is very large. In figure 4.2 the results found using the exact solution and the hydraulic solution for various values of U is compared, we see that apart from the discrepancy for small μ, the hydraulic solution is more or less identical to the exact solution.

In addition to finding approximate solutions for large and small μ, we can also use basic calculus to find some interesting information about the hold-up equation (4.15). We know that any equation of odd order has at least

one real solution, hence, this hold-up equation must have at least one real solution. The remaining four solutions are either all complex, two complex and two real, or all four real. The only physical solutions are obviously H in the interval $[0, 1]$, but it is not obvious whether the solution could be multi-valued in this interval. Some graphical experiments indicates that there are always at least three real solutions, and most often there is only one physically acceptable solution. But when U is very small, without μ being equally small, there is a possibility of five real solutions, and more than one physically acceptable solution have been observed. An example of this is shown in figure 4.3, where the value of the hold-up equation is plotted against dimensionless interface height in the relevant interval $H \in [0, 1]$ for different values of U and $\mu = 20$. The hold-up equation is fulfilled in the points where it becomes zero. For the lowest values for U, the equation actually tends to a double root as the only possible solution. Increasing U a little gives more solutions, there are two possible solutions for $U = 0.005$ and actually three for $U = 0.0028$. When U increases above 0.028 the possibility for multiple solutions in the relevant interval seems to disappear for this viscosity ratio. It also seems that the relation $H < \sqrt{\frac{U}{U+1}}$ is able to remove any extra solutions, thus, any extra solutions to the hold-up equation seems to be unstable solutions with $u_1 - u_2 < 0$. It could actually be questioned whether such solutions are realizable at all, but it is sufficient for us to know that such solutions are at least unstable. Since the hold-up equation will be solved numerically in the following, care must be taken to find the correct solution, as one in principle is not guaranteed that a numerical solution will converge to the correct solution.

4.2 A transient solution

As we saw in chapter 3, the solution can only be assumed to be stationary for a certain distance upstream from the front of the core of water. After this section of quasi-steady flow, the flow is unsteady, and a transient solution has to be found. In that case, one in principle has to solve the entire equation set (4.1)-(4.3). But if some of the terms in the momentum equations can be shown to be small, it would be possible to neglect them to simplify the system. The only terms that could potentially be neglected are the inertia terms $\frac{\partial}{\partial z}\left(c_k A_k \rho_k u_k^2\right)$ and the diffusion terms $2\frac{\partial}{\partial z}\left(A_k \mu_k \frac{\partial u_k}{\partial z}\right)$ for $k = \{1, 2\}$.

First, we compare the inertia term in the water phase with the interfacial shear. The inertia term $\frac{\partial}{\partial z}\left(c_1 A_1 \rho_1 u_1^2\right)$ can by dimensional argument be represented by $\frac{\rho_1 A_1 u_1^2}{L}$, where L is some length scale characteristic for the flow. The interfacial shear $\tau_I s_I = \frac{1}{8}\rho_1 \left(u_1 - u_2\right)|u_1 - u_2| f_I$ can by dimensional argument, again, be represented by $\frac{1}{8}\rho_1 u_1^2 \theta \frac{64}{Re_1} 2\pi h$. The ratio of the

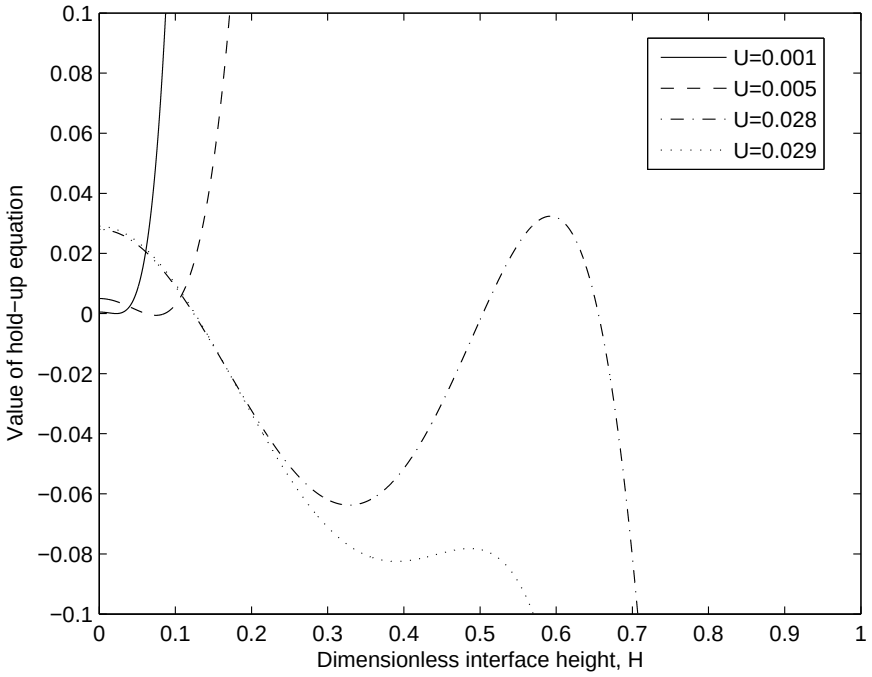

Figure 4.3: *Figure showing the possibility of multiple solutions of the hold-up equation for* $\mu = 20$

two terms is then given as

$$\frac{\frac{\rho_1 A_1 u_1^2}{L}}{\frac{1}{8}\rho_1 u_1^2 \theta \frac{64}{Re_1} 2\pi h} = \frac{\pi h^2 Re_1}{16\pi h L \theta} \tag{4.19}$$

If we assume that a typical dimension is the diameter of the core of water, $L = 2h$, we find the ratio to be $\frac{Re_1}{32\theta}$. Since the Reynolds number of the water phase is $\mathcal{O}\left(10^2\right)$, the ratio of inertia to interfacial shear is at least $\mathcal{O}\left(1\right)$, which means that inertia can not be neglected in the water phase.

Next, we compare the diffusion in water with the interfacial shear. By dimensional arguments we find $2\frac{\partial}{\partial z}\left(A_1\mu_1\frac{\partial u_1}{\partial z}\right) \sim 2\frac{A_1\mu_1 u_1}{L^2}$ for some characteristic dimension L. We then find the ratio between the two terms to be

$$\frac{2\frac{A_1\mu_1 u_1}{L^2}}{\frac{1}{8}\rho_1 u_1^2 \theta \frac{64}{Re_1} 2\pi h} = \frac{h}{8\theta L} \tag{4.20}$$

If we again assume that the typical dimension is the diameter of the core of water, we find that the ratio is $\frac{1}{16\theta}$, and since we in the steady solution found $\theta = 1$, the ratio is quite small. It would therefore be a reasonably good approximation to neglect the diffusion term in the water phase.

We can now repeat this procedure for the oil phase, and compare inertia and diffusion with wall shear. By the same dimensional argument inertia can be represented by $\frac{\rho_2 A_2 u_2^2}{L}$, where L is some length scale. Wall shear is given by $\tau_w s_w = \frac{1}{8}\rho_2 u_2^2 f_2 2\pi R = \frac{1}{4}\rho_2 u_2^2 \pi R \frac{32}{Re_2}$. The ratio is then given by

$$\frac{\frac{\rho_2 A_2 u_2^2}{L}}{\frac{1}{4}\rho_2 u_2^2 \pi R \frac{32}{Re_2}} = \frac{\left(R^2 - h^2\right) Re_2}{8LR} \tag{4.21}$$

If we assume the typical dimension to be equal to the thickness of the layer of oil, we can rewrite the ratio as $\frac{R^2-h^2}{R^2-Rh}\frac{Re_2}{8}$, which is approximately $\frac{Re_2}{4}$. In the oil phase, the mean velocity is $\mathcal{O}\left(10^{-3}\right)$, a length scale $\mathcal{O}\left(10^{-2}\right)$ and kinematic viscosity $\mathcal{O}\left(10^{-5}\right)$. From this we find $Re_2 \approx \mathcal{O}\left(1\right)$, which gives that the ratio between inertia and wall shear is $\mathcal{O}\left(10^{-1}\right)$, such that this term with reasonably good accuracy can be neglected.

The diffusion term can again be represented by $2\frac{A_2 \mu_2 u_2}{L^2}$ for some characteristic dimension L, and we find the ratio of diffusion to wall shear to be given by

$$\frac{2\frac{A_2 \mu_2 u_2}{L^2}}{\frac{1}{4}\rho_2 u_2^2 \pi R \frac{32}{Re_2}} = \frac{R^2 - h^2}{8LR} \tag{4.22}$$

Assuming again that the typical dimension L is equal to the thickness of the layer of oil, we can find the ratio to be $\mathcal{O}\left(10^{-1}\right)$, and thereby it should be possible to neglect the diffusion term as well.

With the simplifications we have found here, the momentum equations are now reduced to

$$\frac{\partial}{\partial t}\left(A_1 \rho_1 u_1\right) + \frac{\partial}{\partial z}\left(c_1 A_1 \rho_1 u_1^2\right) = -A_1 \frac{\partial p_{1I}}{\partial z} - \tau_I s_I \tag{4.23}$$

$$\frac{\partial}{\partial t}\left(A_2 \rho_2 u_2\right) = -A_2 \frac{\partial p_{2I}}{\partial z} - \tau_w s_w + \tau_I s_I \tag{4.24}$$

Although we have found that the diffusion terms are quite small, and thereby can be neglected, it is well known that diffusion terms tends to stabilize numerical solutions. If we at a later stage run into severe stability problems when solving the hydraulic equations numerically, it would possibly become necessary to include the diffusion terms after all.

If we take the derivative of the jump condition for pressure with respect to z, we can find the relation

$$\frac{\partial p_{1I}}{\partial z} - \frac{\partial p_{2I}}{\partial z} = 2\sigma \frac{\partial \mathcal{C}}{\partial z} \tag{4.25}$$

Using this relation, the momentum equations can be combined to eliminate the pressure. In addition, since the fluids are assumed to be incompressible, the density is a constant. From this, we can find the system

$$A_1 \rho_2 \frac{\partial}{\partial t}\left(A_2 u_2\right) - A_2 \rho_1 \frac{\partial}{\partial t}\left(A_1 u_1\right) - A_2 \rho_1 \frac{\partial}{\partial z}\left(c_1 A_1 u_1^2\right)$$

$$= 2\sigma A_1 A_2 \frac{\partial \mathcal{C}}{\partial z} + \tau_I s_I (A_1 + A_2) - \tau_w s_w A_1 \quad (4.26)$$

$$\frac{\partial A_1}{\partial t} + \frac{\partial}{\partial z}(A_1 u_1) = 0 \quad (4.27)$$

$$\frac{\partial A_2}{\partial t} + \frac{\partial}{\partial z}(A_2 u_2) = 0 \quad (4.28)$$

We now have three equations and four unknowns, u_1, u_2, A_1 and A_2. Obviously, we need to add one constraint. We know that $A_1 + A_2 = A$, where A is the entire cross sectional area of the pipe. Introducing this, we can reduce the number of unknowns to three, but to simplify notation we retain A_2 in the equations.

If we now add equations (4.27) and (4.28) and use that $A_2 = A - A_1$, we can find the equation

$$\frac{\partial}{\partial z}(A_1 u_1) + \frac{\partial}{\partial z}(A_2 u_2) = 0 \quad (4.29)$$

Integrating this equation, we find

$$A_1 u_1 + A_2 u_2 = D \quad (4.30)$$

where D is some constant. Mass conservation, and the fact that the fluids are incompressible, gives that this constant is equal to Q, the total volume flow in the pipe. Rearranging a bit, we can then find

$$u_2 = \frac{Q - A_1 u_1}{A_2} \quad (4.31)$$

Inserting this relation in equation (4.28), we find a result that is equal to equation (4.27). Hence, using this relation for u_2 we remove one equation and one unknown from the system. The final system for us to solve, then, is

$$(A_1\rho_2 + A_2\rho_1)\frac{\partial}{\partial t}(A_1 u_1) + A_2\rho_1 \frac{\partial}{\partial z}\left(c_1 A_1 (u_1)^2\right)$$
$$= -2\sigma A_1 A_2 \frac{\partial \mathcal{C}}{\partial z} + \tau_w s_w A_1 - \tau_I s_I A \quad (4.32)$$

$$\frac{\partial A_1}{\partial t} + \frac{\partial}{\partial z}(A_1 u_1) = 0 \quad (4.33)$$

To simplify notation, we now introduce $M = (A_1\rho_2 + A_2\rho_1)$ and the volume flow of phase 1, $Q_1 = A_1 u_1$, from which we find the system

$$M\frac{\partial Q_1}{\partial t} = -A_2\rho_1 \frac{\partial}{\partial z}\left(c_1 \frac{Q_1^2}{A_1}\right) - 2\sigma A_1 A_2 \frac{\partial \mathcal{C}}{\partial z}$$
$$+\tau_w s_w A_1 - \tau_I s_I A \quad (4.34)$$

$$\frac{\partial A_1}{\partial t} = -\frac{\partial Q_1}{\partial z} \quad (4.35)$$

These are the equations we will later solve numerically in chapter 5.

4.3 Linear stability of interfacial waves

To study the behaviour of waves on the interface, it is common to do a linear stability analysis, from which we will see if the interface is stable with respect to pertubations. For this purpose, it is convenient to write the system (4.34) and (4.35) on the form

$$\begin{aligned}
\left(A_1\rho_2 + A_2\rho_1\right)\frac{\partial}{\partial t}\left(A_1 u_1\right) &+ A_2\rho_1\frac{\partial}{\partial z}\left(c_1 A_1\left(u_1\right)^2\right) \\
= -2\sigma A_1 A_2\frac{\partial \mathcal{C}}{\partial z} &+ \tau_w s_w A_1 - \tau_I s_I A \qquad (4.36)\\
\frac{\partial A_1}{\partial t} + \frac{\partial}{\partial z}\left(A_1 u_1\right) &= 0 \qquad (4.37)
\end{aligned}$$

We now assume that these equations permit a steady state solution of the form

$$A_1 = \bar{A}_1, u_1 = \bar{u}_1, A_2 = \bar{A}_2 \text{ and } u_2 = \bar{u}_2 \qquad (4.38)$$

where barred quantities denote constants. The mass conservation equation (4.37) is obviously satisfied by any steady state solution. The momentum equation (4.36) is satisfied if the steady state solution is a solution to the hold-up equation (4.15). To study the behaviour of interfacial waves, we now introduce the following pertubations to the steady state:

$$A_1 = \bar{A}_1 + \widetilde{A}_1, u_1 = \bar{u}_1 + \tilde{u}_1, A_2 = \bar{A}_2 + \widetilde{A}_2 \text{ and } u_2 = \bar{u}_2 + \tilde{u}_2 \qquad (4.39)$$

If we now insert this solution into the conservation equations (4.36) and (4.37), and assume that the magnitude of the pertubations is small so that terms that are products of perturbed quantities can be neglected, we can find the system

$$\begin{aligned}
&\left(\bar{A}_1\rho_2 + \bar{A}_2\rho_1\right)\left(\bar{A}_1\frac{\partial \tilde{u}_1}{\partial t} + \bar{u}_1\frac{\partial \widetilde{A}_1}{\partial t}\right) \\
+ \;& \bar{A}_2\rho_1\left(2\bar{c}_1\bar{A}_1\bar{u}_1\frac{\partial \tilde{u}_1}{\partial z} + \bar{c}_1\left(\bar{u}_1\right)^2\frac{\partial \widetilde{A}_1}{\partial z} + \bar{A}_1\left(\bar{u}_1\right)^2\frac{\partial \tilde{c}_1}{\partial z}\right) \\
= \;& -2\sigma\bar{A}_1\bar{A}_2\frac{\partial \widetilde{\mathcal{C}}}{\partial z} \\
+ \;& \frac{8\pi R\mu_2\bar{u}_2\bar{A}_1}{R-\bar{h}}\left(\frac{\tilde{u}_2}{\bar{u}_2} + \frac{\widetilde{A}_1}{\bar{A}_1} + \frac{\tilde{h}}{R-\bar{h}}\right) \\
- \;& \frac{8\pi\mu_1 A\left(\bar{u}_1-\bar{u}_2\right)^2}{\bar{u}_1}\left(\frac{2\tilde{u}_1}{\bar{u}_1-\bar{u}_2} - \frac{2\tilde{u}_2}{\bar{u}_1-\bar{u}_2} - \frac{\tilde{u}_1}{\bar{u}_1}\right) \qquad (4.40)
\end{aligned}$$

$$\frac{\partial \widetilde{A}_1}{\partial t} + \bar{A}_1\frac{\partial \tilde{u}_1}{\partial z} + \bar{u}_1\frac{\partial \widetilde{A}_1}{\partial z} = 0 \qquad (4.41)$$

Here, we have introduced $\tilde{c}_1$ and $\tilde{h}$ representing the change in the profile parameter c_1 and interface height h corresponding to the pertubation in A_1, and $\widetilde{\mathcal{C}}$ which is the change in interface curvature due to the change in h.

Using the definition of c_1 (4.8), inserting $A_1 = \bar{A}_1 + \widetilde{A}_1$ and neglecting terms that are second order and higher in $\widetilde{A}_1$, we can find

$$\begin{aligned}\tilde{c}_1 &= \frac{\bar{c}_1\widetilde{A}_1}{\bar{A}_1}\left(\frac{\frac{2\mu^2\bar{A}_1^2}{3}+\mu\bar{A}_1\left(\bar{A}_2-\bar{A}_1\right)-2\bar{A}_1\bar{A}_2}{\frac{\mu^2\bar{A}_1^2}{3}+\mu\bar{A}_1\bar{A}_2+\bar{A}_2^2}-\frac{\frac{\mu^2\bar{A}_1^2}{2}+\mu\bar{A}_1\left(\bar{A}_2-\bar{A}_1\right)-2\bar{A}_1\bar{A}_2}{\left(\frac{\mu\bar{A}_1}{2}+\bar{A}_2\right)^2}\right)\\ &\equiv \frac{\bar{c}_1\widetilde{A}_1}{\bar{A}_1}\gamma \qquad (4.42)\end{aligned}$$

in which γ is the term inside the set of parentheses.

Since h is related to A_1 through the expression $h = \sqrt{\frac{A_1}{\pi}}$, we can, if we neglect terms that are second order and higher in $\widetilde{A}_1$ find $\tilde{h}$ to be given by

$$\tilde{h} = \frac{\bar{h}}{2\bar{A}_1}\tilde{A}_1 \qquad (4.43)$$

Inserting $h = \bar{h}+\tilde{h}$ in the expression for interface curvature (4.7), neglecting, again, terms that are second order and higher in $\tilde{h}$, and using equation (4.43) to eliminate $\tilde{h}$ we find

$$\frac{\partial\widetilde{\mathcal{C}}}{\partial z} = -\frac{1}{4\bar{h}\bar{A}_1}\frac{\partial\widetilde{A}_1}{\partial z}-\frac{\bar{h}}{4\bar{A}_1}\frac{\partial^3\widetilde{A}_1}{\partial z^3} \qquad (4.44)$$

It is now convenient, in addition, to eliminate $\tilde{u}_2$ from the momentum equation. Since $u_2 = \frac{Q-u_1A_1}{A_2}$, we can insert the perturbed quantities from (4.39) to find the expression

$$\tilde{u}_2 = -\bar{u}_2\left(\frac{\bar{A}_1\tilde{u}_1+\widetilde{A}_1\bar{u}_1}{Q-\bar{A}_1\bar{u}_1}-\frac{\widetilde{A}_1}{\bar{A}_2}\right) \qquad (4.45)$$

Inserting the expressions for $\tilde{c}_1$, $\tilde{h}$, $\frac{\partial\widetilde{\mathcal{C}}}{\partial z}$ and $\tilde{u}_2$ in the momentum equation and rearranging, we now find the system

$$\begin{aligned}&\left(\bar{A}_1\rho_2+\bar{A}_2\rho_1\right)\left(\bar{A}_1\frac{\partial\tilde{u}_1}{\partial t}+\bar{u}_1\frac{\partial\widetilde{A}_1}{\partial t}\right)\\ +\;&\bar{A}_2\rho_1\bar{c}_1\bar{u}_1\left(2\bar{A}_1\frac{\partial\tilde{u}_1}{\partial z}+\bar{u}_1\frac{\partial\widetilde{A}_1}{\partial z}+\bar{u}_1\gamma\frac{\partial\widetilde{A}_1}{\partial z}\right)\\ =\;&\frac{\sigma\bar{A}_2}{2}\left(\frac{1}{\bar{h}}\frac{\partial\widetilde{A}_1}{\partial z}+\bar{h}\frac{\partial^3\widetilde{A}_1}{\partial z^3}\right)\\ +\;&\frac{8\pi R\mu_2\bar{u}_2\bar{A}_1}{R-\bar{h}}\left(-\frac{1}{\bar{u}_2\bar{A}_2}\left(\bar{A}_1\tilde{u}_1+\widetilde{A}_1\bar{u}_1\right)+\frac{\widetilde{A}_1}{\bar{A}_2}+\frac{\widetilde{A}_1}{\bar{A}_1}+\frac{\bar{h}\widetilde{A}_1}{2\bar{A}_1\left(R-\bar{h}\right)}\right)\end{aligned}$$

$$- \quad \frac{8\pi\mu_1 A\left(\bar{u}_1-\bar{u}_2\right)}{\bar{u}_1}\left(2\tilde{u}_1+2\frac{\left(\bar{A}_1\tilde{u}_1+\widetilde{A}_1\bar{u}_1\right)}{\bar{A}_2}-\frac{2\bar{u}_2\widetilde{A}_1}{\bar{A}_2}-\frac{\left(\bar{u}_1-\bar{u}_2\right)\tilde{u}_1}{\bar{u}_1}\right) \tag{4.46}$$

$$\frac{\partial\widetilde{A}_1}{\partial t}+\bar{A}_1\frac{\partial\tilde{u}_1}{\partial z}+\bar{u}_1\frac{\partial\widetilde{A}_1}{\partial z}=0 \tag{4.47}$$

To further study the behaviour of the waves described by these equations, we insert the separate Fourier components of the pertubations by substituting $\widetilde{A}_1 = A_0 e^{i(kz-\omega t)}$ and $\tilde{u}_1 = u_0 e^{i(kz-\omega t)}$, where A_0 and u_0 are assumed to be constants. With these forms for $\widetilde{A}_1$ and $\tilde{u}_1$ we see that we can replace each occurrence of $\frac{\partial}{\partial t}$ with $-i\omega$, while each $\frac{\partial}{\partial z}$ can be replaced by ik. Using this, and cancelling the exponential part that appears in every term, we now find the system

$$\begin{aligned}
& -i\omega\left(\bar{A}_1\rho_2+\bar{A}_2\rho_1\right)\left(\bar{A}_1u_0+\bar{u}_1A_0\right)\\
+\quad & ik\bar{A}_2\rho_1\bar{c}_1\bar{u}_1\left(2\bar{A}_1u_0+\bar{u}_1A_0+\bar{u}_1\gamma A_0\right)\\
=\quad & \frac{\sigma\bar{A}_2}{2}\left(\frac{1}{\bar{h}}ikA_0-ik^3\bar{h}A_0\right)\\
+\quad & \frac{8\pi R\mu_2\bar{u}_2\bar{A}_1}{R-\bar{h}}\left(-\frac{1}{\bar{u}_2\bar{A}_2}\left(\bar{A}_1u_0+A_0\bar{u}_1\right)+\frac{A_0}{\bar{A}_2}+\frac{A_0}{\bar{A}_1}+\frac{\bar{h}A_0}{2\bar{A}_1\left(R-\bar{h}\right)}\right)\\
-\quad & \frac{8\pi\mu_1 A\left(\bar{u}_1-\bar{u}_2\right)}{\bar{u}_1}\left(2\frac{\left(\bar{A}_1u_0+A_0\bar{u}_1\right)}{\bar{A}_2}-\frac{2\bar{u}_2A_0}{\bar{A}_2}+\frac{\left(\bar{u}_1+\bar{u}_2\right)u_0}{\bar{u}_1}\right)
\end{aligned} \tag{4.48}$$

$$-i\omega A_0+ik\bar{A}_1u_0+ik\bar{u}_1A_0=0 \tag{4.49}$$

We can now solve equation (4.49) for u_0, which gives $u_0 = -\frac{k\bar{u}_1-\omega}{k\bar{A}_1}A_0$. Substituting this result for u_0 in equation (4.48) and cancelling the A_0 terms we find

$$\begin{aligned}
& -i\frac{\omega^2}{k}\left(\bar{A}_1\rho_2+\bar{A}_2\rho_1\right)\\
+\quad & ik\bar{A}_2\rho_1\bar{c}_1\bar{u}_1\left(\frac{2\omega}{k}+\bar{u}_1\left(\gamma-1\right)\right)\\
=\quad & \frac{\sigma\bar{A}_2}{2}\left(\frac{ik}{\bar{h}}-ik^3\bar{h}\right)\\
+\quad & \frac{8\pi R\mu_2\bar{u}_2\bar{A}_1}{R-\bar{h}}\left(-\frac{\omega}{k\bar{u}_2\bar{A}_2}+\frac{A}{\bar{A}_1\bar{A}_2}+\frac{\bar{h}}{2\bar{A}_1\left(R-\bar{h}\right)}\right)\\
-\quad & \frac{8\pi\mu_1 A\left(\bar{u}_1-\bar{u}_2\right)}{\bar{u}_1}\left(\frac{\omega}{k}\left(\frac{2}{\bar{A}_2}+\frac{\bar{u}_1+\bar{u}_2}{\bar{A}_1\bar{u}_1}\right)-\frac{2\bar{u}_2}{\bar{A}_2}-\frac{\bar{u}_1+\bar{u}_2}{\bar{A}_1}\right)
\end{aligned} \tag{4.50}$$

It is now convenient to write this equation on dimensionless form. For this purpose, we introduce the dimensionless interface height $H = \frac{\bar{h}}{R}$, from which we can find $\bar{A}_1 = AH^2$ and $\bar{A}_2 = A\left(1 - H^2\right)$. We also introduce the superficial velocities, which can be written $U_{1,SL} = \bar{u}_1 H^2$ and $U_{2,SL} = \bar{u}_2\left(1 - H^2\right)$, the ratio of superficial velocities $U = \frac{U_{1,SL}}{U_{2,SL}}$, the density ratio $\rho = \frac{\rho_2}{\rho_1}$ and the viscosity ratio $\mu = \frac{\mu_2}{\mu_1}$. Then we define the Weber number $We = \frac{\rho_1 U_{1,SL}^2 R}{\sigma}$, the Reynolds number $Re = \frac{\rho_1 U_{1,SL} R}{\mu_1}$ and $\Gamma = \gamma - 1$. If we now write the wavenumber k and ω on dimensionless form as $\hat{k} = kR$ and $\hat{\omega} = \frac{R\omega}{U_{2,SL}}$ and rearrange a bit, we can simplify the notation by introducing new variables as follows:

$$
\begin{aligned}
\mathbf{P} &= H^2(\rho - 1) + 1 \\
\mathbf{Q} &= 2U\bar{c}_1 \frac{1 - H^2}{H^2} \\
\mathbf{R} &= \frac{8U}{Re}\left(\frac{\mu H^2}{(1-H)(1-H^2)} + \frac{U^2 - (U+1)^2 H^4}{H^2 U^2 (1-H^2)^2}\right) \\
\mathbf{S} &= U^2 \frac{1 - H^2}{H}\left(\frac{\bar{c}_1 \Gamma}{H^3} - \frac{1}{2We}\right) \\
\mathbf{T} &= \frac{U^2}{2We} H(1 - H^2) \\
\mathbf{V} &= \frac{8U}{Re}\left[\frac{\mu}{(1-H)(1-H^2)}\left(\frac{1}{1-H^2} + \frac{H}{2(1-H)}\right)\right. \\
&+ \left.\frac{1}{(1-H^2)^2}\left(2 - \frac{1+H^2}{U(1-H^2)} + \frac{U}{H^4}\right)\right]
\end{aligned}
$$

We now have a dimensionless dispersion relation that can be written as a quadratic equation

$$
\hat{\omega}^2 \mathbf{P} + \hat{\omega}\left(i\mathbf{R} - \hat{k}\mathbf{Q}\right) - \hat{k}^2 \mathbf{S} - \hat{k}^4 \mathbf{T} - i\hat{k}\mathbf{V} = 0 \tag{4.51}
$$

We can now notice that if we multiply equation (4.51) by We, the terms $\mathbf{R}$ and $\mathbf{V}$ would depend on the capillary number, since we have $Ca = \frac{\mu We}{Re}$.

It will become obvious that the sign of the factor $\mathbf{R}$ is important in understanding the implications of this equation. $\mathbf{R}$ is in fact always positive, which can be shown using the inequality

$$
\mathbf{R} = \frac{8U}{Re}\left(\frac{\mu H^2}{(1-H)(1-H^2)} + \frac{U^2 - (U+1)^2 H^4}{H^2 U^2 (1-H^2)^2}\right) > 0 \tag{4.52}
$$

This inequality can be simplified to

$$
\mu H^4 + \frac{1}{1+H} > \left(\frac{U+1}{U}\right)^2 \frac{H^4}{1+H} \tag{4.53}
$$

From section 4.1 we know that $H < \sqrt{\frac{U}{U+1}}$. That means that our inequality is also fulfilled if

$$\mu H^4 + \frac{1}{1+H} > \left(\frac{U+1}{U}\right)^2 \left(\frac{U}{U+1}\right)^2 \frac{1}{1+H} \tag{4.54}$$

which immediately simplifies to

$$\mu H^4 > 0 \tag{4.55}$$

This is obviously always fulfilled, since both μ and H is by its definition positive, and thus $\mathbf{R}$ is always positive.

The solution to an equation on the form (4.51) is well known, and we find

$$\hat{\omega}_\pm = \frac{\hat{k}\mathbf{Q} - i\mathbf{R} \pm \left(-\mathbf{R}^2 + 2i\hat{k}\left(2\mathbf{PV} - \mathbf{QR}\right) + \hat{k}^2\left(\mathbf{Q}^2 + 4\mathbf{PS}\right) + 4\hat{k}^4\mathbf{PT}\right)^{\frac{1}{2}}}{2\mathbf{P}} \tag{4.56}$$

In principle, we must expect the solutions to this equation to have both real and imaginary parts. For a pertubation on the form $\alpha e^{i(kz-\omega t)}$, where α is some constant, the pertubation will be proportional to

$$e^{i(kz-\omega t)} = e^{i(kz-\mathrm{Re}(\omega)t)} e^{\mathrm{Im}(\omega)t} \tag{4.57}$$

where $\mathrm{Re}(\omega)$ and $\mathrm{Im}(\omega)$ denote the real and the imaginary part of ω, respectively. The role of $\mathrm{Re}(\omega)$ and $\mathrm{Im}(\omega)$ is now obvious, we can notice that $\frac{\mathrm{Re}(\omega)}{k}$ gives the wave speed of a pertubation with wave number k and $\mathrm{Im}(\omega)$ gives the growth rate of a pertubation. To have stable waves, we must obviously demand $\mathrm{Im}(\omega) < 0$. Since the scaling of ω and k does not introduce any sign change, the same must hold for $\hat{\omega}$.

It is now interesting to see if we can find simplified solutions when $\hat{k}$ is either very small or very large. Using a series expansion of the square root for small $\hat{k}$, which corresponds to long waves, we can find

$$\hat{\omega} \approx \frac{\hat{k}\mathbf{Q} - i\mathbf{R}}{2\mathbf{P}} \pm \frac{i\mathbf{R}}{2\mathbf{P}}\left(1 - i\hat{k}\frac{2\mathbf{PV} - \mathbf{QR}}{\mathbf{R}^2} + \mathcal{O}\left(\hat{k}^2\right)\right) \tag{4.58}$$

Neglecting terms that are $\mathcal{O}\left(\hat{k}^2\right)$ we can find two separate solutions:

$$\hat{\omega}_+ = \hat{k}\left(\frac{\mathbf{Q}}{\mathbf{P}} - \frac{\mathbf{V}}{\mathbf{R}}\right) \tag{4.59}$$

$$\hat{\omega}_- = \hat{k}\frac{\mathbf{V}}{\mathbf{R}} - \frac{i\mathbf{R}}{\mathbf{P}} \tag{4.60}$$

We can notice that the plus solution has zero growth rate in the limit of long waves, whereas the minus solution has negative growth rate, and

hence stable interfacial waves, if $\frac{\mathbf{R}}{\mathbf{P}} > 0$. The importance of the sign of $\mathbf{R}$ is now obvious, and since $\mathbf{P}$ and $\mathbf{R}$ are always positive, the relation is always fulfilled.

For short waves, we have $\hat{k} \gg 1$. It is now convenient to rewrite the dispersion equation as

$$\omega_{\pm} = \frac{\hat{k}\mathbf{Q} - i\mathbf{R}}{2\mathbf{P}} \pm \frac{\hat{k}^2}{2\mathbf{P}} \left(-\frac{\mathbf{R}^2}{\hat{k}^4} + \frac{2i\left(2\mathbf{PV} - \mathbf{QR}\right)}{\hat{k}^3} + \frac{\mathbf{Q}^2 + 4\mathbf{PS}}{\hat{k}^2} + 4\mathbf{PT} \right)^{\frac{1}{2}} \tag{4.61}$$

Assuming short waves and neglecting terms that are $\mathcal{O}\left(\hat{k}^{-2}\right)$, we can now approximate this equation as

$$\omega_{\pm} \approx \frac{\hat{k}\mathbf{Q} - i\mathbf{R}}{2\mathbf{P}} \pm \frac{\hat{k}^2}{2\mathbf{P}} \left(4\mathbf{PT}\right)^{\frac{1}{2}} = \frac{\hat{k}\mathbf{Q} - i\mathbf{R}}{2\mathbf{P}} \pm \hat{k}^2 \left(\frac{\mathbf{T}}{\mathbf{P}}\right)^{\frac{1}{2}} \tag{4.62}$$

We can notice that short waves are always stable, since it is easy to see that both $\mathbf{P}$ and $\mathbf{T}$ is always positive. In addition, both $\hat{\omega}_+$ and $\hat{\omega}_-$ seems to converge to the same growth rate in the limit of short waves.

A plot of wave speed versus wave number for various values of U is given in figure 4.4, where in addition the approximate behaviour for large and small $\hat{k}$ is given for $U = 16$. We can notice that our approximations fit well. We also see that each pair of plus and minus solutions seems to be symmetric about some line. This behaviour should be expected, since solutions to quadratic equations always come in complex conjugated pairs.

The growth rate of interfacial waves versus wave number for various values of U is presented in figure 4.5. The expected behaviour in the limits of small and large wave number is marked with asterisks. We can notice that the exact solution fits excellent with the approximate solutions. Another interesting observation is that for $U = 1$ the growth rate is always less than or equal to zero. Hence, the interface is stable. On closer inspection, one can find that this is valid for a quite small interval near $U = 1$. If the viscosity ratio μ is reduced, the interval with stable interface shrinks, and ultimately disappears entirely. For other combinations of U and μ, there seem to always be an interval with unstable wave numbers, and we should thus expect pertubations to grow in time for the majority of combinations of values for U, Re, ρ, μ and We.

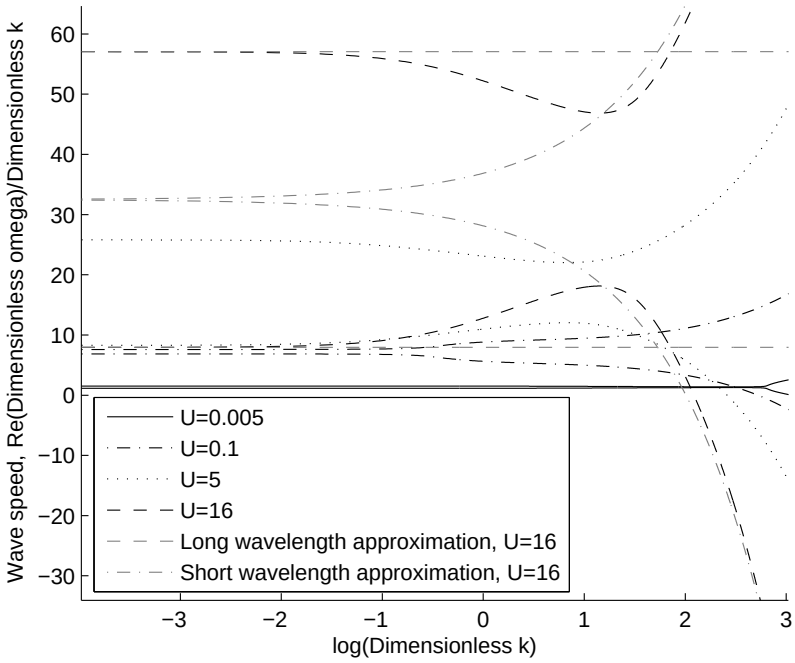

Figure 4.4: *Dimensionless wave speed of interfacial waves, equal to real part of $\hat{\omega}$ divided by $\hat{k}$. For each pair of curves with the same line style, the top curve and bottom curve corresponds to $\hat{\omega}_+$ and $\hat{\omega}_-$, respectively.*

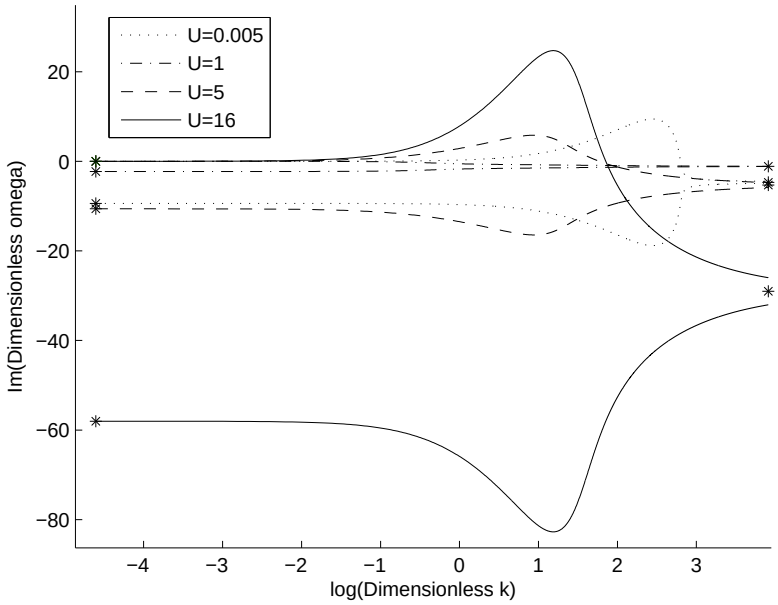

Figure 4.5: *Growth rate of interfacial waves, equal to imaginary part of omega. Asterisks mark expected growth rates in the limit of small or large wave number for different values of U. For each pair of curves with the same line style, the top curve and bottom curve corresponds to $\hat{\omega}_+$ and $\hat{\omega}_-$, respectively.*

Chapter 5

A numerical solution of the hydraulic model

The topic of this chapter is to develop a numerical solution of the problem defined by the hydraulic model in equations (4.34) and (4.35), namely

$$\begin{aligned} M\frac{\partial Q_1}{\partial t} &= -A_2\rho_1\frac{\partial}{\partial z}\left(c_1\frac{Q_1^2}{A_1}\right) - 2\sigma A_1 A_2\frac{\partial \mathcal{C}}{\partial z} \\ &+ \tau_w s_w A_1 - \tau_I s_I A \qquad (5.1) \\ \frac{\partial A_1}{\partial t} &= -\frac{\partial Q_1}{\partial z} \qquad (5.2) \end{aligned}$$

5.1 Discretizing the system

When discretizing the system it is convenient to start by defining the new variables

$$\begin{aligned} g_1 &= -A_2\rho_1\frac{\partial}{\partial z}\left(c_1\frac{Q_1^2}{A_1}\right) - 2\sigma A_1 A_2\frac{\partial \mathcal{C}}{\partial z} \\ &+ \tau_w s_w A_1 - \tau_I s_I A \\ g_2 &= -\frac{\partial Q_1}{\partial z} \end{aligned}$$

The entire system can then be given as the matrix-vector equation

$$\begin{bmatrix} M & 0 \\ 0 & 1 \end{bmatrix} \frac{\partial}{\partial t} \begin{bmatrix} Q_1 \\ A_1 \end{bmatrix} = \begin{bmatrix} g_1 \\ g_2 \end{bmatrix}$$

Defining

$$\mathbf{B} = \begin{bmatrix} M & 0 \\ 0 & 1 \end{bmatrix}, \mathbf{v} = \begin{bmatrix} Q_1 \\ A_1 \end{bmatrix}, \mathbf{g} = \begin{bmatrix} g_1 \\ g_2 \end{bmatrix}$$

the system can be written in the compact form

$$\frac{\partial \mathbf{v}}{\partial t} = \mathbf{B}^{-1}\mathbf{g} \equiv \hat{\mathbf{g}} \tag{5.3}$$

To discretize the system, we introduce the spatial points $i \in [0, n]$ and temporal points $l \in [0, m]$, and use the notation α_i^l for some quantity α which is a function of time and space at temporal point l and spatial point i. For flexibility, we utilize a Θ-rule in time, from which we can find the discretized system

$$\frac{\mathbf{v}_i^{l+1} - \mathbf{v}_i^l}{\Delta t} = \Theta \hat{\mathbf{g}}_i^{l+1} + (1 - \Theta)\, \hat{\mathbf{g}}_i^l \tag{5.4}$$

In this system, $\Theta = 0$ gives the standard explicit scheme, $\Theta = \frac{1}{2}$ gives the Crank-Nicholson-scheme, and $\Theta = 1$ gives the implicit scheme. Each scheme has its own advantages, the explicit scheme being the simplest and fastest to solve, but potensially with stability problems, the Crank-Nicholson-scheme giving second-order accurate solutions in time, and the implicit scheme offering much better stability, and in some cases being unconditionally stable, though giving a system that is much harder to solve. In the equations, we have introduced the time step length Δt, which is assumed to be constant, and equal to $\frac{T}{m}$, where T is the total flow time.

5.1.1 The explicit scheme

Setting $\Theta = 0$ in the general scheme, we can find the explicit scheme

$$\frac{\mathbf{v}_i^{l+1} - \mathbf{v}_i^l}{\Delta t} = \hat{\mathbf{g}}_i^l \tag{5.5}$$

which leads to the necessary explicit updates

$$\mathbf{v}_i^{l+1} = \mathbf{v}_i^l + \Delta t \hat{\mathbf{g}}_i^l \tag{5.6}$$

To simplify the final equations, we now introduce a new discretized variable for each term in the momentum equation. Earlier we defined M, to discretize it we introduce

$$M_i^l = A_{1,i}^l \rho_2 + \left(A - A_{1,i}^l\right) \rho_1 \tag{5.7}$$

For the surface tension term, we find a discretized expression for $\frac{\partial \mathcal{C}}{\partial z}$:

$$\begin{aligned} \left.\frac{\partial \mathcal{C}}{\partial z}\right|_i^l &= \frac{1}{2h_{i+1}^l \sqrt{4\Delta z^2 + \left(h_{i+2}^l - h_i^l\right)^2}} - \frac{1}{2h_{i-1}^l \sqrt{4\Delta z^2 + \left(h_i^l - h_{i-2}^l\right)^2}} \\ &- 2\left(\frac{h_{i+2}^l - 2h_{i+1}^l + h_i^l}{\left(4\Delta z^2 + \left(h_{i+2}^l - h_i^l\right)^2\right)^{\frac{3}{2}}} - \frac{h_i^l - 2h_{i-1}^l + h_{i-2}^l}{\left(4\Delta z^2 + \left(h_i^l - h_{i-2}^l\right)^2\right)^{\frac{3}{2}}} \right) \end{aligned} \tag{5.8}$$

The advective term, given by $-A_2\rho_1\frac{\partial}{\partial z}\left(c_1\frac{Q_1^2}{A_1}\right)$, can be discretized using a second order upwind scheme, to minimize numerical diffusion:

$$F^l_{advection,i} = \frac{\rho_1\left(A - A^l_{1,i}\right)}{2\Delta z}\left(3c^l_{1,i}\frac{\left(Q^l_{1,i}\right)^2}{A^l_{1,i}} - 4c^l_{1,i-1}\frac{\left(Q^l_{1,i-1}\right)^2}{A^l_{1,i-1}} + c^l_{1,i-2}\frac{\left(Q^l_{1,i-2}\right)^2}{A^l_{1,i-2}}\right) \tag{5.9}$$

The wall shear, which is given by $\tau_w s_w A_1$, can be discretized by

$$F^l_{wall\ shear,i} = \frac{8\pi R\mu_2 A^l_{1,i}u^l_{2,i}}{R - h^l_i} \tag{5.10}$$

and interfacial shear, which is given by $\tau_I s_I A$, can be written in the discretized version as

$$F^l_{interface,i} = \frac{8\pi\mu_1 A}{u^l_{1,i}}\left(u^l_{1,i} - u^l_{2,i}\right)\left|u^l_{1,i} - u^l_{2,i}\right| \tag{5.11}$$

In these definitions, we have introduced the cell length Δz, which is assumed to be a constant equal to $\frac{L}{n}$, where L is the length of the pipe. We have also used the expressions for shear stresses introduced in section 4. In addition, we have used the variables u_1, u_2 and h in the equations. These variables are not primary unknowns, u_1 is by definition equal to $\frac{Q_1}{A_1}$, u_2 can be found using equation (4.31) once we know A_1 and u_1, and h is given by $h = \sqrt{\frac{A_1}{\pi}}$. Using these relations, u_1, u_2 and h could be eliminated from the equations, but since all the terms are needed more than once, it is more effective to calculate the values once, and then use the computed value in the equations. The final equations is, then

$$A^{l+1}_{1,i} = A^l_{1,i} - \frac{\Delta t}{2\Delta z}\left(3Q^l_{1,i} - 4Q^l_{1,i-1} + Q^l_{1,i-2}\right) \tag{5.12}$$

$$\begin{aligned} Q^{l+1}_{1,i} &= Q^l_{1,i} \\ &+ \frac{\Delta t}{M^l_i}\Bigg[F^l_{wall\ shear,i} - F^l_{interface,i} \\ &- F^l_{advection,i} - 2\sigma A^l_{1,i}\left(A - A^l_{1,i}\right)\left.\frac{\partial\mathcal{C}}{\partial z}\right|^l_i\Bigg] \end{aligned} \tag{5.13}$$

We then need to define the correct boundary conditions. For the inflow at $z = 0$ it is obvious to choose a Dirichlet condition, and define $A^l_{1,0} = \alpha$ and $Q^l_{1,0} = \beta$ for all l, where α and β are constants describing the cross sectional area occupied by phase 1 and the volume flow of phase 1 at the inlet. α and β could be allowed to be functions of time, without introducing new problems, as long as some explicit function of time is given. For the outflow at $z = L$, it is reasonable to choose a Neumann condition, and define

$\frac{\partial A_1}{\partial z}|_{z=L} = 0$ and $\frac{\partial Q_1}{\partial z}|_{z=L} = 0$. If we start with the condition for A_1, we see that we can discretize the condition as $\frac{\partial A_1}{\partial z}|_{z=L} \approx \frac{1}{\Delta z}\left(A_{1,n}^{l+1} - A_{1,n-1}^{l+1}\right) = 0$, which leads to

$$A_{1,n}^{l+1} = A_{1,n-1}^{l+1} \tag{5.14}$$

Now we turn to the condition for Q_1. The condition can be discretized $\frac{\partial Q_1}{\partial z}|_{z=L} \approx \frac{1}{\Delta z}\left(Q_{1,n}^{l+1} - Q_{1,n-1}^{l+1}\right) = 0$,and it gives

$$Q_{1,n}^{l+1} = Q_{1,n-1}^{l+1} \tag{5.15}$$

In the expression for surface curvature, we see that we need information about the interface heights h_{-1}^l and h_{n+1}^l, which are outside our domain. It is reasonable to assume no gradients in interface height at both inlet and outflow, and thereby we can find $h_{-1}^l = h_0^l$ and $h_{n+1}^l = h_n^l$.

In addition, some initial condition must be chosen. This, then, completes the explicit model.

5.1.2 The implicit scheme

In the implicit scheme, we set $\Theta = 1$ in the general scheme. For this purpose, it is convenient to reintroduce $A_1 u_1$ instead of Q_1, and to simplify the equations a bit, we use first order upwind discretization of the advective term. We then find

$$\begin{aligned}
&\frac{A_{1,i}^{l+1}\rho_2 + \left(A - A_{1,i}^{l+1}\right)\rho_1}{\Delta t}\left(A_{1,i}^{l+1}u_{1,i}^{l+1} - A_{1,i}^{l}u_{1,i}^{l}\right) \\
+ \;& \frac{\rho_1}{2\Delta z}\left[\left(A - A_{1,i}^{l+1}\right)\left(c_{1,i+1}^{l+1}A_{1,i+1}^{l+1}\left(u_{1,i+1}^{l+1}\right)^2 - c_{1,i-1}^{l+1}A_{1,i-1}^{l+1}\left(u_{1,i-1}^{l+1}\right)^2\right)\right] \\
= \;& -2\sigma A_{1,i}^{l+1}\left(A - A_{1,i}^{l+1}\right)\left.\frac{\partial \mathcal{C}}{\partial z}\right|_i^{l+1} + \left[\tau_w s_w A_1 - \tau_I s_I A\right]_i^{l+1}
\end{aligned} \tag{5.16}$$

$$\frac{A_{1,i}^{l+1} - A_{1,i}^{l}}{\Delta t} + \frac{1}{2\Delta z}\left(A_{1,i+1}^{l+1}u_{1,i+1}^{l+1} - A_{1,i-1}^{l+1}u_{1,i-1}^{l+1}\right) = 0 \tag{5.17}$$

The curvature term, wall shear stress and interfacial shear stress can be written on discretized form in the same way as in equations (5.8), (5.10) and (5.11), respectively, but evaluated at time step $l+1$. Rearranging a bit, we can write the equations

$$-\left(\frac{\Delta t}{2\Delta z}u_{1,i-1}^{l+1}\right)A_{1,i-1}^{l+1} + A_{1,i}^{l+1} + \left(\frac{\Delta t}{2\Delta z}u_{1,i+1}^{l+1}\right)A_{1,i+1}^{l+1} = A_{1,i}^{l} \tag{5.18}$$

$$-\frac{\rho_1\Delta t}{2\Delta z}\left(\left(A - A_{1,i}^{l+1}\right)c_{1,i-1}^{l+1}A_{1,i-1}^{l+1}u_{1,i-1}^{l+1}\right)u_{1,i-1}^{l+1}$$

$$
\begin{aligned}
&+ \left(\rho_2\left(A_{1,i}^{l+1}\right)^2 + \rho_1\left(A - A_{1,i}^{l+1}\right)A_{1,i}^{l+1}\right.\\
&\quad \left. + \frac{\Delta t}{u_{1,i}^{l+1}}\left(2\sigma A_{1,i}^{l+1}\left(A - A_{1,i}^{l+1}\right)\left.\frac{\partial \mathcal{C}}{\partial z}\right|_i^{l+1} - \left[F_{wall\ shear} - F_{interface}\right]_i^{l+1}\right)\right)u_{1,i}^{l+1}\\
&+ \frac{\rho_1 \Delta t}{2\Delta z}\left(\left(A - A_{1,i}^{l+1}\right)c_{1,i+1}^{l+1}A_{1,i+1}^{l+1}u_{1,i+1}^{l+1}\right)u_{1,i+1}^{l+1}\\
&= \left(\rho_1\left(A - A_{1,i}^{l+1}\right) + \rho_2 A_{1,i}^{l+1}\right)A_{1,i}^{l}u_{1,i}^{l} \qquad (5.19)
\end{aligned}
$$

We can notice that this is a nonlinear system of two equations for two unknowns. This type of system needs to be solved by iterative methods. It is tempting to try the method of successive substitutions, since this method is easier than the more robust Newton-Rhapson's method. The concept of the successive substitution model is to make an initial guess to what $A_{1,i}^{l+1}$ and $u_{1,i}^{l+1}$ is, use this value to remove the nonlinearities in the system, and then solve the now linear system to find new values for $A_{1,i}^{l+1}$ and $u_{1,i}^{l+1}$. This procedure is then repeated until the solution has converged to within some convergence criteria. We now introduce the notation $A_{1,i}^{l+1,k}$ and $u_{1,i}^{l+1,k}$ for the solution at iteration k for time step $l+1$. The system can then be written

$$
\begin{aligned}
&- \left(\frac{\Delta t}{2\Delta z}u_{1,i-1}^{l+1,k}\right)A_{1,i-1}^{l+1,k+1}\\
&+ A_{1,i}^{l+1,k+1} + \left(\frac{\Delta t}{2\Delta z}u_{1,i+1}^{l+1,k}\right)A_{1,i+1}^{l+1,k+1} = A_{1,i}^{l} \qquad (5.20)
\end{aligned}
$$

$$
\begin{aligned}
&- \frac{\rho_1 \Delta t}{2\Delta z}\left(\left(A - A_{1,i}^{l+1,k+1}\right)c_{1,i-1}^{l+1,k+1}A_{1,i-1}^{l+1,k+1}u_{1,i-1}^{l+1,k}\right)u_{1,i-1}^{l+1,k+1}\\
&+ \left(\rho_2\left(A_{1,i}^{l+1,k+1}\right)^2 + \rho_1\left(A - A_{1,i}^{l+1,k+1}\right)A_{1,i}^{l+1,k+1}\right.\\
&\quad + \frac{\Delta t}{u_{1,i}^{l+1,k}}\left(2\sigma A_{1,i}^{l+1,k+1}\left(A - A_{1,i}^{l+1,k+1}\right)\left.\frac{\partial \mathcal{C}}{\partial z}\right|_i^{l+1,k+1}\right.\\
&\quad \left.\left. - \left[F_{wall\ shear} - F_{interface}\right]_i^{l+1,k}\right)\right)u_{1,i}^{l+1,k+1}\\
&+ \frac{\rho_1 \Delta t}{2\Delta z}\left(\left(A - A_{1,i}^{l+1,k+1}\right)c_{1,i+1}^{l+1,k+1}A_{1,i+1}^{l+1,k+1}u_{1,i+1}^{l+1,k}\right)u_{1,i+1}^{l+1,k+1}\\
&= \left(\rho_1\left(A - A_{1,i}^{l+1,k+1}\right) + \rho_2 A_{1,i}^{l+1,k+1}\right)A_{1,i}^{l}u_{1,i}^{l} \qquad (5.21)
\end{aligned}
$$

This is now a linear system that can be solved in two steps, first, we find $A_{1,i}^{l+1,k+1}$ from the linear system defined by equation (5.20), then we can insert the values for $A_{1,i}^{l+1,k+1}$ in the linear system defined by equation (5.21) and find $u_{1,i}^{l+1,k+1}$. We can notice that the terms c_1 and $\frac{\partial \mathcal{C}}{\partial z}$ is determined

by A_1 only, so no nonlinearities are introduced by using these values from iteration $k+1$ in the momentum equation. The same reasoning for boundary conditions as in section 5.1.1 is still valid, we have $A^l_{1,0} = \alpha$, $u^l_{1,0} = \beta$, $A^{l+1}_{1,n} = A^{l+1}_{1,n-1}$ and $u^{l+1}_{1,n} = u^{l+1}_{1,n-1}$

We now have everything we need to set up the system. For A_1, we define the matrix $\mathbf{B}$

$$\mathbf{B} = \begin{bmatrix} 1 & 0 & \dots & \dots & \dots & 0 & 0 \\ -\frac{\Delta t}{2\Delta z}u^{l+1,k}_{1,0} & 1 & \frac{\Delta t}{2\Delta z}u^{l+1,k}_{1,2} & 0 & \dots & & \vdots \\ 0 & & \ddots & & & & \vdots \\ \vdots & & & \ddots & & & \vdots \\ & & 0 & -\frac{\Delta t}{2\Delta z}u^{l+1,k}_{1,i-1} & 1 & \frac{\Delta t}{2\Delta z}u^{l+1,k}_{1,i+1} & 0 \\ & & & & & \ddots & \vdots \\ 0 & \dots & & & 0 & -1 & 1 \end{bmatrix}$$

And the system is then, simply

$$\mathbf{B}\begin{bmatrix} A^{l+1,k+1}_{1,0} \\ A^{l+1,k+1}_{1,1} \\ \vdots \\ A^{l+1,k+1}_{1,i} \\ \vdots \\ A^{l+1,k+1}_{1,n-1} \\ A^{l+1,k+1}_{1,n} \end{bmatrix} = \begin{bmatrix} \alpha \\ A^l_{1,1} \\ \vdots \\ A^l_{1,i} \\ \vdots \\ A^l_{1,n-1} \\ 0 \end{bmatrix}$$

To set up the system for u_1, it is useful to simplify notation by defining the following variables:

$$f^{l,k}_i = -\frac{\rho_1 \Delta t}{2\Delta z}\left(\left(A - A^{l+1,k+1}_{1,i+1}\right)c^{l+1,k+1}_{1,i}A^{l+1,k+1}_{1,i}u^{l+1,k}_{1,i}\right) \quad (5.22)$$

$$\begin{aligned} g^{l,k}_i = &\left(\rho_2\left(A^{l+1,k+1}_{1,i}\right)^2 + \rho_1\left(A - A^{l+1,k+1}_{1,i}\right)A^{l+1,k+1}_{1,i}\right. \\ &+\frac{\Delta t}{u^{l+1,k}_{1,i}}\left(2\sigma A^{l+1,k+1}_{1,i}\left(A - A^{l+1,k+1}_{1,i}\right)\frac{\partial \mathcal{C}}{\partial z}\Big|^{l+1,k+1}_i\right. \\ &\left.\left.-\left[F_{wall\ shear} - F_{interface}\right]^{l+1,k}_i\right)\right) \end{aligned} \quad (5.23)$$

$$h^{l,k}_i = \frac{\rho_1 \Delta t}{2\Delta z}\left(\left(A - A^{l+1,k+1}_{1,i-1}\right)c^{l+1,k+1}_{1,i}A^{l+1,k+1}_{1,i}u^{l+1,k}_{1,i}\right) \quad (5.24)$$

$$b^{l,k}_i = \left(\rho_1\left(A - A^{l+1,k+1}_{1,i}\right) + \rho_2 A^{l+1,k+1}_{1,i}\right)A^l_{1,i} \quad (5.25)$$

The system for u_1 now becomes

$$\begin{bmatrix} 1 & 0 & \dots & \dots & \dots & 0 & 0 \\ f_0^{l,k} & g_1^{l,k} & h_2^{l,k} & 0 & \dots & & \vdots \\ 0 & & \ddots & & & & \vdots \\ \vdots & & & \ddots & & & \vdots \\ & & 0 & f_{i-1}^{l,k} & g_i^{l,k} & h_{i+1}^{l,k} & 0 \\ & & & & & \ddots & \vdots \\ 0 & \dots & & & 0 & -1 & 1 \end{bmatrix} \begin{bmatrix} u_{1,0}^{l+1,k+1} \\ u_{1,1}^{l+1,k+1} \\ \vdots \\ u_{1,i}^{l+1,k+1} \\ \vdots \\ u_{1,n-1}^{l+1,k+1} \\ u_{1,n}^{l+1,k+1} \end{bmatrix} = \begin{bmatrix} \beta \\ b_1^{l,k} \\ \vdots \\ b_i^{l,k} \\ \vdots \\ b_{n-1}^{l,k} \\ 0 \end{bmatrix}$$

5.2 Implementation and testing

A numerical implementation of the explicit model from section 5.1.1 can be summarized in the pseudocode given in table (5.1).

```
for i in [0,n]
    Set initial condition for A1[i] and Q1[i]
while time<total time
    for i in [1,n-1]
        Compute Q1[i] from momentum equation
        Compute A1[i] from mass conservation equation
    Set boundary conditions for A1 and Q1
Print result to file
```

Table 5.1: *Pseudocode for solving the explicit version of the hydraulic equations.*

The model is implemented using the programming language C++. The implementation is given in appendix A, with details on how to use the program in appendix A.1.

It is now time to verify that the implementation actually works as it is supposed to. In the following tests, we assume that fluid properties are as introduced in section 3.2, and in addition we set $\sigma = 0.00032$ N/m. We use a spatial step length $\Delta z = 0.01$ m, as this is close to the dimension of the smallest structures the hydraulic model is able to describe. First, it is interesting to see if the hold-up equation (4.15) is fulfilled. To do that, we set an initial condition with a volume flow that corresponds to $U = 15.57$ in equation (4.15), which is the same value for U as what was used to generate figure 3.14, where the analytical and numerical velocity profile is compared. Then we set an area occupied by phase 1 that corresponds to a liquid height which is not a solution to the hold-up equation. Boundary condition at $z = 0$ is set to a constant equal to the initial condition. As shown in figure 5.1, the

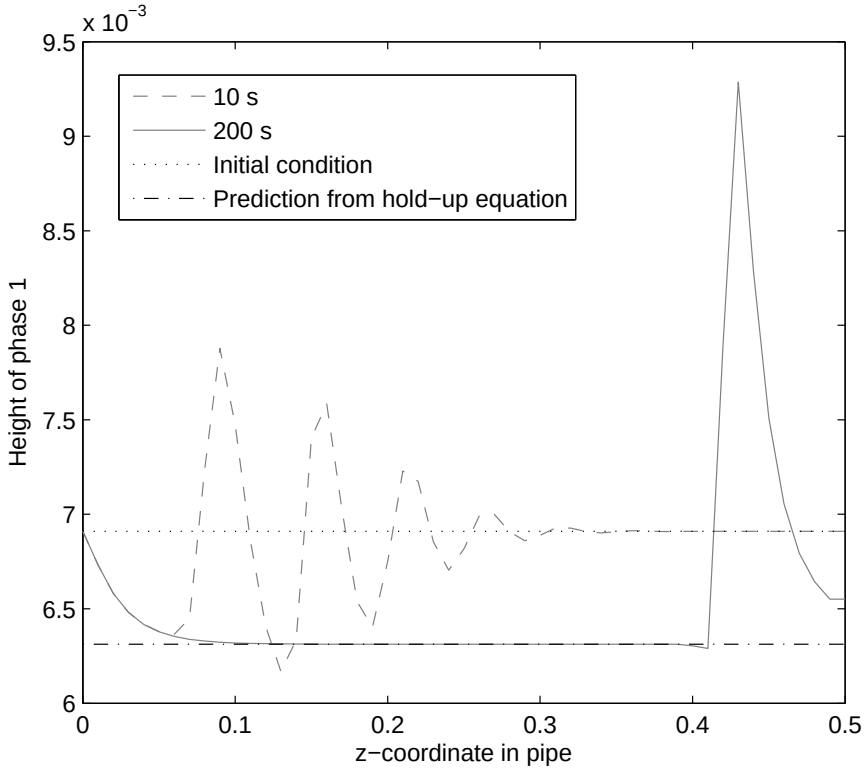

Figure 5.1: *Interface height predicted by the program compared with initial condition and liquid height predicted by hold-up equation, unstable case.*

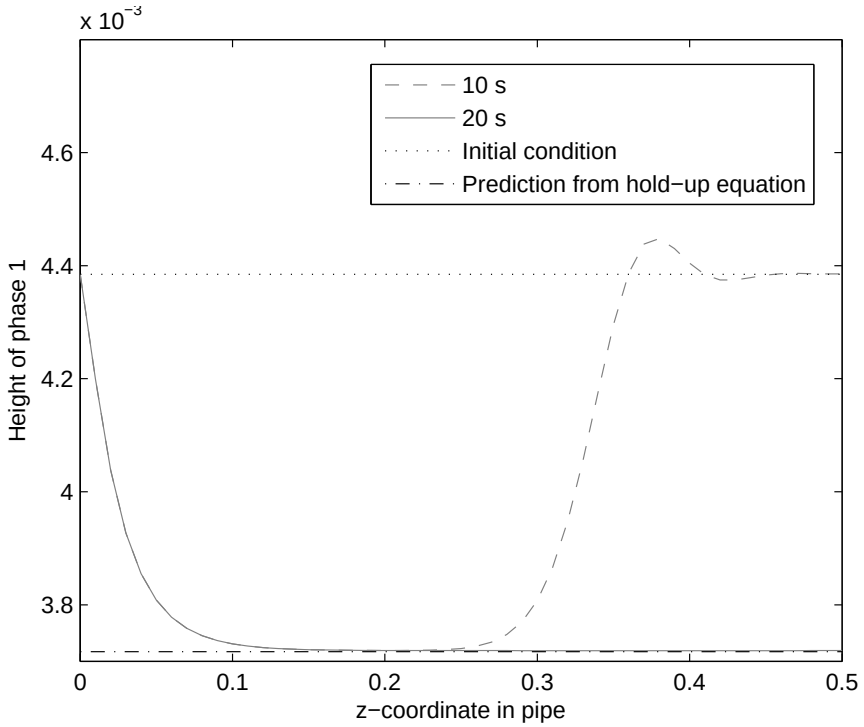

Figure 5.2: *Interface height predicted by the program compared with initial condition and liquid height predicted by hold-up equation, stable case.*

initial condition is not stable. Waves quickly appear, but we see that the interface relatively fast reaches the height predicted by the hold-up equation. The wave formation should not come as a surprise, we saw in section 4.3 that any pertubation of a stable interface would grow exponentially, except for a small interval with values for U close to one, where the interface was predicted to be unconditionally stable. It is now interesting to redo the same calculations as above, now with a volume flow that corresponds to $U = 1$, to see if the interface is actually found to be stable. We now get the result shown in figure 5.2. This time we can notice that the waves grow much slower, and that the interface reaches the stable height predicted by the hold-up equation much faster. There is still a small disturbance that is not dying out, which we in principle did not expect in this case. But we should keep in mind that this is possibly not the best way to test stability, since an entire interface located at the wrong height is by no means a small pertubation. A better way to test stability is to use a stable interface height as initial condition, and add some small pertubation. An example of this, with $U = 1$, is given in figure 5.3. As expected, the waves are decaying. Returning to the case $U = 15.57$, we now expect exponential growth of waves. As shown in figure 5.4, the waves are now growing to a stable height, where the waves have a

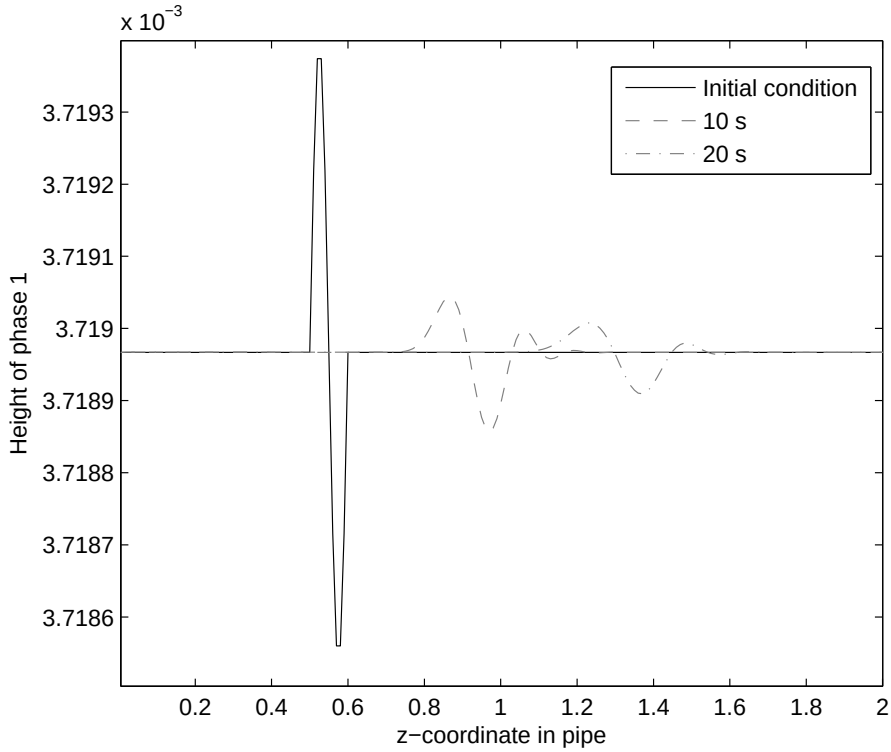

Figure 5.3: *Predicted wave shape at different time steps, with a flow that should have a stable interface. We see dacaying waves, as expected.*

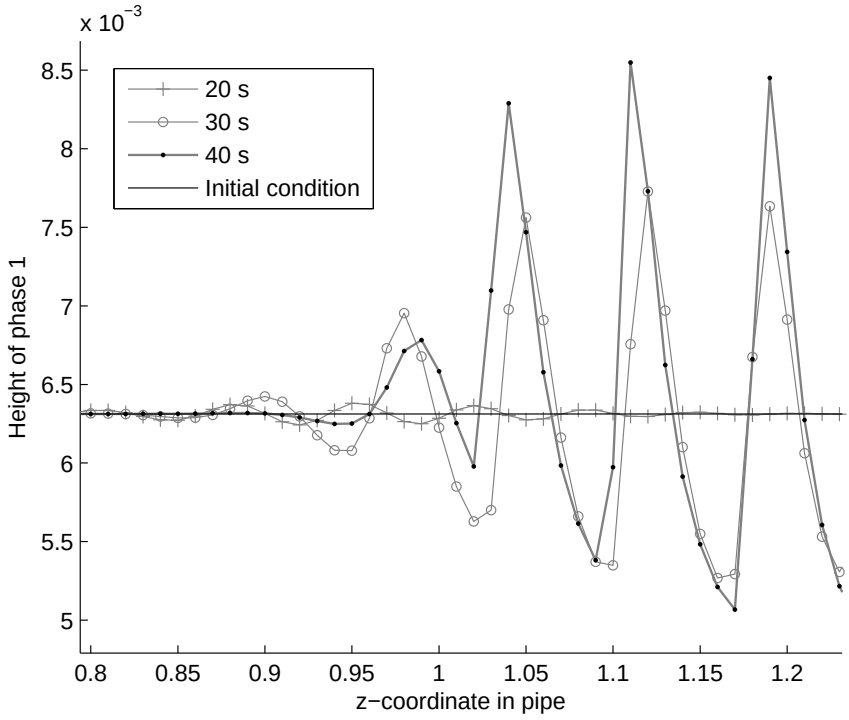

Figure 5.4: *Predicted wave shape at different time steps, with a flow that should have an unstable interface. The waves are growing to a stable height, where the character of the waves is no longer linear. The initial pertubation is so small that it is no longer possible to detect it, since the scale of the largest waves are much larger.*

highly nonlinear character.

The waves that form seem to have a typical wavelength λ of approximately $0.07 - 0.09$ m. If we assume $\lambda = 0.08$ m, we can solve the dispersion equation (4.56) numerically, and we find the growth rate to be given by $\mathrm{Im}(\omega) \approx 0.32$. This growth rate is plotted together with the actual growth rate found by solving the hydraulic system (5.12)-(5.13), we find the result given in figure 5.5. The two solutions fit quite well, but the numerical solution has a growth rate somewhat smaller than what is found from the dispersion relation. Two effects can cause this, first, nonlinear effects would tend to reduce growth, and second, even with second order upwind discretization, we must expect some numerical diffusion. From the real part of the dispersion relation we can find a prediction for the wave speed, for this flow we find $\frac{\mathrm{Re}(\omega)}{k} \approx 7.3 \cdot 10^{-3}$ m/s. From checking the position of the waves found by solving the hydraulic system at different time steps, we find the wave speed to be approximately 0.01 m/s, which is reasonably close to the

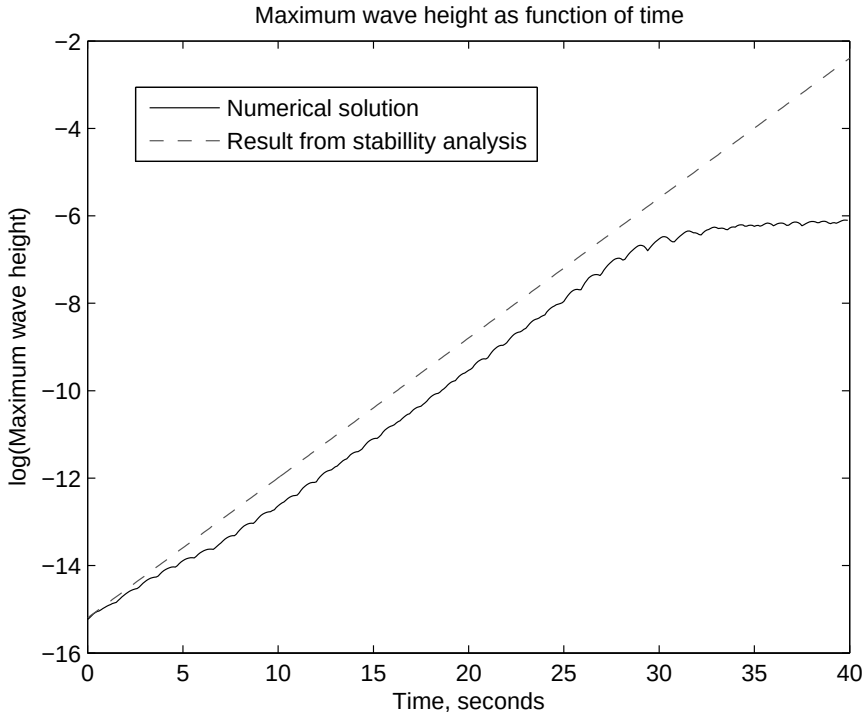

Figure 5.5: *Maximum wave height, numerical result and prediction by dispersion relation.*

prediction. But if we look at the plot of $\mathrm{Im}(\hat{\omega})$ versus $\hat{k}$ in figure 4.5, we find that we should expect maximum wave growth for a wave number close to 330 for $U = 16$. This corresponds to a wave length of approximately 2 cm, which is much shorter than the waves we actually observe. It seems limited grid resolution dampens waves shorter than seven times Δz.

The surface tension coefficient used in these tests is quite small. If we redo the tests with a higher σ, qualitatively the same results are found, but the tendency to form waves are much higher. In addition, the interface is not stable with $U = 1$ any more. This can be confirmed by the dispersion equation, which gives positive growth rate when the surface tension coefficient is increased, instead of the negative growth rate we found for low σ.

Chapter 6

The hydraulic model with a discontinuity

In the hydraulic model derived in chapter 4 we assumed that both phases were present at every cross section of the pipe. In the opposite case, with one of the phases occupying the entire cross section, the model would not work. For instance, the mean velocity of a phase that is not present is undefined, thus giving problems in computing the shear stresses. That means that the model is not able to solve the problem we solved using FLUENT in chapter 3, where we used water to displace oil from a pipe initially entirely filled with oil. In this chapter we try to adjust the hydraulic model so that it becomes able to handle this problem, with a discontinuous phase 1 penetrating into the pipe, as well.

6.1 Main challenges for the modelling

A drawing of the typical situation in the case of a finger of phase 1 penetrating into the pipe filled with phase 2 is given in figure 6.1. In the hydraulic model, the only information initially available is the cross sectional area occupied by phase 1 and the volume flow rate of phase 1 at the separate grid points, in the drawing denoted $[\ldots, s-2, s-1, s, s+1, \ldots]$. From here on, we define the point s to be the last grid point phase 1 has reached, with the front of phase 1 thus located between s and the next point, $s+1$.

The shape of the interface in the interval $[s, s+1]$ is unknown in the hydraulic model, and the shape given in figure 6.1 is only intended to illustrate a typical situation. Goldsmith and Mason[11] have described the front as an oblate spheroid where the ratio of the axis of revolution to diametrical axis depends on the speed of propagation of the front and the choice of fluids, but this observation can not be used as a predictive tool in our case.

To model this problem, we now introduce a circular disc with radius h_δ located a distance δ from s, as shown in the figure. We will in the following

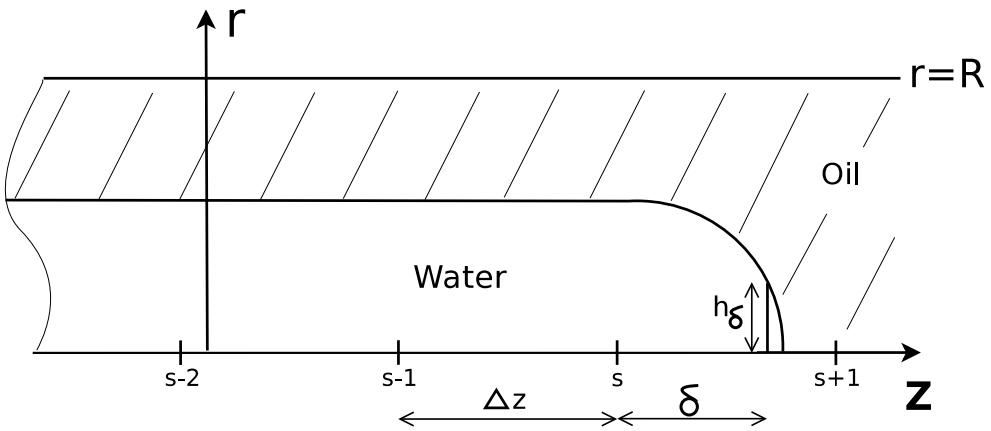

Figure 6.1: *Geometry for a discontinuous phase 1 in the hydralic model.*

use δ itself to denote the distance, and δ as a subscript to denote the value of some variable at the point $s+\delta$. The volume of phase 1 that is between δ and the actual front of phase 1 is from here on ignored, as it is quite small. The actual position of the interface in the interval $[s, \delta]$ is still unknown, but as it turns out, it will not become necessary with more detailed information regarding this interface. But somehow we need to determine the distance δ, to know when the discontinuity advances past the point $s+1$. In addition, when the discontinuity advances past $s+1$, we will need a means to compute values for A_1 and Q_1 in that point without having access to those values from the previous time step. It is not necessarily obvious how one should do that.

We now assume that the interface is continuous in the interval $[0, s]$, that is, the interface is continuous upstream from the discontinuity at δ. In that case, the standard explicit numerical solution from chapter 5 is applicable in the interval $[0, s-2]$. Downstream from the discontinuity, the solution is simply $A_1 = 0$ and $Q_1 = 0$. Thus, we have to treat $s-1$ and s in a special way. $s-1$ is quite simple, the only problem with using the standard explicit equations (5.12) and (5.13) is the way the curvature term is defined in equation (5.8), namely, for the point $s-1$ the equation would include the interface height at the point $s+1$, where the interface is not present at all. The same problem occur for the point s, here, equation (5.8) would include the points $s+1$ and $s+2$, which the interface has not reached. In addition, it seems reasonable to assume that there is some sort of drag on the front of the interface, and that this drag would tend to decrease the volume flow of phase 1 at point s. One could argue that if we superimpose a velocity $-U$ on the flow, where U is the actual penetration speed of the front of

phase 1, the system would have similarities with a stationary object, here the front of phase 1, positioned in a free stream. In that case it is obvious that there is some drag on the object, working in the negative z-direction. If the front had the shape of a perfect hemisphere, one could model the drag using tabulated values for the drag coefficient of a hemisphere in a free stream, but unfortunately the shape is not hemispherical, although quite close. It is even worse for this type of model that the confined space of a pipe can not be expected to behave as a free stream, and certainly not when the the typical dimension of the object is of the same order as the dimension of the pipe itself.

6.2 Modelling

To find new expressions for the curvature term at the point $s-1$ we first of all find a new expression for $\frac{\partial \mathcal{C}}{\partial z}$. Using the definition of $\mathcal{C}$ from equation (4.7) and calculating the derivative using basic calculus, we find the expression

$$\frac{\partial \mathcal{C}}{\partial z} = -\frac{h^2 \frac{\partial^3 h}{\partial z^3} + \frac{\partial h}{\partial z}\left(1 + \left(\frac{\partial h}{\partial z}\right)^2 + h\frac{\partial^2 h}{\partial z^2}\right)}{h^2\left(1+\left(\frac{\partial h}{\partial z}\right)^2\right)^{\frac{3}{2}}} + \frac{3\frac{\partial h}{\partial z}\left(\frac{\partial^2 h}{\partial z^2}\right)^2}{\left(1+\left(\frac{\partial h}{\partial z}\right)^2\right)^{\frac{5}{2}}} \tag{6.1}$$

We now have to define discretized values for $\frac{\partial h}{\partial z}$, $\frac{\partial^2 h}{\partial z^2}$ and $\frac{\partial^3 h}{\partial z^3}$ at $s-1$. The first two are easy, since we can use standard discretizations, and find

$$\left.\frac{\partial h}{\partial z}\right|_{s-1}^{l} = \frac{h_s^l - h_{s-2}^l}{2\Delta z} \tag{6.2}$$

$$\left.\frac{\partial^2 h}{\partial z^2}\right|_{s-1}^{l} = \frac{h_s^l - 2h_{s-1}^l + h_{s-2}^l}{\Delta z^2} \tag{6.3}$$

The third order term is a bit harder. First, we assume

$$\left.\frac{\partial^3 h}{\partial z^3}\right|_{s-1} = Ah_{s-3} + Bh_{s-2} + Ch_{s-1} + Dh_s \tag{6.4}$$

where A, B, C, D denote constants. Doing Taylor expansions of the interface height at each point, we find

$$\begin{aligned}
\left.\frac{\partial^3 h}{\partial z^3}\right|_{s-1} &= A\left(h_{s-1} - 2\Delta z\left.\frac{\partial h}{\partial z}\right|_{s-1} + 2\Delta z^2\left.\frac{\partial^2 h}{\partial z^2}\right|_{s-1} - \frac{4\Delta z^3}{3}\left.\frac{\partial^3 h}{\partial z^3}\right|_{s-1}\right) \\
&+ B\left(h_{s-1} - \Delta z\left.\frac{\partial h}{\partial z}\right|_{s-1} + \frac{\Delta z^2}{2}\left.\frac{\partial^2 h}{\partial z^2}\right|_{s-1} - \frac{\Delta z^3}{6}\left.\frac{\partial^3 h}{\partial z^3}\right|_{s-1}\right) \\
&+ Ch_{s-1} \\
&+ D\left(h_{s-1} + \Delta z\left.\frac{\partial h}{\partial z}\right|_{s-1} + \frac{\Delta z^2}{2}\left.\frac{\partial^2 h}{\partial z^2}\right|_{s-1} + \frac{\Delta z^3}{6}\left.\frac{\partial^3 h}{\partial z^3}\right|_{s-1}\right)
\end{aligned}$$

Rearranging a bit, we find

$$\begin{aligned}\left.\frac{\partial^3 h}{\partial z^3}\right|_{s-1} &= h_{s-1}\left(A+B+C+D\right)\\ &+ \left.\frac{\partial h}{\partial z}\right|_{s-1}\left(-2A\Delta z - B\Delta z + D\Delta z\right)\\ &+ \left.\frac{\partial^2 h}{\partial z^2}\right|_{s-1}\left(2A\Delta z^2 + B\frac{\Delta z^2}{2} + D\frac{\Delta z^2}{2}\right)\\ &+ \left.\frac{\partial^3 h}{\partial z^3}\right|_{s-1}\left(-A\frac{4\Delta z^3}{3} - B\frac{\Delta z^3}{6} + D\frac{\Delta z^3}{6}\right)\end{aligned}$$

We now have to demand $A+B+C+D=0$, $-2A\Delta z - B\Delta z + D\Delta z = 0$, $2A\Delta z^2 + B\frac{\Delta z^2}{2} + D\frac{\Delta z^2}{2} = 0$ and $-A\frac{4\Delta z^3}{3} - B\frac{\Delta z^3}{6} + D\frac{\Delta z^3}{6} = 1$, and we then have a system of four equations and four unknowns, which is easy to solve. If we insert the result in equation (6.4) we end up with the expression

$$\left.\frac{\partial^3 h}{\partial z^3}\right|_{s-1}^{l} = \frac{-h_{s-3}^l + 3h_{s-2}^l - 3h_{s-1}^l + h_s^l}{\Delta z^3} \tag{6.5}$$

We now have everything we need to solve the mass conservation equation and the momentum equation at point $s-1$. Then we turn to point s, and find expressions for the same derivatives, now using the interface heights h_{s-1}, h_s and h_δ for the first and second order derivative, and in addition h_{s-2} for the third order derivative. Using the exact same method as above, we can now find

$$\left.\frac{\partial h}{\partial z}\right|_{s}^{l} = \frac{-\delta^2 h_{s-1}^l + \left(\delta^2 - \Delta z^2\right)h_s^l + \Delta z^2 h_\delta}{\Delta z\delta\left(\Delta z+\delta\right)} \tag{6.6}$$

$$\left.\frac{\partial^2 h}{\partial z^2}\right|_{s}^{l} = \frac{2\delta h_{s-1}^l - 2\left(\Delta z+\delta\right)h_s^l + 2\Delta z h_\delta}{\Delta z\delta\left(\Delta z+\delta\right)} \tag{6.7}$$

$$\begin{aligned}\left.\frac{\partial^3 h}{\partial z^3}\right|_{s}^{l} &= -\frac{3}{\Delta z^2\left(2\Delta z+\delta\right)}h_{s-2}^l + \frac{6}{\Delta z^2\left(\Delta z+\delta\right)}h_{s-1}^l\\ &\quad -\frac{3}{\Delta z^2\delta}h_s^l + \frac{6}{\delta\left(\Delta z+\delta\right)\left(2\Delta z+\delta\right)}h_\delta\end{aligned} \tag{6.8}$$

One should notice that in the special case $\delta = \Delta z$ the expressions for the derivatives simplifies to the same form as the expressions for derivatives at point $s-1$. It is now obvious that we can not let δ become zero, as the derivatives would then become $\pm\infty$. That means that we have to let the front move some distance further than to the point $s+1$ before we can use the standard equations for that point. We therefore wait until $\delta \geq 1.5\Delta z$

before we use the standard equations for $s+1$. At the same time as we start using standard equations for $s+1$, we must reduce δ by Δz, since we have moved the last point we use the standard equations for the distance Δz forward.

Now we must solve the problem of determining δ. It is tempting to use the expressions for derivatives at point s in a Taylor expansion to express the shape of the front in the entire interval $[s, \delta]$, but unfortunately, the resulting expression proves not to be accurate enough to give a reasonable value for δ. Instead, we apply the consept of mass conservation at the point $s+\delta$. Equation (4.35) for this point gives

$$\left.\frac{\partial A_1}{\partial t}\right|_\delta^l = -\left.\frac{\partial Q_1}{\partial z}\right|_\delta^l \tag{6.9}$$

Since h_δ is a constant, we see that the left hand side of the above equation is identically zero. Using, again, Taylor expansions, we can express the right hand side in terms of $Q^l_{1,s-1}$, $Q^l_{1,s}$ and $Q^l_{1,\delta}$, we find

$$\frac{\Delta z + 2\delta}{\delta\left(\Delta z+\delta\right)}Q^l_{1,\delta} - \frac{\Delta z+\delta}{\Delta z\delta}Q^l_{1,s} + \frac{\delta}{\Delta z\left(\Delta z+\delta\right)}Q^l_{1,s-1} = 0 \tag{6.10}$$

Here, we can notice that this discretization is equal to the standard second order upwind discretization if $\delta = \Delta z$. Rearranging a bit, we find

$$Q^l_{1,\delta} = \frac{\delta\left(\Delta z+\delta\right)}{\Delta z+2\delta}\left(\frac{\Delta z+\delta}{\Delta z\delta}Q^l_{1,s} - \frac{\delta}{\Delta z\left(\Delta z+\delta\right)}Q^l_{1,s-1}\right) \tag{6.11}$$

If we now knew the area this volume flow flows through, it would be simple to find the velocity of the front, and thus determine δ. One choice is $A_{1,\delta} = \pi h_\delta^2$, but that would obviously be wrong, since we would then assume that the interface in the interval $[s, s+\delta]$ is stationary, and that the entire volume flow is forced out through the circular disc at the front, like a nozzle. This would significantly overestimate the velocity of the front. Another choice would be $A^l_{1,s}$. If we define a control volume bounded by $A^l_{1,s}$, $A_{1,\delta}$ and the entire interface in the interval $[s, s+\delta]$ we find that everything that flow into the control volume at s must increase the volume through pushing the entire interface and $A_{1,\delta}$ forward. The projection of $A_{1,\delta}$ and the interface in the z-direction is identical to $A^l_{1,s}$, and it could thus be justified to use $A^l_{1,s}$ as the appropriate area. Thus, we could compute the velocity of the front as

$$u^l_\delta = \frac{Q^l_{1,\delta}}{A^l_{1,s}} \tag{6.12}$$

But when we tried to justify using $A^l_{1,s}$ as the area, we assumed that the interface had a constant shape, and was only pushed forward. This is not

necessarily entirely correct, and it might become necessary to include a constant α, preferrably close to one, to correct for this error, with the final equation

$$u_\delta^l = \alpha \frac{Q_{1,\delta}^l}{A_{1,s}^l} \tag{6.13}$$

The value of α can be found from numerical experiments, the velocity u_δ must be adjusted so that no mass is lost at the front. If u_δ is set too small, we will see a net loss of phase 1 at the front, and in the opposite case, we will have the effect of a source of phase 1 close to the front.

With the definition of u_δ finished, we have all the information we need to find δ at each time step, and thus determine when we are supposed to start using the standard explicit equations (5.12) and (5.13) at the point after s as well. But since these equations include values from the previous time step, which we do not have the first time we try to find $A_{1,s+1}^l$ and $Q_{1,s+1}^l$, we will need to treat this point in a special way the first time. We now use a Taylor expansion to express the interface height h_{s+1}^l in terms of the derivatives $\frac{\partial h}{\partial z}$, $\frac{\partial^2 h}{\partial z^2}$ and $\frac{\partial^3 h}{\partial z^3}$ at s:

$$h_{s+1}^l = h_s^l + \Delta z \frac{\partial h}{\partial z}\bigg|_s^l + \frac{\Delta z^2}{2}\frac{\partial^2 h}{\partial z^2}\bigg|_s^l + \frac{\Delta z^3}{6}\frac{\partial^3 h}{\partial z^3}\bigg|_s^l \tag{6.14}$$

It is now obvious that $A_{1,s+1}^l = \pi \left(h_{s+1}^l\right)^2$. To find $Q_{1,s+1}^l$ we assume, again, that the front has constant shape, and insert $\delta = \Delta z$ in equation (6.11) to find the expression

$$Q_{1,s+1}^l = \frac{4Q_{1,s}^l - Q_{1,s-1}^l}{3} \tag{6.15}$$

Even though it is quite obvious that $A_{1,s+1}^l$ and $Q_{1,s+1}^l$ are not zero when $\delta \in [\Delta z, 1.5\Delta z]$, we set $A_{1,s+1}^l$ and $Q_{1,s+1}^l$ to zero anyway, since the values for $A_{1,s+1}^l$ and $Q_{1,s+1}^l$ will not have any impact on the flow until $\delta \geq 1.5\Delta z$.

If we now assume that drag on the front is insignificant, our model for a moving front is complete. But it will become clear that drag is actually essential in describing the flow, so we need to model this term in some way. As shown in section 3.4.3, the flow ahead of the front is quite complex, and we can not expect to be able to describe this complexity at all in a hydraulic model. Thus, we will have to try to model drag from the few details we actually know. We want to find an extra drag term to insert in the momentum equation for the last point, so that we end up with the equation

$$\begin{aligned} Q_{1,s}^{l+1} &= Q_{1,s}^l + \frac{\Delta t}{\tilde{A}_s^l}\Bigg[F_{wall\ shear,s}^l - F_{interface,s}^l \\ &- F_{advection,s}^l - 2\sigma A_{1,s}^l \left(A - A_{1,s}^l\right)\frac{\partial \mathcal{C}}{\partial z}\bigg|_s^l - F_{drag}^l\Bigg] \end{aligned} \tag{6.16}$$

Simple dimensional analysis shows that the term F_{drag} must have dimension Nm. It is obvious that there is a lot of ways to combine variables to reproduce the dimension Nm, and it is not necessarily easy to decide which combination is the best one. Trial and error, assisted by some physical insight, is our best choice. The standard drag equation reads $F = \frac{1}{2}\rho C_D u_{diff}^2 A_f$, where ρ is some characteristic density, u_{diff} is the velocity of the flow relative to the object in question, A_f is the frontal area of the object and C_D is the drag coefficient. This equation gives a force, N, and we must multiply by some relevant length scale L to find the dimension we want. If we introduce a Reynolds number $Re_{drag} = \frac{\rho u_{diff} L}{\mu}$, we can rewrite the equation as

$$F_{drag} = \frac{1}{2}\mu Re_{drag} C_D u_{diff} A_f \tag{6.17}$$

The dimensionless drag coefficient C_D is unknown, and probably some complex function of our four main dimensionless quantities, Reynolds number, Capillary number, viscosity ratio and density ratio. Re_{drag} can also be written as a function of the same dimensionless quantities, and we can thus simplify the equation by introducing the new dimensionless variable $B = \frac{1}{2} Re_{drag} C_D$. Further, it is assumed that μ_2 is the relevant viscosity, since the drag essentially is due to the front forcing away phase 2. It also seems a reasonable assumption that $A_{1,s}$ is the relevant area, since this area is the frontal area of phase 1, and the frontal area should be connected with the drag. We then find the equation

$$F_{drag} = B\mu_2 u_{diff} A_{1,s} \tag{6.18}$$

It now remains to define what the relevant velocity u_{diff} is. We need a velocity that can represent the difference between the velocity of the front and the velocity of the fluid downstream of the front. As we saw in figure 3.14, our analytical results from chapter 2 are quite close to the velocity profile found in FLUENT. Thus, it seems reasonable to find the mean velocity in phase 1 using results from chapter 2. Rearranging the hold-up equation (2.33) a bit, we can end up with the equation

$$\overline{u}_1 = \frac{Q\left(H^2(\mu - 2) + 2\right)}{A\left(H^4(\mu - 1) + 1\right)} \tag{6.19}$$

where H is, as before, dimensionless interface height, defined by $H = \frac{h}{R}$. Far downstream of the front, the flow is a fully developed Poiseuille flow. We now find the mean velocity $\overline{u}_2$ of this flow over the area $A_{1,s}$, since it is this area that excerts a force on the front. This mean velocity can be given by

$$\overline{u}_2 = \frac{Q}{A}\left(2 - H^2\right) \tag{6.20}$$

We then define u_{diff} as

$$u_{diff} = \overline{u}_1 - \overline{u}_2 \tag{6.21}$$

Reintroducing dimensional variables, we finally find the relevant velocity to be

$$u_{diff} = \frac{Q\left(A_{1,s}\left(A - A_{1,s}\right)^2\left(\mu - 1\right)\right)}{A^2\left(A_{1,s}^2\left(\mu - 1\right) + A^2\right)} \tag{6.22}$$

With this, we have finished a model of the drag:

$$F_{drag}^{l} = B\frac{Q\left(A_{1,s}^2\mu_2\left(A - A_{1,s}\right)^2\left(\mu - 1\right)\right)}{A^2\left(A_{1,s}^2\left(\mu - 1\right) + A^2\right)} \tag{6.23}$$

Correct values for B needs to be determined from numerical experiments. This reduces the value of our numerical solution as a predictive tool significantly, since we need some unknown constant in order to find the results we want.

Boundary values can be treated in exactly the same way as in section 5.1.1, but some special initial condition is necessary. To be able to start the simulation at all, we need to define volume flow and interface height for a few points closest to the pipe inlet. An obvious choice is to let the pipe be entirely filled with phase 1 at the inlet, and then reduce both $Q_{1,i}^0$ and $A_{1,i}^0$ linearly until both values reach zero after a few points. It is chosen to let let the last point s initially be point 6, and that δ initially has the value $\frac{\Delta z}{2}$. The rest of the pipe is entirely filled with phase 2, that is, $Q_{1,i}^0$ and $A_{1,i}^0$ are both zero in the rest of the pipe. As we saw in section 4.3, the interface is unstable in most cases, and we should expect any pertubation of a stable interface to grow in time. It seems hard to find an initial condition that is actually a stable situation, so we should expect some formation of waves on the interface.

6.3 A numerical solution

This model can be implemented by extending the pseudocode listed in table 5.1. The main differences are that special treatment is needed for the points $s-1$ and s, and that the front has to be tracked. The pseudocode listed in table (6.1) has these functions included.

The implementation given in appendix A is able to handle this problem as well, by choosing the correct options, as described in appendix A.1.

It is now tempting to test the program with no added drag on the front. In the following tests, we again assume that fluid properties are as introduced in section 3.2, and adjust σ to find a result for different capillary numbers. We find as shown in figure 6.2 that we get a reasonable solution only for very small capillary numbers, where drag should be expected to be of little importance. With higher capillary numbers, we get a wavy interface after 30 s, which is not what we expect at all. If we check interface shape after a

```
for i in [0,n]
    Set initial condition for A1[i] and Q1[i]
while time<total time
    for i in [1,s-2]
        Compute Q1[i] from momentum equation
        Compute A1[i] from mass conservation equation
    Compute Q1[s-1] from special version of momentum equation
    Compute A1[s-1] from mass conservation equation
    Compute Q1[s] from special version of momentum equation
    Compute A1[s] from mass conservation equation
    Recalculate position of front, delta
    if delta>1.5*dz
        Compute Q1[s+1] and A1[s+1] from special equations
        s = s+1
        delta = delta-dz
    for i in [s+1,n-1]
        Q1[i] = 0
        A1[i] = 0
    Set boundary conditions for A1 and Q1
Print result to file
```

Table 6.1: *Pseudocode for solving the explicit version of the hydraulic equations, now with a discontinuity. "s" is defined to be the last point the front has reached.*

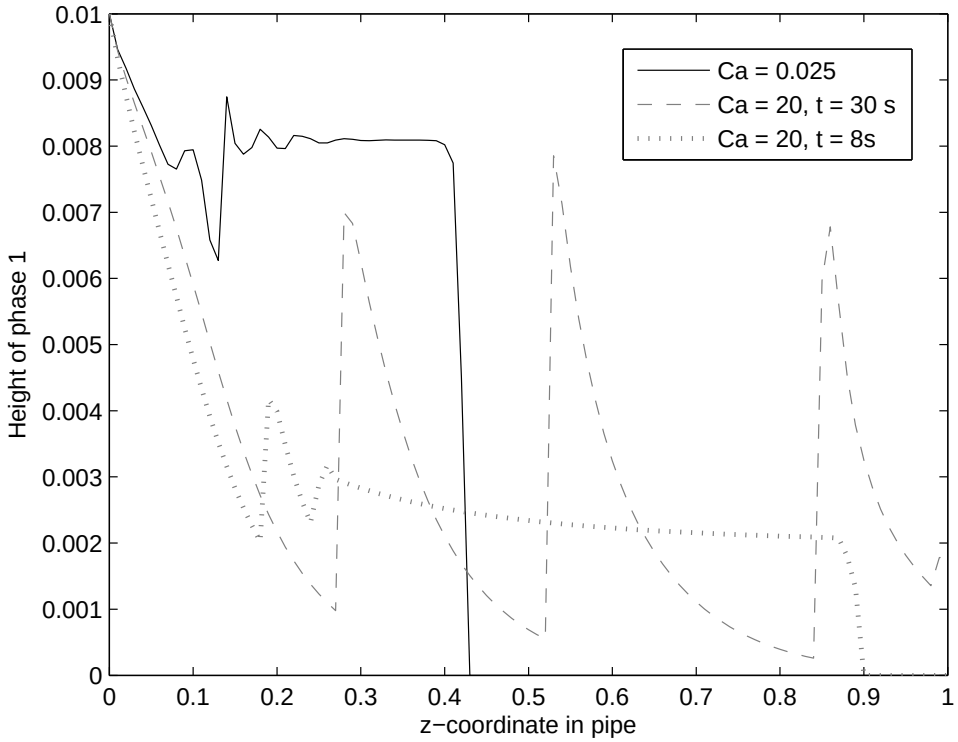

Figure 6.2: *Figure showing an initial test of the numerical model. Solid line shows a low capillary number after* 30 s *flow time, where the interface shape is qualitatively as we expect. The dashed line is for a higher capillary number after* 30 s *flow time, this time the solution is not as we expect at all. The dotted line shows the high capillary number after* 8 s *flow time.*

few seconds of flow, we find that with a high capillary number a front with interface height a little above h_δ is formed, and that this front moves with a very large velocity. This large front velocity makes the capillary number quite high. The waves seem to form after the front itself has moved out of the domain. For the low capillary number the fraction of oil left on the wall is far too high as compared to the results found by Soares et al[17]. It should be noticed that the mass conservation is not perfect in this case, but this can be remedied by adjustment of the factor α in equation (6.13). However, we still get qualitatively the same results when loss of mass is minimized. An added drag should be able to slow down the front, and thus prevent these discrepancies from the Soares result.

We now add the drag given by equation (6.23) as defined in the momentum equation (6.16) for the last point before the front. By adjusting the value B from equation (6.23) and α from equation (6.13) correctly, we are

now able to get exactly the same result as Soares et al, except that close to the inlet, we get the same type of waves that we got for the low capillary number case in figure 6.2. These waves seem not to have been reported in other works, and are probably unphysical. As mentioned in section 6.2, the initial condition is probably not a stable situation, and we should expect any disturbance of a stable interface to grow in time, except in the quite unusual configurations with low U where the interface is actually stable. Although we are now able to reproduce the results we want, neither B nor α seem to be independent of capillary number, so the value of this model is so far limited.

We have one not so obvious problem with the formulation used so far. Since we have used upwind discretization, the only term that transfers information regarding the front upstream to previous points is the curvature term. Every other term use only information from points upstream. In the limit of infinite capillary number the curvature has no effect, and this gives that no information is transferred upstream at all. It seems reasonable to assume that it is important in this case to let information flow upstream, and one way to do that is to reintroduce the diffusive terms that were left out in constructing the original hydraulic model in section 4.2. A discretized version of the terms can be given by

$$\begin{aligned} F_{diffusion,1,i} &= \frac{(A - A_{1,i})\,\mu_1}{\Delta z^2}\Bigg[(A_{1,i+1} + A_{1,i}) \left(\frac{Q_{1,i+1}}{A_{1,i+1}} - \frac{Q_{1,i}}{A_{1,i}} \right) \\ &\quad - (A_{1,i} + A_{1,i-1}) \left(\frac{Q_{1,i}}{A_{1,i}} - \frac{Q_{1,i-1}}{A_{1,i-1}} \right) \Bigg] \qquad (6.24) \\ F_{diffusion,2,i} &= \frac{A_{1,i}\mu_2}{\Delta z^2}\Bigg[(A - (A_{1,i+1} + A_{1,i})) \left(\frac{Q - Q_{1,i+1}}{A - A_{1,i+1}} - \frac{Q - Q_{1,i}}{A - A_{1,i}} \right) \\ &\quad - (A - (A_{1,i} + A_{1,i-1})) \left(\frac{Q - Q_{1,i}}{A - A_{1,i}} - \frac{Q - Q_{1,i-1}}{A - A_{1,i-1}} \right) \Bigg] \qquad (6.25) \end{aligned}$$

and the momentum equation for a point i can now be given by

$$\begin{aligned} Q_{1,i}^{l+1} &= Q_{1,i}^{l} \\ &+ \frac{\Delta t}{\tilde{A}_i^l}\Bigg[F^l_{wall\ shear,i} - F^l_{interface,i} - F^l_{advection,i} \\ &\quad -2\sigma A^l_{1,i} \left(A - A^l_{1,i} \right) \left. \frac{\partial \mathcal{C}}{\partial z} \right|_i^l + F^l_{diffusion,1,i} - F^l_{diffusion,2,i} \Bigg] \end{aligned} \qquad (6.26)$$

Using this momentum equation for $i \in [1, s-1]$ we find a somewhat improved performance. If we insert $\alpha = 1.57$ and $B = 72.6$ we get quite good results compared to the results found by Soares et al for large capillary

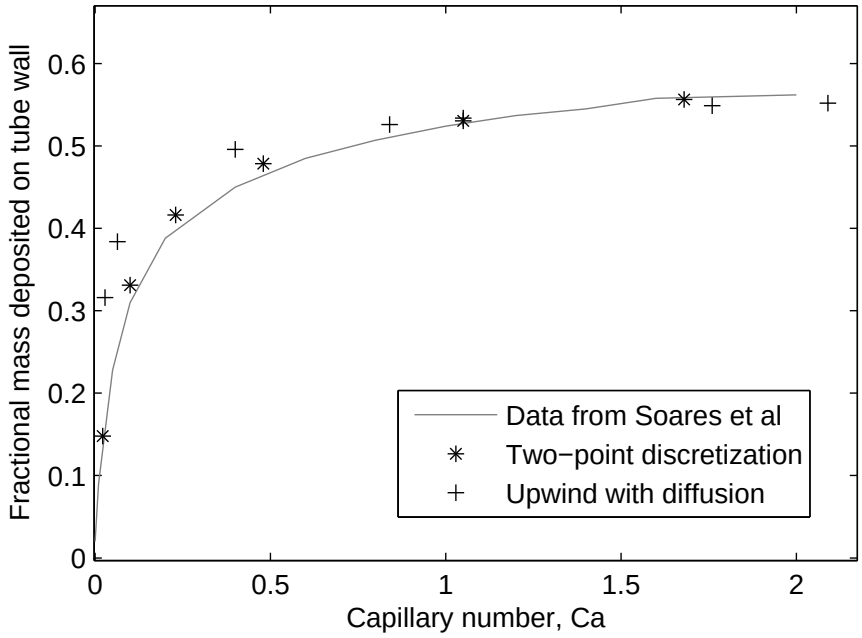

Figure 6.3: *Predictions from two versions of the hydraulic model, compared with the results reported by Soares et al*

numbers, as shown marked with plus-signs (+) in figure 6.3. But we still get overprediction of the fraction of oil left when the capillary number is small. And mass conservation is still not perfect, α should probably be adjusted a little as function of Ca, but the error in having α constant is now quite small.

Another way to increase flow of information upstream is to use standard two-point discretization of first order terms instead of using upwind. This would probably impair stability, but it is worth trying. The advective term now becomes

$$F^l_{advection,i} = \frac{\rho_1 \left(A - A^l_{1,i}\right)}{2\Delta z} \left(c^l_{1,i+1} \frac{\left(Q^l_{1,i+1}\right)^2}{A^l_{1,i+1}} - c^l_{1,i-1} \frac{\left(Q^l_{1,i-1}\right)^2}{A^l_{1,i-1}} \right) \quad (6.27)$$

and the mass conservation equation becomes

$$A^{l+1}_{1,i} = A^l_{1,i} - \frac{\Delta t}{\Delta z} \left(Q^l_{1,i+1} - Q^l_{1,i-1}\right) \quad (6.28)$$

With these formulations in the standard hydraulic model, we get the results marked with asterisks (*) in figure 6.3. In this case $B = 43$ and $\alpha = 1$. It is interesting to see that this formulation allows α equal to unity for the

entire range tested, without introducing large errors. Also, the results are now remarkably close to what Soares et al found over the entire range of capillary numbers. We can notice that B seems not to depend on Ca, but that it is still a function of Reynolds number, viscosity ratio and density ratio. Changing one or more of those factors makes it necessary to change B, and the function $B(Re, \mu, \rho)$ seems to be quite complex. No good expression for B has been found. In addition, extra wave formation have now appeared, as we expected, and if the volume flow is increased we quite quickly get severe stability problems. This further limits the value of the model.

Chapter 7

Case studies

The topic of this chapter is use of the numerical applications developed in chapters 4–6 to find out what results we are able to find, and to compare what we find with results reported in other publications, where applicable.

7.1 Equal viscosities

The special case of equal viscosities, and thus viscosity ratio $\mu = 1$, has some features it is interesting to see if the hydraulic model is able to describe. The main difference as compared to the analysis in chapter 2 is that continuity in interfacial shear stress simplifies to $\frac{dv_1}{dr}|_{r=h} = \frac{dv_2}{dr}|_{r=h}$. Thus, in a fully developed flow, the velocity profile for the two-fluid system will be equal to the parabolic profile of a single phase Poiseuille flow. This can be seen by inserting $\mu_1 = \mu_2 \equiv \mu_0$ in the velocity profiles from chapter 2, equations (2.26) and (2.27). With this simplification, the velocity profile in both phases will be given by

$$v_{1,2} = \frac{\Theta}{4\mu_0}\left(R^2 - r^2\right) \tag{7.1}$$

The analytical hold-up equation (2.35) can now be simplified by inserting $\mu = 1$, and we find

$$H = \sqrt{1 - \frac{1}{\sqrt{U+1}}} \tag{7.2}$$

The hydraulic hold-up equation (4.15) can not be equally simplified, and we will still have to solve this equation numerically. But if we solve both hold-up equations for U in the interval $[0.001, 100]$ we find that the difference between the interface height predicted by the two solutions is of the order of 2% of the pipe radius. By using the program developed in chapter 5 with $\mu = 1$ the hold-up predicted by the hydraulic hold-up equation (4.15) is confirmed. Since the two hold-up equations give results that are quite similar in this case, the hydraulic model actually predicts a solution that corresponds to

a velocity profile that is quite close to the parabolic profile we predicted analytically.

Petitjeans and Maxworthy[13] performed experiments with a viscous fluid being displaced by another, less viscous fluid, with the fluids being miscible in all proportions. They argued that this flow with large values for the Péclet number should mimic the situation with immiscible fluids at high capillary number. The reasoning for this was that molecular diffusion, which is by definition zero for immiscible fluids, is negligible when the Péclet number is high, and that surface tension, which is absent for miscible fluids, is negligible when the capillary number is high. With large viscosity ratio, they reproduced the asymptotic value $m = 0.6$ found by Cox[5], but with lower viscosity ratio, they found that the fraction of mass left at the wall was reduced. Soares et al[17] predicted numerically that the fraction of mass should actually increase when the viscosity ratio was reduced, and argued that the reason for the discrepancy was that Petitjeans and Maxworthy used an inaccurate expression for evaluating the fraction of mass left in the tube. The expression they used was proposed by Taylor[19], and given by

$$m = \frac{U - \overline{u}}{U} \tag{7.3}$$

where U is the velocity of the front and $\overline{u}$ is the mean velocity in the fluid downstream from the front. This expression is only valid when the fluid in the thin film left at the wall is stationary, and that is a good approximation only for large viscosity ratios. The velocity profile given in figure 3.14 can serve as an example, the mean velocity of the fluid left at the wall is clearly not negligible. Thus, we should expect an increased fraction of oil left at the wall when we use $\mu = 1$ in the model developed in chapter 6, although the model was not very successful. But one problem with $\mu = 1$ in the model is obvious, since the equation describing drag on the front, equation (6.23), includes the term $(\mu - 1)$, the drag will be identically zero. If we redo the algebra we did to find equation (6.23) assuming $\mu = 1$, we can find the simplified drag expression

$$F_{drag,s} = \frac{Q\mu_2 A_{1,s}^3}{A^3} \tag{7.4}$$

But regardless of which expression for drag we use, we get a very thin film of phase 2 left on the wall, which is the opposite result of what Soares et al reported. Even with a negative drag, which can not be defended by any physical reasoning, we get this very low fraction of oil left in the pipe. The model seems for some reason to run into problems with $\mu = 1$.

7.2 Core annular flow

A core annular flow is in some sense the opposite case of what we have considered so far. The viscosity ratio is reversed, with the most viscous fluid

in the core, and a much less viscous fluid, typically water, in the annulus close to the wall. The practical application of this type of flow is transport of very viscous oils in pipelines. The very viscous core will then move more or less like a rigid body, lubricated by the annulus of less viscous fluid. The major benefit of this is that a very viscous oil can be pumped through a pipe with a pressure drop that is of the same order of magnitude as the pressure drop the same volume flow of the less viscous fluid would have. This is obviously a significant advantage, since smaller pumps can be installed, and thus large cost savings are made possible. This has led to a large amount of research regarding the behaviour and stability of core annular flows, since for instance transition to stratified flow would reduce the volume flow of the oil significantly.

In developing the hydraulic model, no assumption were made about the viscosity ratio. Thus, the model should be able to handle at least some phenomena from core annular flow as well. We can not expect to predict transitions to dispersed flow or stratified flow, as we have assumed an axisymmetric flow with a core of circular cross section. For the same reason, we can not expect to describe phenomena that include the core moving out of the center of the pipe. But it should be possible to describe axisymmetric waves, called bamboo-waves, and stability of a perfect cylindrical core, and it would be interesting to compare results from our hydraulic model with what others have reported previously. Since we now swap position of water and oil from the situation we have regarded previously, the indices of water and oil will also be swapped. In this section, index 1 will denote values in the core of oil, whereas index 2 will denote values in the annulus of water.

Joseph and Renardy[12] states that core annular flow is only possible for very viscous oils with viscosity of more than roughly $0.5\text{Pa}\cdot\text{s}$, and that emulsification into water readily occur for lighter oils. We thus choose the oil viscosity $\mu_1 = 1\text{Pa}\cdot\text{s}$ in the following, to make certain that we are in a region where core annular flow is possible. Oils with this high viscosity generally have a density close to that of water, so we choose for simplicity to set $\rho_1 = \rho_2$.

With the chosen viscosity, the viscosity ratio will become $\mu = 0.001$. It is now interesting to find out what kind of solutions the hydraulic hold-up equation (4.15) will give in this case. It should actually be a quite good approximation to assume $\mu = 0$, from which we in section 4.1 found the approximate solution $H = \sqrt{\frac{U}{U+1}}$. Numerical experiments confirm this assumption, a steady interface height close to the approximate solution is found.

Rodriguez and Bannwart[14] have studied stability of core annular flow using a one-dimensional model quite close to the model we derived in chapter 4. Using the inviscid Kelvin Helmholtz criterion they found that short waves were stable, but that longer waves tended to be unstable. They found that the wavelength of the longest stable interfacial wave for a horizontal flow

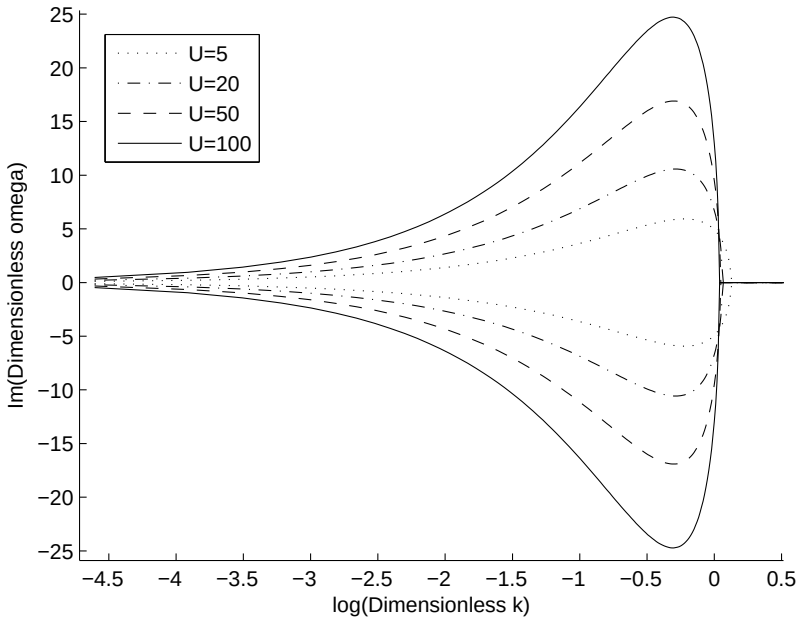

Figure 7.1: *Imaginary part of the dispersion relation for inviscid Kelvin Helmholtz criterion for a core annular flow.* $\mu = 0.001$, $\sigma = 0.029$ N/m. *For each pair of curves with the same line style, the top curve and bottom curve corresponds to* $\hat{\omega}_+$ *and* $\hat{\omega}_-$, *respectively. We see that above a certain wave number, there is no wave growth, and hence, short waves are stable.*

with no density difference could be given by

$$\lambda_{max} = 2R\pi H \tag{7.5}$$

where, as before, R is the pipe radius and H the dimensionless hold-up.

The stability analysis from section 4.3 can quite easily be adapted to using the inviscid Kelvin Helmholtz criterion to find conditions for stability. In this case, using equation (4.56), we set $\mathbf{R} = \mathbf{V} = 0$, and end up with the inviscid equation

$$\hat{\omega}_\pm = \frac{\hat{k}\mathbf{Q} \pm \left(\hat{k}^2\left(\mathbf{Q}^2 + 4\mathbf{PS}\right) + 4\hat{k}^4\mathbf{PT}\right)^{\frac{1}{2}}}{2\mathbf{P}} \tag{7.6}$$

Rodriguez and Bannwart compare their results with experiments where they used an oil which gave an oil-water interface tension of 0.029 N/m, so this coefficient is used in the following. The dispersion relation is readily solved numerically, and a plot of the imaginary part of ω versus wave number is given in figure 7.1. We can notice that the growth rate goes to zero close to $\log \hat{k} = 0$.

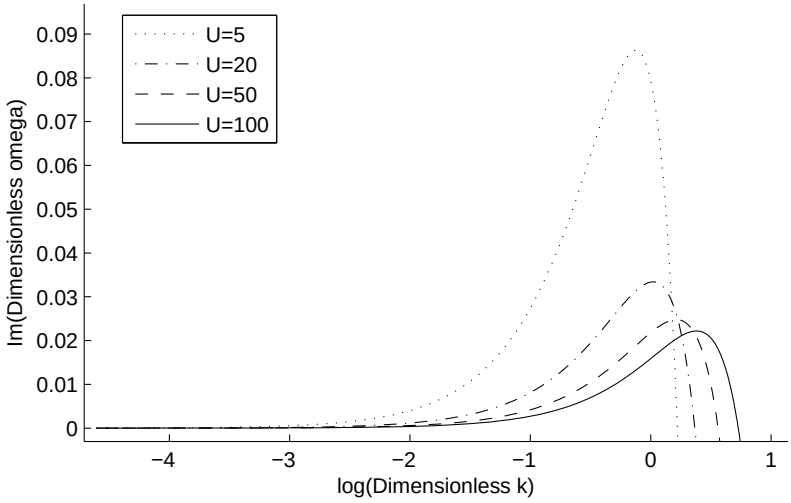

Figure 7.2: *Imaginary part of the dispersion relation for viscous Kelvin Helmholtz criterion for a core annular flow.* $\mu = 0.001$, $\sigma = 0.029$ N/m. *Only solution for* $\hat{\omega}_+$ *is shown, the imaginary part of* $\hat{\omega}_-$ *is very large and negative over the entire range of wave numbers, and thus not very interesting.*

The same growth rate for the viscous Kelvin Helmholtz criterion is given in figure 7.2, where we have reintroduced the definitions of $\mathbf{R}$ and $\mathbf{V}$ from section 4.3. We see that the waves are unstable for even shorter waves when we use this criterion.

The results from this stability analysis can be summarized by the data in table (7.1). We can notice that our results using inviscid Kelvin Helmholtz are close to what we find using the expression derived by Rodriguez and Bannwart[14]. Rodriguez and Bannwart also gives a plot of the actual wavelengths observed for a stable upward vertical core annular flow. It seems that these wavelengths are quite close, at least qualitatively, to the predictions from viscous Kelvin Helmholtz. It is also interesting to notice that this result is in accordance with what Bai et al[1] found. They reported reduced wavelengths when the annulus of water got thinner, and commented that this meant that the waves had the same steepness, regardless of how thick the annulus was.

Joseph and Renardy[12] also mentions that a core annular flow is unstable to short waves if the surface tension is zero for both viscous and inviscid cases, and that the growth rate goes to infinity with the wave number in the inviscid case. This is readily confirmed by inserting zero surface tension in the stability analysis from chapter 4, the growth rate then goes to infinity with the wave number in both the viscous and the inviscid case. A comparison of growth rates plotted versus wave number is given in figure 7.3.

U	λ_{max}	λ_{IKH}	λ_{VKH}
5	5.7 cm	5.5 cm	5 cm
20	6.1 cm	5.9 cm	4.4 cm
50	6.2 cm	6 cm	3.6 cm
100	6.2 cm	6 cm	3 cm

Table 7.1: *Comparison of results for maximum wavelength found using different stability formulations, λ_{max} the expression found by Rodriguez and Bannwart with interface height that is a solution of the hydraulic hold-up equation (4.15), λ_{IKH} the result found using the inviscid Kelvin Helmholtz criterion and λ_{VKH} the result found using viscous Kelvin Helmholtz.*

We see that with no surface tension, the growth rate goes to infinity with the wavenumber in both the viscous and the inviscid case, whereas with surface tension coefficient $\sigma = 0.029$ N/m the growth rate is either zero or negative for large wave numbers. We can also notice that in the viscous case with surface tension coefficient $\sigma = 0.029$ N/m the maximum growth rate is actually very small. From section 5.2 we know that the minimum wavelength we can expect to find with the chosen grid is approximately 6 cm. That is equivalent with $\hat{k} \leq 1.05$, and $\log \hat{k} \leq 0.046$. Below this wave number, the plots for the two viscous cases are more or less equal, in both cases with very small growth rate. With relatively small wave numbers it is reasonable to expect viscous Kelvin Helmholtz to be most important, and we should thus expect a very low growth rate in numerical experiments. Through various numerical tests it is observed that initial pertubations actually seem to display neutral or slightly negative growth rate, despite the expected positive growth. One should observe that the expected growth rate is in this case actually smaller than the difference between expected and actual growth rate seen in figure 5.5 for the case of water in the core, so it seems reasonable to assume that numerical diffusion is able to suppress the slight growth expected from the stability analysis.

7.3 Thinning of oil layer after long time

In chapter 6, we tried to develop a version of the hydraulic model that was able to handle the initial displacement of oil. Although the success was quite limited, we should still be able to use the solver for the standard hydraulic model from chapter 5 to find out what would happen when the front of water has passed through the entire section of pipe considered. As there is a shear at the interface between the phases, it is obvious that the layer of oil will become thinner as time goes by if only water is pumped into the pipe. How fast this oil layer gets thinner is unknown, but it should be possible to make

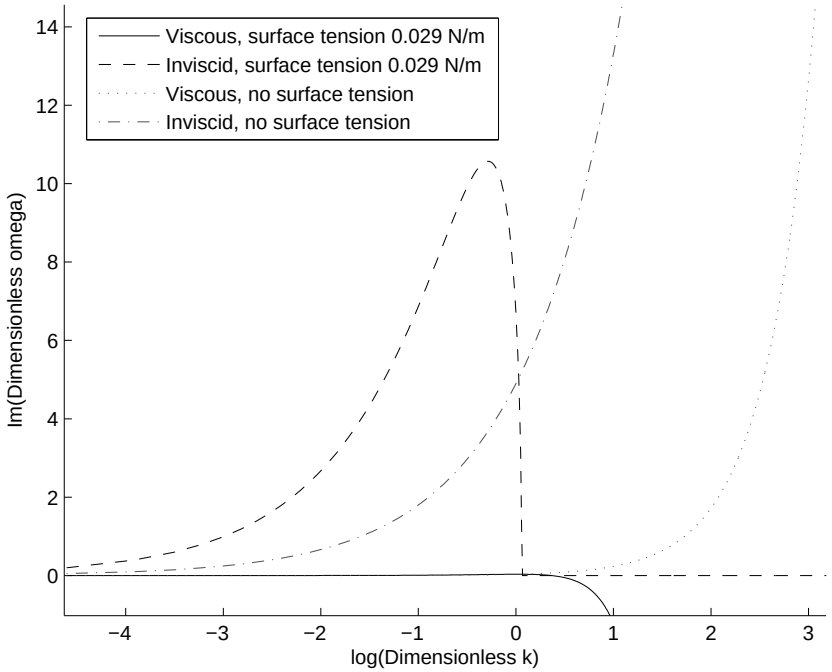

Figure 7.3: *Comparison of growth rates for viscous and inviscid case, with and without surface tension.*$U = 20$.

a prediction using the mentioned numerical solver, at least when the layer is not very thin. When the layer thickness reaches zero, one would again have the problem of a moving contact line, as described in section 3.4.2. The hydraulic model is too simplified to be able to describe this phenomenon, and we can thus not trust the predictions made for very thin oil layers.

As initial condition we choose a solution to the hold-up equation, with constant interface height and volume flow of water in the pipe. Then the inflow of water is gradually increased, until the inflow is pure water that fills the entire cross section. If the initial height is chosen so that the fraction of oil left in the pipe depends on the capillary number as reported previously by e.g. Soares et al[17], this description should be quite close to what would actually happen.

We start with the limit of high capillary numbers, as in this limit the initial interface height is relatively independent of the capillary number. It is thus possible to adjust all the dimensionless groups, capillary number, Reynolds number, viscosity ratio and density ratio without changing the initial interface height. In this limit, we know that we can expect that the fraction of oil left in the pipe $m = 0.6$, which corresponds to $H \approx 0.6325$. Curi-

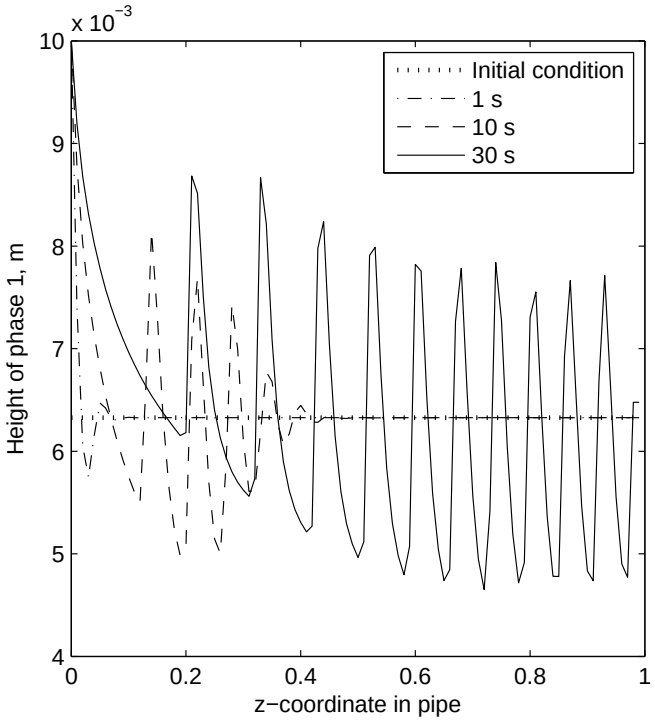

Figure 7.4: *Interface shape after a few seconds.*

ously, this dimensionless interface height is almost exactly $1 - e^{-1}$, where e is Euler's number. From the hold-up equation (4.15) we then find $U \approx 15.8$. We set the surface tension coefficient at the very low value 0.0001 N/m, to make the capillary number large enough, and use the standard fluid properties introduced in section 3.2. The inflow is gradually changed to pure water during 0.5 s. A plot of how the interface shape changes soon after the simulation is started is given in figure 7.4. We can notice that quite early a wave is formed close to the pipe inlet, and that this small wave eventually grows to a wave train filling the entire pipe section. We know from section 4.3 that the interface is usually unstable, and it is not surprising that the major change in boundary condition triggers wave growth. But when the wave has passed, we after 30 s again see a stable interface close to the inlet, where we see quite clearly that the thickness of the oil layer is shrinking. It is thus reasonable to assume that the thickness of the oil layer will be monotonically decreasing after the wave train has been washed out of the pipe.

It is now interesting to see what happens after long flow times. A plot showing interface shape at different time steps is given in figure 7.5. We can notice that the thickness of the oil layer still seems to be monotonically decreasing. We also see that close to the inlet, the contact line has moved

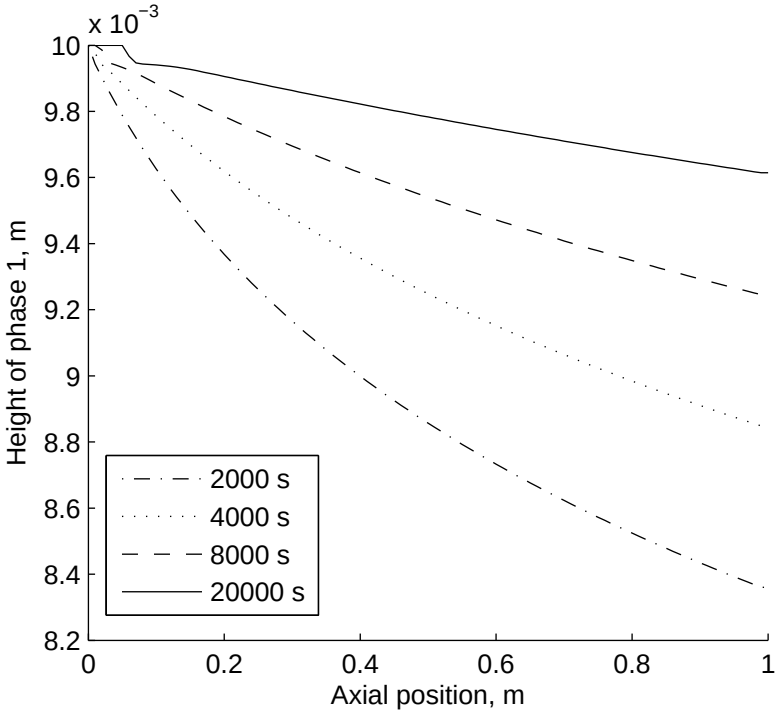

Figure 7.5: *Interface height after long flow times.*

somewhat, and a step is formed. This step is reduced for smaller Δt and increased for larger Δt. It thus seems reasonable to assume that the movement of the contact line and the step formation is due to numerical inaccuracy, and that in the limit $\Delta t \to 0$ these phenomena would not be observed. The shown results have been found using $\Delta t = 4 \cdot 10^{-5}$, and this is considered accurate enough for the current purpose. Finally, it is also clear that the thinner the layer of oil is, the slower it is expelled. Figure 7.6 shows the predicted velocity profile for a fully developed flow for different values of U using the results of chapter 2, and we see that the mean velocity of the layer of oil is significantly reduced as U increases and the layer gets thinner. The observation from the results of the simulation is thus in accordance with what we should expect from the analysis, at least if we assume that the velocity profile of the transient flow discussed in this section is relatively close to the velocity profile of a steady flow.

A plot of time development of oil layer thickness for different cross sections of the pipe is given in figure 7.7. As expected, we see a lot of noise from the waves that form at the beginning of the simulation. We also see that the plots for different cross sections in the pipe are more or less equal when the waves have moved out of the pipe, but that the plots are shifted in time. After long flow time, the rate at which the oil layer thickness is

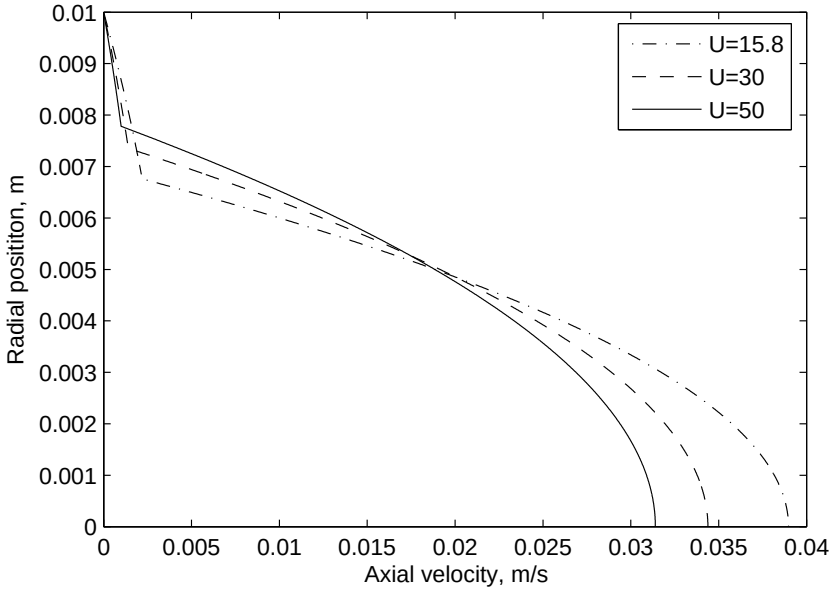

Figure 7.6: *Velocity profile for a fully developed flow at different values for* U.

reduced seems to tend to a constant value, independent of z and t.

When the waves have moved out of the pipe, the thickness of the oil layer seems to be monotonically decreasing. That means that we can try to track the point with a certain interface height, and thus find out how fast the interface moves at different interface heights. It is important to notice that we can not track material points this way, as we must expect material points to have some radial velocity in addition to the axial velocity. Thus, what we find is the velocity of the geometrical point where the interface has a certain height. A plot of the velocity of the points with certain interface heights versus time is given in figure 7.8. We can notice that there is again some wave formation that makes the result hard to interpret at the start of the simulation, but that the results stabilize quite fast. We then see that at every chosen interface height, the geometrical point seems to move with a constant velocity. In a fully developed flow, we are able to find an analytical expression for the axial velocity of the interface. If we combine equations (2.27), (2.31) and (2.33), we find, after some algebra

$$v_{interface}(H) = \frac{2Q\left(1 - H^2\right)}{A\left(H^4\left(\mu - 1\right) + 1\right)} \tag{7.7}$$

In a fully developed flow there will not be any radial velocity component, as that would imply that the flow is not fully developed. If the transient flow is not too far from being fully developed, we could expect the axial velocity of

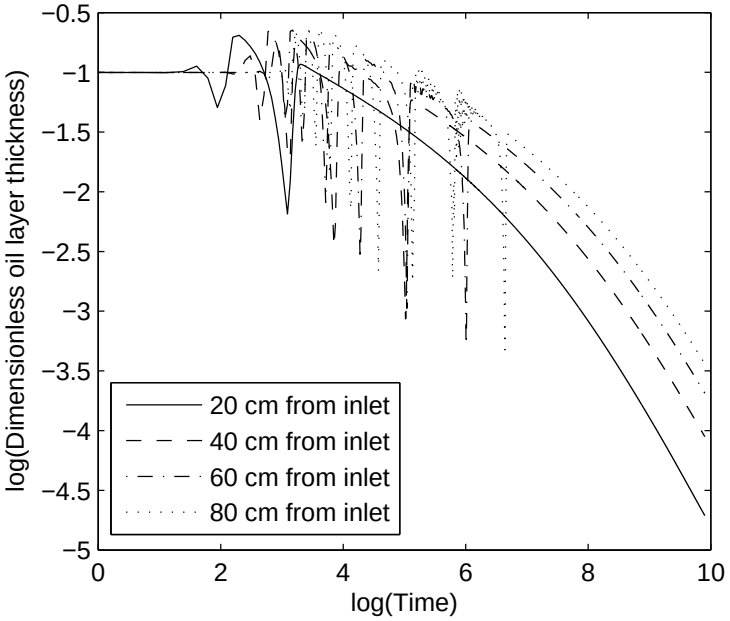

Figure 7.7: *log-log plot of time development of oil layer thickness for different positions in the pipe.*

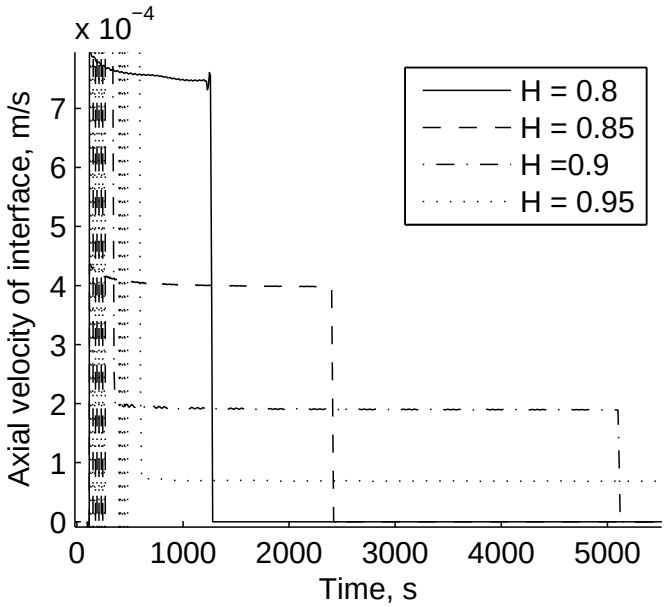

Figure 7.8: *Velocity of the interface at different interface heights.*

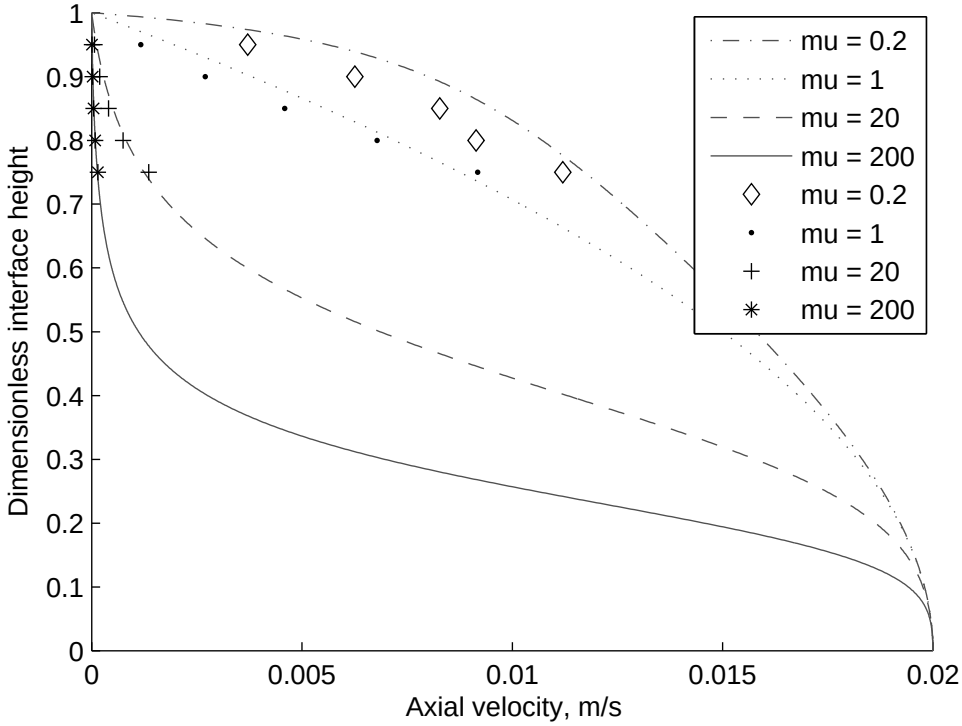

Figure 7.9: *Comparison of the velocity of the interface at different interface heights for different viscosity ratios μ, and with the actual velocity predicted by the hydraulic model.*

a geometrical point at the interface in a transient flow to be quite close to the axial velocity of a material point at the interface in the corresponding fully developed flow. Thus, equation (7.7) would be a relatively good description of the axial velocity of a geometrical point at the interface with interface height H even for the transient flow.

Interface velocity versus interface height predicted by equation (7.7) is plotted for different viscosity ratios in figure 7.9. We can notice that for $\mu = 1$ we find the expected Poiseuille profile. $\mu < 1$ gives a profile with higher interface velocity than the Poiseuille parabola, whereas the interface velocity is significantly reduced when μ is high. Close to the pipe wall, the interface moves very slowly with high viscosity ratios. If equation (7.7) gives a good description of the velocity of the interface for a transient flow, we can notice that the time it takes to remove a certain fraction of oil initially left at the wall from the pipe increases with the viscosity ratio. We should expect this result, as continuity of shear stress at the interface, relation (2.8), gives that the interface shear is reduced with high viscosity ratio.

The actual velocities of the interface observed in numerical experiments is also plotted in figure 7.9. We see that the results are in quite good agreement with the analytical prediction, but that equation (7.7) overestimates the velocity of the interface somewhat. This can be explained by the fact that the flow is in this case obviously not fully developed. In addition, we know from figure 4.2 that the analytical hold-up equation (2.33) and the hydraulic hold-up equation (4.15) do not give the exact same result, and this can perhaps explain some of the discrepancy. We can also notice that the numerical results are closer to the analytical result for large viscosity ratios than for small viscosity ratios. This result can be explained by the fact that the results from the two different hold-up equations are closer for large viscosity ratios, and that the reduced interfacial shear for large viscosity ratios should imply that the transient flow is closer to fully developed than for low viscosity ratios. Thus, for very large viscosity ratios, it should be a good approximation to assume equation (7.7) to be a correct descripiton of the interface velocity. Using this, we can find an analytical expression describing the interface height as a function of time. Inserting $v_{interface} = \frac{z}{t}$ in equation (7.7) and rewriting a bit, we get

$$H_1(z,t) = \sqrt{\frac{Qt}{Az\left(\mu-1\right)}\left(-1+\sqrt{1-\frac{Az\left(\mu-1\right)\left(Az-2Qt\right)}{Q^2t^2}}\right)} \tag{7.8}$$

But in this equation, we have not taken into account that we have an initial interface height H_0. To include this initial interface height, we introduce the Heaviside step function $He[\xi]$ defined by

$$He[\xi] = \begin{cases} 0 & \xi < 0 \\ 1 & \xi \geq 0 \end{cases}$$

We can now write interface height as

$$H(z,t) = H_0 + He\left[v_{interface}t - z\right]\left(H_1(z,t) - H_0\right) \tag{7.9}$$

With this expression, the volume of water in the pipe at any given time could be found by doing the integration

$$V = A\int_0^L \left(H(z,t)\right)^2 dz \tag{7.10}$$

where L is the length of the pipe. No analytical solution of the integral has been found, so the integral will have to be evaluated numerically.

Up till now, we have only changed the viscosities. Changing viscosities obviously changes the viscosity ratio, but it will also change the Reynolds number if we change μ_1 or capillary number if we change μ_2. Thus, we do not know whether the differences in interface velocity observed in the numerical

experiments is only due to changes in μ, or if the changes in Reynolds number and capillary number have also affected the solution. We must thus change Reynolds number and capillary number separately, to see if this changes the result. Fortunately, through further numerical experiments neither of the two dimensionless groups seem to change the velocity of the interface, but it is obvious that a too high Reynolds number would lead to transition to turbulence, and thus invalidate the result. With the lowest capillary number tested, Ca ≈ 0.02, it is found that the interface is still moving with approximately the velocity predicted by equation (7.7). The difference between the prediction from equation (7.7) and the actual interface velocity found numerically seems to be the same for low capillary number as it was for high capillary numbers. The last dimensionless group relevant is the density ratio, and it is observed that this group does not change the velocity of the interface, either. But one should notice that changes to the dimensionless groups are changing the rate at which waves form, and higher wave growth rate makes it harder to interpret the result and find accurate values for the velocity of the interface.

Beresnev and Deng[2] have used another approach for describing concentric two-fluid flows. They assumed that the velocity profile in the core and annulus could be approximated as a Poiseuille flow, but rederived the Poiseuille profile with the possibility of different pressure gradients in the core and the annulus. They used the resulting profile to write the volume flow of each phase as a function of the interface height H and pressure difference. To find the pressure difference across the interface, they used a linearized version of the mean curvature $\mathcal{C}$ defined in equation (4.7):

$$\mathcal{C} = \frac{1}{2}\left(\frac{1}{h} - \frac{\partial^2 h}{\partial z^2}\right) \tag{7.11}$$

They then ended up with an equation for the volume flow of each phase as a function of interface height and fluid properties only. Imposing the demand that the sum of the two volume flows must be equal to the total volume flow, which is a constant, and using the result in the mass conservation equation for the core, they found a partial differential equation with interface height as the only variable. They also included the possibility of letting the pipe radius vary sinusoidally along the pipe axis. The model was used to study break-up of the core, and they compared their results with simulations in FLUENT and the finite element solver COMSOL. They found that the results from the one-dimensional model converged towards the results found using FLUENT and COMSOL when the amplitude of the sinusoidal variation in radius was reduced. It thus seems reasonable to expect the model to perform quite well for a pipe without variation in radius.

With the notation used in this text and with an assumption of a constant

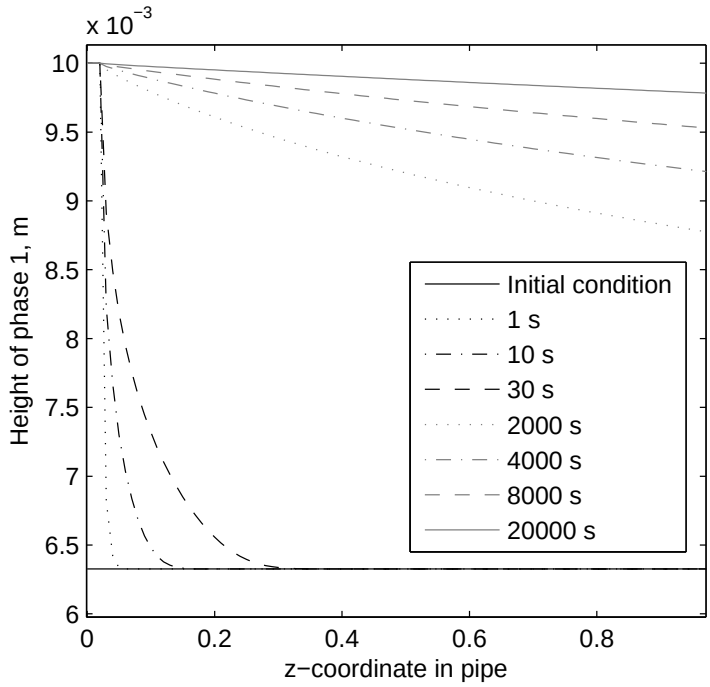

Figure 7.10: *Interface shape at different time steps, as predicted by the model from Beresnev and Deng[2].*

radius pipe the expression found by Beresnev and Deng can be given by

$$\frac{\partial H}{\partial t^*} = -\frac{\mu Q^*}{2\pi H}\frac{\partial}{\partial z^*}\left(\frac{\frac{2}{\mu}\left(\frac{1}{H^2}-1\right)}{\frac{1}{H^4}+\mu-1}\right) + \frac{1}{4H}\frac{\partial}{\partial z^*}\left(H^2\left(\frac{\partial H}{\partial z^*}+H^2\frac{\partial^3 H}{\partial z^{*3}}\right)\left(\frac{\left(\frac{1}{H^2}-1\right)\left(\left(\frac{1}{\mu}-\frac{1}{4}\right)\frac{1}{H^2}+\frac{3}{4}-\frac{1}{\mu}\right)}{\frac{1}{H^4}+\mu-1}+\frac{1}{\mu}\log H\right)\right) \tag{7.12}$$

in which terms marked with an asterisk denotes the dimensionless version of the same term without an asterisk. The dimensionless terms are defined by

$$H = \frac{h}{R}, \qquad z^* = \frac{z}{R}, \qquad t^* = \frac{t\sigma}{\mu_1 R}, \qquad Q^* = \frac{Q\mu_1}{\sigma R^2} \tag{7.13}$$

This model is readily implemented using the framework of the implementation from chapter 5, basically, all we need to do is introducing the scaling and replacing the hydraulic model with the model derived by Beresnev and Deng.

When we use this model to simulate the flow, we can find the result given in figure 7.10. The same settings and flow properties have been used here

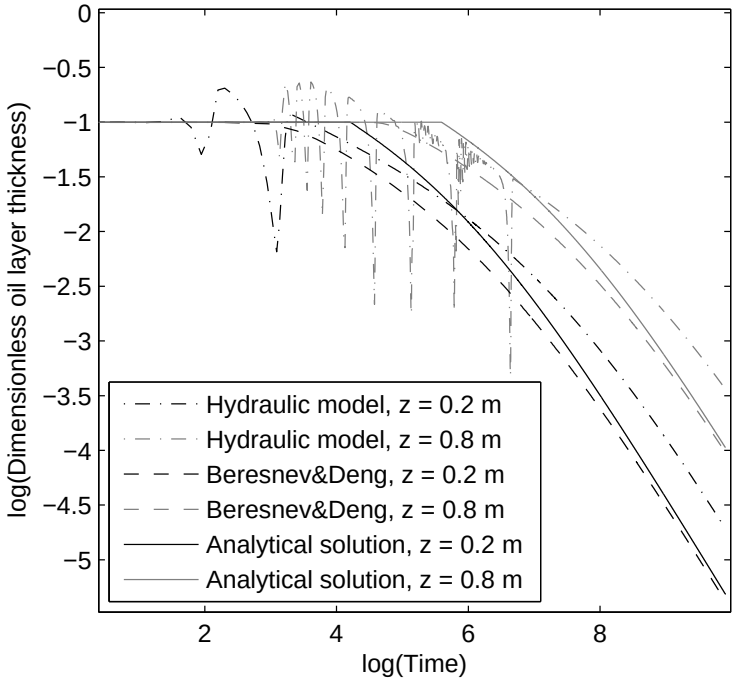

Figure 7.11: *Comparison of oil layer thickness predicted by the hydraulic model, the Beresnev and Deng model and the analytical solution, equation (7.9) at different points in the pipe.* $\mu = 20$.

as those used in the hydraulic model to generate figures 7.4 and 7.5. The most striking difference between the results from the two models is that no waves are present in figure 7.10. While we have shown that the interface in the hydraulic model is in most cases unstable, the interface from the model derived by Beresnev and Deng seems to be stable. This could be due to the linearization of the expression for mean curvature. To investigate this further, we use the definition from equation (7.11) instead of equation (4.7) to describe mean curvature in the hydraulic model. It is observed that the interface is still unstable in the hydraulic model, and the observed stability in the model derived by Beresnev and Deng is thus not due to the linearization of the curvature term. Apart from this difference, the results are quite similar, but the Beresnev and Deng model seems to predict a faster reduction in oil layer thickness.

A comparison of how the oil layer thickness evolve in time for the hydraulic model, the Beresnev and Deng model and the analytical approximation in equation (7.9) is given in figure 7.11. We see that the hydraulic model and the Beresnev and Deng model give at least qualitatively similar results, and that the gradient after a long time seems to be quite similar.

But the most striking observation is that the Beresnev and Deng model seems to predict almost exactly the same behaviour after long flow times as the analytical solution does. Although this might come as a surprise, it could be explained by the fact that Beresnev and Deng actually assumed the flow to be Poiseuillean, and that equation (7.7) thus should be an exact description of the velocity of geometrical points at the interface. We can also notice that all three plots seem to tend to linear in this limit. This can be shown analytically by assuming large t in equation (7.9). With that assumption, the Heaviside step function is always equal to unity, which yields $H(z,t) = H_1(z,t)$. Doing a series expansion of the inner square root in equation (7.8) we find

$$\begin{aligned} H(z,t) &\approx \left[\frac{Qt}{Az(\mu-1)}\left(-1+1-\frac{Az(\mu-1)(Az-2Qt)}{2Q^2t^2}\right.\right. \\ &- \left.\left.\frac{(Az(\mu-1))^2}{2Q^2t^2}+\mathcal{O}\left(t^{-2}\right)\right)\right]^{\frac{1}{2}} \\ &\approx \sqrt{1-\frac{Az\mu}{2Qt}} \end{aligned} \tag{7.14}$$

where we in the last approximation have neglected terms $\mathcal{O}\left(t^{-2}\right)$. Doing another series expansion of the remaining square root, we can simplify the expression to

$$H(z,t) \approx 1-\frac{Az\mu}{4Qt}+\mathcal{O}\left(t^{-2}\right) \approx 1-\frac{Az\mu}{4Qt} \tag{7.15}$$

From this, we see that the thickness of the oil layer is proportional to t^{-1} when t is large. A plot comparing the different results for $z = 0.2$ is given in figure 7.12, and we see that the approximation is close to the analytical result and the Beresnev and Deng model for large t, whereas the hydraulic model predicts nearly the same rate of reduction of oil film thickness for large t, but a somewhat thicker oil film at each time instant.

The main difference between the three approaches lies obviously in the early stages of the flow. The wave formation in the hydraulic model seems to slow down the displacement rate at the earliest stages as compared to the Beresnev and Deng model, while the analytical solution seems to underestimate the displacement rate when the oil layer is thick. This last difference is probably connected with the fact that with large gradients in interface height the flow is relatively far from being fully developed. The situation seems to be identical for a very long pipe and for a faster flow, but it should be noticed that the hydraulic model has stability problems for a flow with relatively high velocity.

When we know the interface position, it is an easy task to perform a numerical integration to find the volume of oil left in the pipe. But the

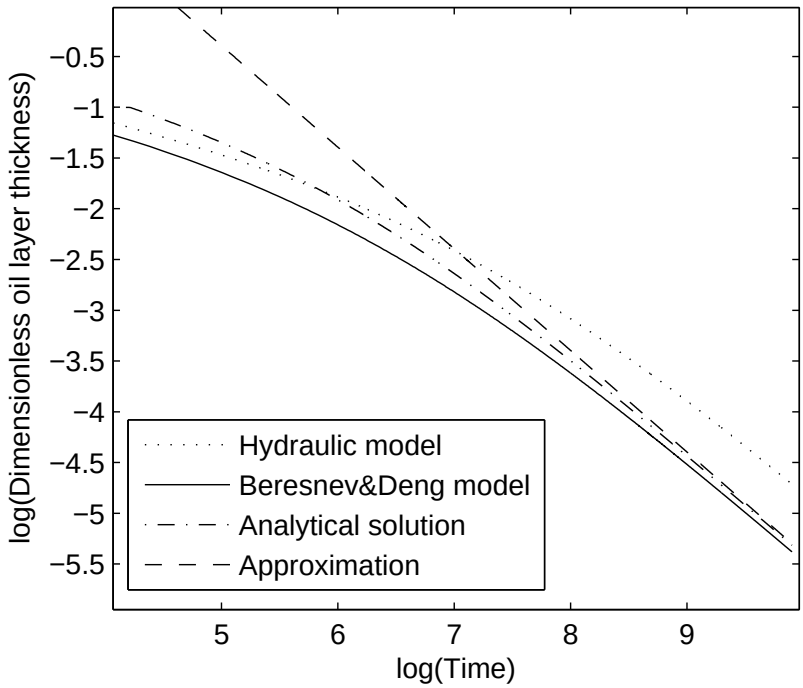

Figure 7.12: *Comparison of the hydraulic model, the Beresnev and Deng model, the analytical solution (7.9) and the approximate solution for large t, (7.15).* $\mu = 20$.

approximate solution for large t, equation (7.15), can be integrated directly, and we find

$$\begin{aligned} V_{oil} &= A\int_0^L (H(z,t))^2\,dz = A\int_0^L \left(1-\frac{Az\mu}{4Qt}\right)^2 dz \\ &= AL\left(1-\frac{AL\mu}{4Qt}+\frac{A^2L^2\mu^2}{48Q^2t^2}\right) \end{aligned} \tag{7.16}$$

where V_{oil} is the total volume of oil in the pipe and L is the pipe length.

We from here on define the volume fraction of oil left in the pipe to be $m_V = \frac{V_{oil}}{V_{total}}$, where V_{total} is the volume of the pipe itself. If the interface height is constant in the entire pipe, this definition is equal to the volume fraction m introduced in equation (1.1). We now introduce the time scale $t_s = \frac{AR}{Q}$, which is the time needed for the mean velocity of the flow to advance one pipe radius, and define the dimensionless time $t^* = \frac{t}{t_s}$. A plot of m_V versus t^* for the different approaches with a pipe length $L = 1$ m is given in figure 7.13. We see that the results from the hydraulic model, the Beresnev and Deng model and the analytical solution are quite equal. Although the analytical solution predicts a somewhat smaller fraction of oil left in the pipe, the analytical solution seems to give results surprisingly close to what is found through the numerical models. The same seems to hold both for smaller and larger viscosity ratios.

An additional change could be made to the analytical description of the interface. From equation (3.6) we know that the velocity of the front as a function of the initial interface height should be given by

$$v_{front}(H_0) = \frac{Q\left(H_0^2(\mu-2)+2\right)}{A\left(H_0^4(\mu-1)+1\right)} \tag{7.17}$$

This could be used to find a new version of equation (7.9) if we introduce a new Heaviside step function, and we find

$$H(z,t) = He\left[v_{front}t - z\right]H_0 + He\left[v_{interface}t - z\right](H_1(z,t) - H_0) \tag{7.18}$$

This equation is able to describe the initial displacement of oil, as well. The first step function describes the initial front propagating through the pipe, and the second step function gives the gradual thinning of the oil layer. Since we know from section 3.4.3 that equation (7.17) is actually a quite good representation of the front velocity, and since we saw in figure 7.13 that equation (7.9) gave a surprisingly good representation of the time development of the fraction of oil left in the pipe when the initial condition is a stable interface, we could hope for equation (7.18) to give a reasonably good description of the interface at any time step. Thus, the problem of finding out how much oil is left in the pipe at any time would be reduced to finding the initial interface height H_0, which is quite well known from

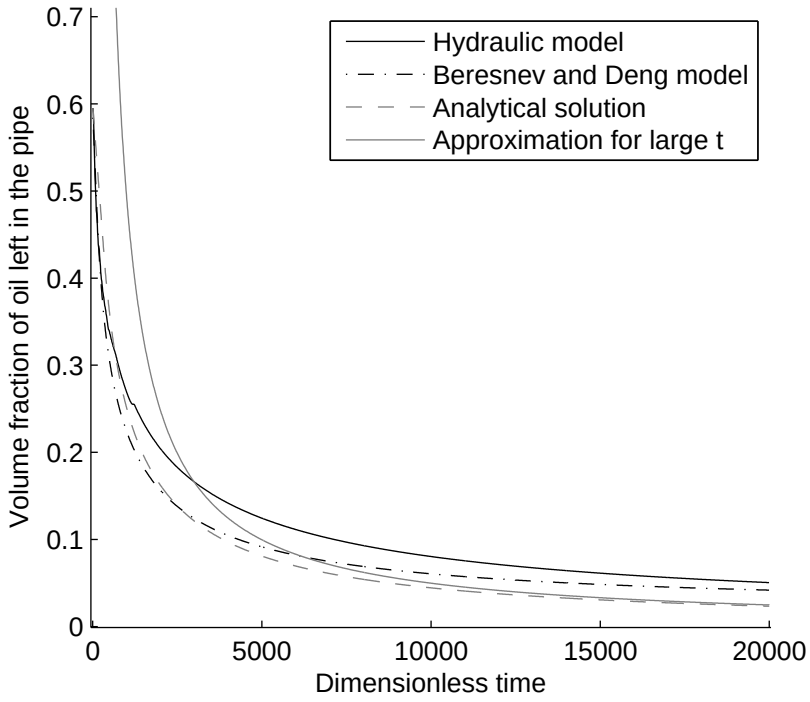

Figure 7.13: *Comparison of time development of the volume fraction of oil left in the pipe for the hydraulic model, the Beresnev and Deng model, the analytical solution and an approximate solution valid for large t.* $\mu = 20$.

the results of e.g. Soares et al[17], and doing a numerical integration of the square of the interface height given by equation (7.18). If equation (7.18) actually holds to any extent, this would be a major simplification of the problem.

Chapter 8

Concluding comments

The subject of this thesis has been the displacement of hydraulic fluid from long hydraulic lines. Through analytical and numerical approaches, we have tried to investigate this type of flow. We have seen that using FLUENT, we are able to produce results that are quite close to what others have reported earlier. There are indications that better results would have been found using finer grid resolution. It seems obvious from the FLUENT simulations that this method would also have worked for finding out how fast the oil film initially left in the pipe would be washed out, but it is equally obvious that this would require a very large computational effort, making this method less attractive. The simplicity and computational efficiency of the hydraulic model makes it a preferrable option, but the we have seen that the simplifications have made it difficult to treat the initial displacement of oil. An empirical correction became necessary, and the value of the hydraulic model as a predictive tool thus became reduced. When the initial condition was set to a stable interface with an interface height as expected from previous works by e.g. Soares et al[17], the hydraulic model actually performed quite well, and gave results in good agreement with the results found using the model derived by Beresnev and Deng[2]. The simple analytical expression in equation (7.9) describing the interface shape showed surprisingly good agreement with the numerical results, although a small deviation was observed. The attempt at describing core annular flow using the hydraulic model did not produce good results, probably due to numerical diffusion suppressing any predicted wave growth, but the stability analysis performed at least gave good agreement with results found by Rodriguez and Bannwart[14].

For further work on this topic, it would be interesting to try to validate the hydraulic model against results reported by others, thereby gaining some confidence in the results we have actually found in this work. A vast variety of axisymmetric flows are described in various articles, and the hydraulic model should in principle be able to simulate any axisymmetric pipe flow. As an example, one could mention the results for break-up of a stationary

core found by Schwartz et al[16]. It would also be interesting to try to predict the rate at which the oil film left at the wall is expelled from the pipe using FLUENT, but this would probably require several weeks of CPU-time.

Finally, it would be an important task to test experimentally the drainage rate found in section 7.3, as that would be the best way of validating the results. It would be especially interesting to know under which conditions, if any, equation (7.18) gives a good description of the interface and the fraction of oil left in the pipe.

Appendix A

Implementation

A.1 Details concerning use of program

The program is implemented with a generic solver architecture, that makes any extensions of the program quite easy. The *main()* method has as its only responsibility to interpret command line input, call the constructor in class *Hydsolver* to make an object of the problem and prepare all data structures, and then call the *solve()* function with the object. First, *solve()* calls *setIC()*, which sets up the required initial condition. Then *solve()* calls *timeLoop()*, which runs the actual numerical simulation in time using various help functions, drop intermediate data to file, and print progress information to screen. When the simulation is finished, *solve()* calls *computeRelatedProperties()* which has as responsibility to compute any values that are decoupled from the equations in the hydraulic model, and for which it is not necessary to find time development. The only value that is computed is the final volume of phase 1 in the pipe, but the solver could easily be extended to find e.g. the final pressure drop in the pipe. Finally, *solve()* calls *resultReport()*, which writes final data to file and screen.

The solver prints data to four different files, which all have different intentions.

result.hyd This file contains final cross sectional area occupied by phase 1 and final volume flow of phase 1 for all points in the pipe. The typical format is

```
A1(0) Q1(0)
A1(1) Q1(1)
A1(2) Q1(2)
  :     :
A1(n) Q1(n)
```

This is the same file format as the program is able to read as initial

condition, and the whole intention of this file is to be able to continue an old simulation.

result-h.hyd This file contains final interface height. The format is a first line containing the letters *i h z*, the following lines contain number of point in first column, interface height in second column and z-coordinate in third column. This file's intention is to plot final interface height using MATLAB, which is quite simple using the code

```
[data, ~, ~] = tblread('..<path>/result-h.hyd');
plot(data(:,2),data(:,1));
```

where <*path*> is the path to the folder containing the file.

liquid-height.hyd This file contains intermediate data with the same format as in *result-h.hyd*. Every ten seconds flow time, a new result is written to the file. This is found to be frequent enough for practical purposes, while still keeping the file size reasonable. The last line in the file contains the letter R, the number of intervals in which the pipe is divided, and the number of results written to the file. The file is intended to be read by MATLAB for post-processing purposes, e.g. finding time development of the oil volume in the pipe, as in section 7.3.

height-certain-positions.hyd This file contains time development of interface height at positions at 1/5, 2/5, 3/5 and 4/5 of the pipe length. The first line contains a heading with the letters *n time p1 p2 p3 p4*, then every ten seconds the number of stored results, time and the four interface heights are written on a new line. The last line contains the total number of stored results, the total flow time and the coordinate of the four points. This file is also intended to be read by MATLAB for post-processing, mainly plotting interface height as function of time, as in section 7.3.

For flexibility, the program is written with the possibility of setting all fluid and solver properties through command line options. For each setting, there is a default setting that will be used if nothing else is included on the command line. The format of the command line options is -x <option>, where "x" refers to a specific setting, and "option" is whatever value one wants the setting to have. Invalid command line input is ignored. The available settings and options are

-L Sets the length of the pipe. Default is 1 m.

-T Sets the total flow time. Default is 2 s.

-dt Sets the length of the time step. Default is 0.001 s.

-dz Sets the length of the spatial step. Default is 0.01 m.

-rho1 Sets the density of phase 1. Default is water, 998.2 kg/m^3.

-rho2 Sets the density of phase 2. Default is a generic oil,800 kg/m^3.

-mu1 Sets the molecular viscosity of phase 1. Default is water, 0.001003 Pa $\cdot$ s.

-mu2 Sets the molecular viscosity of phase 2. Default is a generic oil, 0.02 Pa $\cdot$ s.

-s Sets the surface tension of the interface. Default is 0.02 N/m.

-A Sets the cross sectional area of the pipe. Default is $\pi \cdot 10^{-4}$ m^2, which is the same as a pipe with 1 cm radius.

-Q Sets the total volume flow in the pipe. Default is $\pi \cdot 10^{-6}$ m^3/s, which gives the flow a mean velocity of 0.01 m/s using the default cross sectional area.

-A1 Sets the initial cross sectional area occupied by phase 1. This value is used both as initial condition and boundary condition at inlet, if not overridden by **-c**,**-f** or **-i**. Default is $4\pi \cdot 10^{-5}$ m^2.

-Q1 Sets the initial volume flow of phase 1. This value is used both as initial condition and boundary condition at inlet, if not overridden by **-c**,**-f** or **-i**. Default is $2 \cdot 10^{-6}$ m^3/s.

-f Sets the file name to read initial condition from. The program ends if it is impossible to open the file. The format of the file has to be equal to the format the program writes to the file *result.hyd*. This setting overrides **-A1** and **-Q1**, but the default values for A_1 and Q_1 are used if the input file is too short or instead of any invalid data in the file. The value given for A_1 and Q_1 for $z = 0$ will be used as boundary condition, if not overridden by **-c**. Default is NONE.

-p Toggles on/off pertubation of the interface. Only option is ON, this adds a small sinus-shaped pertubation to the interface. This setting has been used in the stability tests in section 5.2 and 7.2. Default is OFF.

-pl Sets the length of the interface pertubation. If **-p** is not set to ON, this setting will have no effect. Default is 0.1 m.

-c Toggles on/off constant boundary condition. Only option is OFF, this makes the boundary condition change from whatever the initial boundary condition is to pure inflow of phase 1 during 0.5 s. This option overrides any other setting of boundary condition, and is used to find the results given in section 7.3. Default is ON.

-i Toggles on/off initial displacement. Only option is ON, this overrides any setting of initial and boundary condition. Inflow is set to pure phase 1, and an initial amount of phase 1 is set close to the inlet. The rest of the pipe is completely filled with phase 2. This setting is used to find the results for the hydraulic model with a discontinuity with standard two-point discretization instead of upwind in section 6.3. Default is OFF.

-B Sets the empirical adjustment factor B of the front drag, as defined in equation (6.18). Default is 43.

The compiled program can, when compiled, be run under a Linux environment by stating the command

```
./Hydsolver
```

with the required options included, assuming that the name *Hydsolver* is used when linking the compiled file.

A.2 Header file

The following is the C++ header file for the developed numerical solver.

```
using namespace std;

class Hydsolver
{
protected:

//Variables
//Arrays to store solutions
double *Q1;     //new value for mean velocity of phase 1
double *Q1m;    //previous value for mean velocity of phase 1
double *A1;     //new value for area occupied by phase 1
double *A1m;    //previous value for area occupied by phase 1
double *h;      //liquid height
double *hm;     //liquid height, previous time step
double *c1;     //profile parameter
double *c1m;    //profile parameter, previous time step
double *temp;   //temporary pointer, used to swap other pointers

//Temporary variables, used to compute solution
double F_advection_upwind;
double F_pressure;
```

```
double dC_dz_special;
double dh_dz;
double d2h_dz2;
double d3h_dz3;
double c1Q1_A1_prev;
double Q1m_minus2;

//Related properties
double volume1;          //volume of phase 1 present in pipe
double volume1_initial;  //initial volume of phase 1 in pipe
double volume1_inflow;   //inflow volume of phase 1 during
                                //total flow time
double volume1_outflow;  //outflow volume of phase 1 during
                                //total flow time
int resultsStored;       //number of results written to file

//Initial and boundary conditions
double A1_IC;    //initial condition for area occupied by phase 1
double Q1_IC;    //initial condition for mean velocity of phase 1
double A1_BC;    //boundary condition for area occupied by
                            //phase 1 at z=0
double Q1_BC;    //boundary condition for mean velocity of
                            //phase 1 at z=0
double h_BC;     //boundary condition for liquid height at z=0

//Flow properties
double A;         //cross sectional area of pipe
double R;         //radius of pipe
double Q;         //total volume flow through cross section of pipe
double rho1;      //density of phase 1
double rho2;      //density of phase 2
double mu1;       //molecular viscosity of phase 1
double mu2;       //molecular viscosity of phase 2
double mu;        //viscosity ratio, mu2/mu1
double sigma;     //surface tension coefficient
double length;    //total length of pipe
double totalTime; //total flow time
double pi;

//Variables necessary to simulate initial displacement
double h_delta;  //height of interface at the nose of phase 1
double Q_delta;  //volume flow of phase 1 near nose of phase
int lastPoint;   //index of last spatial point before
                       //front of phase 1
```

```
double delta;    //distance from last spatial point to actual
                        //position of front of interface
double B;        //front drag coefficient

//Solution settings
double eps;                //a small value
double dt;                 //length of time step
double dz;                 //length of spatial step
int n;                     //index of last spatial point
int m;                     //index of last temporal point
char* filenameIC;          //name of the file where the initial
                               //condition is stored
bool pertubation;          //whether pertubation is to be added
double pertubation_length; //length of added pertubation
bool read_IC;              //whether IC is supposed to be
                               //read from file
bool constant_BC;          //toggles changing boundary
                               //conditions on/off
bool initial_displacement; //toggles initial displacement
                               //on/off

//Constructor and destructor
public:
Hydsolver (double length_, double totalTime_, double dt_,
            double dz_, double Q1_IC_, double A1_IC_,
            double A_, double Q_, double mu1_, double mu2_,
            double rho1_, double rho2_, double sigma_,
            bool pertubation_, double pertubation_length_,
            char* filenameIC_, bool read_IC_ , bool constant_BC_,
            bool initial_displacement_, double B_);
~Hydsolver () {};

//Class functions
void solve ();

protected:
//Main functions, called one time
void setIC ();
void setPertubation ();
void timeLoop ();
void resultReport ();
void computeRelatedProperties ();

//Help functions, called multiple times
```

```
double computeC1 (double h);
double u1 (int i);
double u2 (int i);
double F_wall_shear (int i);
double F_interface (int i);
double F_diffusion1 (int i);
double F_diffusion2 (int i);
double F_advection (int i);
double dC_dz (int i);
double M (int i);
double computeVolumeIntegral ();
void updateStructures (double t, double adjustmentTime);
void solveThisTimeStep ();
};
```

A.3 Cpp-file

The following is a listing of the .cpp-file written for the numerical solver.

```
#include "Hydsolver.h"
#include <cmath>
#include <iostream>
#include <sstream>
#include <fstream>

using namespace std;

template <class T> bool from_string(T& t, const std::string& s,
                 std::ios_base& (*f)(std::ios_base&))
{
    std::istringstream iss(s);
    return !(iss >> f >> t).fail();
}

/*Constructor for the problem, initializes data and
        prepares necessary structures*/
Hydsolver:: Hydsolver(double length_, double totalTime_, double dt_,
               double dz_, double Q1_IC_, double A1_IC_, double A_,
               double Q_, double mu1_, double mu2_, double rho1_,
               double rho2_, double sigma_, bool pertubation_,
```

```
                double pertubation_length_, char* filenameIC_, bool read_IC_ ,
                bool constant_BC_, bool initial_displacement_, double B_)
{
    //Read arguments
    length = length_;
    totalTime = totalTime_;
    dt = dt_;
    dz = dz_;
    A = A_;
    A1_IC = A1_IC_;
    Q = Q_;
    Q1_IC = Q1_IC_;
    pertubation_length = pertubation_length_;
    mu1 = mu1_;
    mu2 = mu2_;
    rho1 = rho1_;
    rho2 = rho2_;
    sigma = sigma_;
    filenameIC = filenameIC_;
    read_IC = read_IC_;
    constant_BC = constant_BC_;
    pertubation = pertubation_;
    initial_displacement = initial_displacement_;
    B = B_;

    //Definition of various constants
    pi = 3.141592654;
    eps = 1e-13;      //A small epsilon-value
    R = sqrt(A/pi);   //Pipe radius

    //Calculate number of spatial intervals
    n = int(length/dz);

    //Initialize arrays
    Q1 = new double [n+1];
    Q1m = new double [n+1];
    A1 = new double [n+1];
    A1m = new double [n+1];
    c1 = new double [n+1];
    c1m = new double [n+1];
    h = new double [n+3];
    hm = new double [n+3];

    //Initialize variables for volume computation
```

```
    volume1 = 0;
    volume1_initial = 0;
    volume1_inflow = 0;
    volume1_outflow = 0;

    //Write report to screen
    cout << "The following system is set up:" << endl;
    cout << "Length of pipe: " << length << endl;
    cout << "Total flow time: " << totalTime << endl;
    cout << "dt: " << dt << "  dz: " << dz << endl;
    cout << "Spatial points i in [0," << n << "]" << endl;
    cout << endl;
}

/*The solve-function solves the system set up by the constructor,
    using other functions*/
void Hydsolver:: solve()
{
    cout << "Starting simulator" << endl;

    setIC();
    timeLoop();
    computeRelatedProperties();
    resultReport();
}

/*Set the required initial condition*/
void Hydsolver:: setIC()
{
    /*If the initial displacement of oil from the pipe is to be
     modelled, only a small amount of water close to the inlet
     is set in the initial condition*/
    if(initial_displacement)
    {
        //The last point the front of water has reached:
        lastPoint = 6;
        //The distance the front has moved past the last point:
        delta = 0.5*dz;

        Q1_BC = Q-.01*eps;
        A1_BC = A-eps;
        //Set gradually reduced volume of water
        for(int i = 0; i<=lastPoint; i++)
        {
```

```
            Q1[i] = Q1_BC*(lastPoint+1-i)/(lastPoint+1);
            A1[i] = A1_BC*(lastPoint+1-i)/(lastPoint+1);
            h[i+1]= sqrt(A1[i]/pi);
            c1[i] = computeC1(h[i+1]);
        }
        //Set rest of points to zero
        for(int i = lastPoint+1; i<=n; i++)
        {
            Q1[i] = 0;
            A1[i] = 0;
            h[i+1]= 0;
            c1[i] = 0;
        }
    }

    /*If the initial displacement is not to be modelled, an
    initial amount of water is set in the entire pipe*/
    else
    {
        if(read_IC)
        {
            ifstream fin(filenameIC);
            string line;
            int linenumber = 0;

            /*Read initial condition from file. The read input
            values are typecast to double, the value will be used
            as initial condition if it is in a physically
            acceptable interval. If not, the default value will
            be used. If a line has only one entry, this entry
            will be used for A1, and the default value will be used
            for Q1. If more than two entries are present on
            a line, the remaining entries will not be used.*/

            while (!fin.eof() && linenumber <= n)
            {
                getline (fin, line);
                if(!line.empty())
                {
                    char* char_line = (char*)line.c_str();
                    char* pEnd;
                    A1[linenumber]  = strtod (char_line,&pEnd);
                    if(A1[linenumber]<eps || A1[linenumber]>A-eps)
                        {A1[linenumber] = A1_IC;}
```

```
                Q1[linenumber]  = strtod(pEnd, NULL);
                if(Q1[linenumber]<0.01*eps || Q1[linenumber]>Q)
                    {Q1[linenumber] = Q1_IC;}
                h[linenumber+1] = sqrt(A1[linenumber]/pi);
                c1[linenumber]  = computeC1(h[linenumber+1]);
                linenumber++;
            }
        }
        fin.close();

        /*Set default values for rest of pipe if the
        data on file is too short*/
        if(linenumber<n)
        {
            for(int i = linenumber; i<=n; i++)
            {
                Q1[i] = Q1_IC;
                A1[i] = A1_IC;
                h[i+1]= sqrt(A1[i]/pi);
                c1[i] = computeC1(h[i+1]);
            }
        }
    }
    else
    {
    /*Set default values for Q1 and A1 if initial
    condition is not read from file*/
        for(int i = 0; i<=n; i++)
        {
            Q1[i] = Q1_IC;
            A1[i] = A1_IC;
            h[i+1]= sqrt(A1[i]/pi);
            c1[i] = computeC1(h[i+1]);
        }
    }
    //Add small pertubation to initial condition if required.
    if(pertubation)
        {setPertubation();}
    A1_BC = A1[0];
    Q1_BC = Q1[0];
}
h[n+1] = h[n];
h[n+2] = h[n];
h[0] = h[1];
```

```
    h_BC = h[1];

    //Find initial volume of phase 1 in pipe
    volume1_initial = computeVolumeIntegral();
}

/*Add small pertubation to the interface, if required*/
void Hydsolver:: setPertubation()
{
    double coordinate_start = 0.5; //Point where pertubation start
    int point_start = int((coordinate_start+1e-6)/dz);
    int point_end = int((coordinate_start+pertubation_length)/dz);
    if(point_end>n)
        {point_end = n;}
    if(point_end<point_start)
        {point_end = point_start+1;}
    cout << "Adding sinus-shaped pertubation" << endl;
    for (int i = point_start; i<=point_end; i++)
    {
        A1[i] = A1[i] + 1e-8*sin(2*pi*(i-point_start)*dz
                            /pertubation_length);
        h[i+1]= sqrt(A1[i]/pi);
        c1[i] = computeC1(h[i+1]);
    }
}

/*Start simulation of the system*/
void Hydsolver:: timeLoop()
{
    //Set up progress-bar on screen
    cout << "|-----------------PROGRESS-----------------|" << endl;
    //Interval between printing a '*'
    double updateInterval = totalTime/42;
    /*Total time at which next '*' is printed*/
    double nextUpdate = updateInterval;

    cout << "|";
    flush(cout);

    //Add first time step to integrals of inflow and outflow
    volume1_inflow += 0.5*Q1m[0]*dt;
    volume1_outflow += 0.5*Q1m[n]*dt;

    /*Open file and prepare for printing intermediate
```

```
    data of liquid height in entire pipe*/
ofstream fout("liquid-height.hyd");   //Open file
fout << "i    h      z" << endl;      //Print header to file
fout.precision(16);

/*Open file and prepare for printing intermediate
    data of liquid height at certain positions*/
ofstream fout2("height-certain-positions.hyd"); //Open file
fout2.precision(16);
//Define positions to print data for
int position1 = n/5;
int position2 = 2*n/5;
int position3 = 3*n/5;
int position4 = 4*n/5;
fout2 << "n time p1 p2 p3 p4" << endl; //Print header to file

//Keep track of when data is to be written to file
double print          = 0;  /*Time since result was
                              printed to file last time*/
double print_interval = 10; /*Time interval between
                              results printed to file*/
int resultsStored     = 0;  //Number of results printed to file

//Initialize counter for total time
double t = 0;

/*Set time to use to change boundary condition from the
    initial to pure phase 1 at inflow, if the inlet
    boundary condition is not constant*/
double adjustmentTime = 0.5;

while (t<totalTime)
{
    //Prepare data structures for this time step
    updateStructures(t, adjustmentTime);

    //Solve the system at this time step
    solveThisTimeStep();

    //Set boundary conditions
    Q1[0] = Q1_BC;
    A1[0] = A1_BC;
    Q1[n] = Q1[n-1];
    A1[n] = A1[n-1];
```

```
        h[0]  = h_BC;
        h[1]  = h_BC;
        h[n+1]= h[n];
        h[n+2]= h[n];
        c1[0] = computeC1(h[1]);
        c1[n] = computeC1(h[n+1]);

        //Add inflow and outflow to integrals
        volume1_inflow += Q1[0]*dt;
        volume1_outflow += Q1[n]*dt;

        //Update time counters
        t += dt;
        print += dt;

        //Write report if necessary
        if(print > print_interval)
        {
            for(int i = 0; i<=n; i++)
            {
                fout << "h[" << i << "] " << h[i+1] << " "
                        << i*dz << endl;
            }
            fout2 << resultsStored << " " << t << " "
                << h[position1] << " " << h[position2] << " "
                << h[position3] << " " << h[position4] << endl;
            resultsStored++;
            print = 0;
        }

        //Update progress on screen
        if(t>nextUpdate)
        {
            cout << "*";
            flush(cout);
            nextUpdate += updateInterval;
        }
    }

    //Complete print to file, and close file
    fout << "R " << n << " " << resultsStored << endl;
    fout.close();
    fout2 << resultsStored << " " << totalTime << " "
        << position1*dz << " " << position2*dz << " "
```

```
        << position3*dz << " " << position4*dz << endl;
    fout2.close();

    //Finish progress-bar
    cout << "|" << endl;
}

void Hydsolver:: solveThisTimeStep()
{
    int j = 2;

    if(initial_displacement && lastPoint<n)
    {
        int i;
        for(i = 1; i<=lastPoint-2; i++)
        {
            A1[i] = A1m[i]
                - (dt/(2*dz))*(Q1[i+1]-Q1[i-1]);
            //Prevent unphysical values
            if(A1[i]>=A-eps)
                {A1[i] = A-eps;}
            if(A1[i]<=eps)
                {A1[i] = eps;}

            Q1[i] = Q1m[i] + (dt/M(i))*(F_wall_shear(i)
                - F_interface(i) - F_advection(i)
                - sigma*A1m[i]*(A-A1m[i])*dC_dz(i)
                - F_diffusion2(i) + F_diffusion1(i));
            //Prevent unphysical values
            if(Q1[i]>Q)
                {Q1[i] = Q-.01*eps;}
            if(Q1[i]<.01*eps)
                {Q1[i] = .01*eps;}

            h[j] = sqrt(A1[i]/pi);
            c1[i]= computeC1(h[i+1]);
            j++;
        }

        //Special treatment of last points close to discontinuity
        //Second last point, special expression for interface curvature
        dh_dz   = (-hm[j-1]+hm[j+1])/(2*dz);
        d2h_dz2 = (1/(dz*dz))*hm[j-1]-(2/(dz*dz))*hm[j]
            +(1/(dz*dz))*hm[j+1];
```

```
d3h_dz3 = -(1/(dz*dz*dz))*hm[j-2]+(3/(dz*dz*dz))*hm[j-1]
    -(3/(dz*dz*dz))*hm[j]+(1/(dz*dz*dz))*hm[j+1];
dC_dz_special = (-hm[j]*hm[j]*d3h_dz3-dh_dz*(1+dh_dz*dh_dz
    + hm[j]*d2h_dz2))/(hm[j]*hm[j]*pow(1+dh_dz*dh_dz,1.5))
    +(3*dh_dz*d2h_dz2*d2h_dz2)/(pow(1+dh_dz*dh_dz,2.5));

A1[i] = A1m[i]
    - (dt/(2*dz))*(Q1m[i+1] - Q1m[i-1]);
//Prevent unphysical values
if(A1[i]>=A-eps)
    {A1[i] = A-eps;}
if(A1[i]<=eps)
    {A1[i] = eps;}

Q1[i] = Q1m[i] + (dt/M(i))*(F_wall_shear(i)
    - F_interface(i) - F_advection(i)
    - sigma*A1m[i]*(A-A1m[i])*dC_dz_special
    - F_diffusion2(i) + F_diffusion1(i));
//Prevent unphysical values
if(Q1[i]>Q)
    {Q1[i] = Q-.01*eps;}
if(Q1[i]<.01*eps)
    {Q1[i] = .01*eps;}

h[i+1] = sqrt(A1[i]/pi);
c1[i]  = computeC1(h[i+1]);

i++;
j++;

//Last point:
//Upwind expression for advection:
F_advection_upwind = rho1*((A-A1m[i])/(2*dz))
            *(3*c1m[i]*Q1m[i]*u1(i)
            - 4*c1m[i-1]*Q1m[i-1]*Q1m[i-1]/A1m[i-1]
            +c1m[i-2]*Q1m[i-2]*Q1m[i-2]/A1m[i-2]);

//special expression for interface curvature:
dh_dz = (-delta*delta*hm[j-1]+(delta*delta-dz*dz)*hm[j]
    +dz*dz*h_delta)/(dz*delta*(dz+delta));
d2h_dz2 = (2/(dz*(dz+delta)))*hm[j-1]-(2/(dz*delta))*hm[j]
            +(2/(delta*(dz+delta)))*h_delta;
d3h_dz3 = -(3/(dz*dz*(2*dz+delta)))*hm[j-2]
        +(6/(dz*dz*(dz+delta)))*hm[j-1]
```

```
        -(3/(dz*dz*delta))*hm[j]
        +(6/(delta*(dz+delta)*(2*dz+delta)))*h_delta;

dC_dz_special = (-hm[j]*hm[j]*d3h_dz3-dh_dz
        *(1+dh_dz*dh_dz + hm[j]*d2h_dz2))
        /(hm[j]*hm[j]*pow(1+dh_dz*dh_dz,1.5))
        +(3*dh_dz*d2h_dz2*d2h_dz2)/(pow(1+dh_dz*dh_dz,2.5));

//Modelled drag on the front:
F_pressure = (Q*mu2*A1m[i]*(A-A1m[i])*(A-A1m[i])*(mu-1)
            /(A*A*((mu-1)*A1m[i]*A1m[i]+A*A)))*A1m[i];

A1[i]   = A1m[i]
    - (dt/(2*dz))*(3*Q1m[i] -4*Q1m[i-1]+Q1m[i-2]);
//Prevent unphysical values
if(A1[i]>=A-eps)
    {A1[i] = A-eps;}
if(A1[i]<=eps)
    {A1[i] = eps;}

Q1[i] = Q1m[i] + (dt/M(i))*(F_wall_shear(i)
    - F_interface(i) - F_advection_upwind
    - sigma*A1m[i]*(A-A1m[i])*dC_dz_special
    - B*F_pressure);
//Prevent unphysical values
if(Q1[i]>Q)
    {Q1[i] = Q-.01*eps;}
if(Q1[i]<.01*eps)
    {Q1[i] = .01*eps;}

h[i+1] = sqrt(A1[i]/pi);
c1[i]  = computeC1(h[i+1]);

//Update delta
Q_delta = (delta*(dz+delta)/(dz+2*delta))
            *((dz+delta)*Q1[i]/(dz*delta)
            - delta*Q1[i-1]/(dz*(dz+delta)));
delta += 1*Q_delta*dt/A1[lastPoint];

//Set rest of points to zero
for(i = lastPoint+1; i<=n; i++)
{
    Q1[i] = 0;
    A1[i] = 0;
```

```
            h[i+1] = 0;
        }

        //Update lastPoint, if necessary
        if(delta>(1.5*dz))
        {
            h[lastPoint+2]  = h[lastPoint+1]+dz*dh_dz
                    +0.5*dz*dz*d2h_dz2+dz*dz*dz*d3h_dz3/6;
            A1[lastPoint+1] = pi*h[lastPoint+2]*h[lastPoint+2];
            Q1[lastPoint+1] = (4*Q1[lastPoint]-Q1[lastPoint-1])/3;
            lastPoint++;
            delta -= dz;
        }
    }
    /*Standard numerical solution, with no
        treatment of discontinuity*/
    else
    {
        /*Values for the point [i-1], the
        boundary condition is used for [-1]*/
        c1Q1_A1_prev = c1m[0]*Q1m[0]*Q1m[0]/A1m[0];
        Q1m_minus2  = Q1m[0];
        for(int i = 1; i<n; i++)
        {
            F_advection_upwind  = rho1*((A-A1m[i])/(2*dz))
                        *(3*c1m[i]*Q1m[i]*u1(i)
                        - 4*c1m[i-1]*Q1m[i-1]*Q1m[i-1]/A1m[i-1]
                        +c1Q1_A1_prev);

            A1[i] = A1m[i]
                - (dt/(2*dz))*(3*Q1m[i]-4*Q1m[i-1]+Q1m_minus2);
            //Prevent unphysical values
            if(A1[i]>=A-eps)
                {A1[i] = A-eps;}
            if(A1[i]<=eps)
                {A1[i] = eps;}

            Q1[i] = Q1m[i] + (dt/M(i))*(F_wall_shear(i)
                - F_interface(i) - F_advection_upwind
                - sigma*A1m[i]*(A-A1m[i])*dC_dz(i));

            //Prevent unphysical values
            if(Q1[i]>Q)
                {Q1[i] = Q-.01*eps;}
```

```
            if(Q1[i]<.01*eps)
                {Q1[i] = .01*eps;}

            h[i+1] = sqrt(A1[i]/pi);
            c1[i]  = computeC1(h[i+1]);

            c1Q1_A1_prev = c1m[i-1]*Q1m[i-1]*Q1m[i-1]/A1m[i-1];
            Q1m_minus2   = Q1m[i-1];
        }
    }
}

/*Find any properties that are decoupled from the
    equations in the hydraulic model*/
void Hydsolver:: computeRelatedProperties()
{
    volume1 = computeVolumeIntegral();
}

/*Find the volume of phase 1 in the pipe,
    doing a simple numerical integration*/
double Hydsolver:: computeVolumeIntegral()
{
    double volume = 0;
    for(int i = 1; i<n; i++)
    {
        volume += A1[i]*dz;
    }
    volume += 0.5*(A1[0]+A1[n])*dz;
    return volume;
}

/*Write final results to screen and file*/
void Hydsolver:: resultReport()
{
    //Print final interface height in entire pipe to file
    ofstream fout_h("result-h.hyd");
    fout_h << "i    h      z" << endl;
    fout_h.precision(16);
    for(int i = 0; i<=n; i++)
    {
        fout_h << "h[" << i << "] "
            << h[i+1] << " " << i*dz << endl;
    }
```

```
    fout_h.close();

    /*Print final cross sectional area occupied by
    phase 1 and volume flow of phase 1*/
    ofstream fout("result.hyd");
    fout.precision(16);
    for(int i = 0; i<=n; i++)
        {fout << A1[i] << "  " << Q1[i] << endl;}
    fout.close();

    //Print to screen report on how well mass is conserved
    cout << "Initial volume of phase 1: "
        << volume1_initial << endl;
    cout << "Final volume of phase 1: "
        << volume1 << endl;
    double diff = volume1_initial - volume1
        - volume1_outflow + volume1_inflow;
    cout << "Total loss of phase 1: "
        << diff << " m^3" << endl;
}

/*Compute the profile parameter c1*/
inline double Hydsolver:: computeC1(double h)
{
    return (mu*mu*h*h*h*h/3 + mu*(R*R*h*h-h*h*h*h)
        + (R*R-h*h)*(R*R-h*h))/(mu*mu*h*h*h*h/4
        + mu*(R*R*h*h-h*h*h*h) + (R*R-h*h)*(R*R-h*h));
}

/*Compute mean velocity of phase 1*/
inline double Hydsolver:: u1(int i)
{
    return Q1m[i]/A1m[i];
}

/*Compute mean velocity of phase 2*/
inline double Hydsolver:: u2(int i)
{
    return (Q-Q1m[i])/(A-A1m[i]);
}

/*Compute wall shear term*/
inline double Hydsolver:: F_wall_shear(int i)
{
```

```
    return 8*pi*R*mu2*u2(i)*A1m[i]/(R-hm[i+1]);
}

/*Compute interface shear term*/
inline double Hydsolver:: F_interface(int i)
{
    return (8*pi*mu1*A/u1(i))*(u1(i)-u2(i))
            *abs(u1(i)-u2(i));
}

/*Compute diffusion term in phase 1*/
inline double Hydsolver:: F_diffusion1(int i)
{
    return (A-A1m[i])*(mu1/(dz*dz))*((A1m[i+1]+A1m[i])
            *(Q1m[i+1]/A1m[i+1]-Q1m[i]/A1m[i])
            - (A1m[i]+A1m[i-1])*(Q1m[i]/A1m[i]-Q1m[i-1]/A1m[i-1]));
}

/*Compute diffusion term in phase 2*/
inline double Hydsolver:: F_diffusion2(int i)
{
    return (A1m[i]*mu2/(dz*dz))*((A-(A1m[i+1]+A1m[i]))
        *((Q-Q1m[i+1])/(A-A1m[i+1])-(Q-Q1m[i])/(A-A1m[i]))
        -(A-(A1m[i]+A1m[i-1]))*((Q-Q1m[i])/(A-A1m[i])
        -(Q-Q1m[i-1])/(A-A1m[i-1])));
}

/*Compute M-term*/
inline double Hydsolver:: M(int i)
{
    return A1m[i]*rho2+(A-A1m[i])*rho1;
}

/*Compute advective term with standard two-point centered difference*/
inline double Hydsolver:: F_advection(int i)
{
    return rho1*((A-A1m[i])/(2*dz))*(c1m[i+1]*Q1m[i+1]*Q1m[i+1]/A1m[i+1]
            - c1m[i-1]*Q1m[i-1]*Q1m[i-1]/A1m[i-1]);;
}

/*Compute surface curvature*/
inline double Hydsolver:: dC_dz(int i)
{
    return 1/(hm[i+2]*sqrt(4*dz*dz+(hm[i+3]-hm[i+1])*(hm[i+3]-hm[i+1])))
```

```
        - 1/(hm[i]*sqrt(4*dz*dz+(hm[i+1]-hm[i-1])*(hm[i+1]-hm[i-1])))
        - 4*((hm[i+3]-2*hm[i+2]+hm[i+1])
            /(pow(4*dz*dz+(hm[i+3]-hm[i+1])*(hm[i+3]-hm[i+1]),1.5))
        - (hm[i+1]-2*hm[i]+hm[i-1])
            /(pow(4*dz*dz+(hm[i+1]-hm[i-1])*(hm[i+1]-hm[i-1]),1.5)));
}

/*Prepare data structures and boundary
conditions for next time step*/
void Hydsolver:: updateStructures(double t,
                        double adjustmentTime)
{
    //Adjust boundary conditions if necessary
    if(t<(adjustmentTime+.5*dt)&&!constant_BC)
    {
        A1_BC = A1_IC+(A-A1_IC)*t/adjustmentTime;
        Q1_BC = Q1_IC+(Q-Q1_IC)*t/adjustmentTime;
        h_BC = sqrt(A1_BC/pi);
        if(t>(adjustmentTime-.5*dt))
        {
            A1_BC = A;
            Q1_BC = Q;
            h_BC = sqrt(A1_BC/pi);
        }
    }
    //Swap array pointers
    temp = Q1m;
    Q1m = Q1;
    Q1 = temp;
    temp = A1m;
    A1m = A1;
    A1 = temp;
    temp = c1m;
    c1m = c1;
    c1 = temp;
    temp = hm;
    hm = h;
    h = temp;
}

/*Interpret command line options*/
char* getCmdOption(char ** begin, char ** end,
                    const std::string & option)
{
```

```
    char ** itr = std::find(begin, end, option);
    if (itr != end && ++itr != end)
    {
        return *itr;
    }
    return 0;
}

int main (int argc, char * argv[])
{
    //Default values:
    //Default pipe length:
    double length = 1;
    //Default flow time:
    double totalTime = 1;
    //Default length of time step:
    double dt = 0.001;
    //Default spatial step:
    double dz = 0.01;
    //Default cross sectional area of pipe:
    double A = 3.141592654*1e-4;
    //Default cross sectional area occupied by phase 1:
    double A1 = 0.4*A;
    //Default total volume flow:
    double Q = 3.141592654*1e-6;
    //Default volume flow of phase 1:
    double Q1 = Q*0.6366197724;
    //Default viscosity of phase 1:
    double mu1 = 0.001003;
    //Default viscosity of phase 2:
    double mu2 = 0.02;
    //Default density of phase 1:
    double rho1 = 998.2;
    //Default density of phase 2:
    double rho2 = 800;
    //Default interface tension:
    double sigma = 0.02;
    //Default filename for initial condition:
    char* filename = "NONE";
    /*Default for whether a pertubation is
    to be added to the initial condition*/
    bool pertubation = false;
    //Default length of pertubation:
    double pertubation_length = 0.1;
```

```
/*Default for whether initial condition
is to be read from file*/
bool read_IC = false;
/*Default for whether the boundary condition
at the inlet is constant*/
bool constant_BC = true;
/*Default for whether initial displacement
of oil is to be modelled*/
bool initial_displacement = false;
//Default coefficient of drag
double B = 43;

//Try to read input values from command line
float f;
//Read length of pipe
char* input_length = getCmdOption(argv, argv + argc, "-L");
if (input_length)
{
    if(from_string<float>
            (f, std::string(input_length), std::dec))
        {length = f;}
}
//Read total flow time
char* input_time = getCmdOption(argv, argv + argc, "-T");
if (input_time)
{
    if(from_string<float>
            (f, std::string(input_time), std::dec))
        {totalTime = f;}
}
//Read length of time step
char* input_dt = getCmdOption(argv, argv + argc, "-dt");
if (input_dt)
{
    if(from_string<float>
            (f, std::string(input_dt), std::dec))
        {dt = f;}
}
//Read length of spatial step
char* input_dz = getCmdOption(argv, argv + argc, "-dz");
if (input_dz)
{
    if(from_string<float>
            (f, std::string(input_dz), std::dec))
```

```
        {dz = f;}
}
//Read viscosity of phase 1
char* input_mu1 = getCmdOption(argv, argv + argc, "-mu1");
if (input_mu1)
{
    if(from_string<float>
            (f, std::string(input_mu1), std::dec))
        {mu1 = f;}
}
//Read viscosity of phase 2
char* input_mu2 = getCmdOption(argv, argv + argc, "-mu2");
if (input_mu2)
{
    if(from_string<float>
            (f, std::string(input_mu2), std::dec))
        {mu2 = f;}
}
//Read density of phase 1
char* input_rho1 = getCmdOption(argv, argv + argc, "-rho1");
if (input_rho1)
{
    if(from_string<float>
            (f, std::string(input_rho1), std::dec))
        {rho1 = f;}
}
//Read density of phase 2
char* input_rho2 = getCmdOption(argv, argv + argc, "-rho2");
if (input_rho2)
{
    if(from_string<float>
            (f, std::string(input_rho2), std::dec))
        {rho2 = f;}
}
//Read interface tension coefficient
char* input_sigma = getCmdOption(argv, argv + argc, "-s");
if (input_sigma)
{
    if(from_string<float>
            (f, std::string(input_sigma), std::dec))
        {sigma = f;}
}
//Read filename where initial condition is located
char* filename_ = getCmdOption(argv, argv + argc, "-f");
```

```
if (filename_)
{
    ifstream fin(filename_);
    if (fin.is_open()) //Check if file is actually open
    {
        filename = filename_;
        read_IC = true;
        fin.close();
    }
    else  //Abort if it is not possible to open file
    {
        cout << "File '" << filename_
            << "' not found, aborting." << endl;
        return 0;
    }
}
//Read boundary condition for A1
char* input_A1 = getCmdOption(argv, argv + argc, "-A1");
if (input_A1)
{
    if(from_string<float>
            (f, std::string(input_A1), std::dec))
        {A1 = f;}
}
//Read boundary condition for Q1
char* input_Q1 = getCmdOption(argv, argv + argc, "-Q1");
if (input_Q1)
{
    if(from_string<float>
            (f, std::string(input_Q1), std::dec))
        {Q1 = f;}
}
//Read whether boundary conditions are constant
char* input_constant = getCmdOption(argv, argv + argc, "-c");
if (input_constant)
{
    if(!strcmp(input_constant,"OFF"))
        {constant_BC = false;}
}
//Read whether pertubation of surface is included
char* input_pert = getCmdOption(argv, argv + argc, "-p");
if (input_pert)
{
    if(!strcmp(input_pert,"ON"))
```

```
            {pertubation = true;}
    }
    //Read whether initial displacement is to be included
    char* input_i = getCmdOption(argv, argv + argc, "-i");
    if (input_i)
    {
        if(!strcmp(input_i,"ON"))
            {initial_displacement = true;}
    }
    //Read front drag coefficient
    char* input_B = getCmdOption(argv, argv + argc, "-B");
    if (input_B)
    {
        if(from_string<float>
                (f, std::string(input_B), std::dec))
            {B = f;}
    }
    //Read length of pertubation
    char* input_pert_length = getCmdOption(argv, argv + argc, "-pl");
    if (input_pert_length)
    {
        if(from_string<float>
                (f, std::string(input_pert_length), std::dec))
        {
            pertubation_length = f;
            //Round off pertubation length to a multiple of dz
            int intervals = int(pertubation_length/dz);
            pertubation_length = intervals*dz;
            cout << "Pertubation length adjusted to "
                    << pertubation_length << endl;
        }
    }
    //Call constructor to set up system
    Hydsolver simulator(length, totalTime, dt, dz, Q1, A1, A, Q,
                    mu1, mu2, rho1, rho2, sigma, pertubation,
                    pertubation_length, filename, read_IC,
                    constant_BC, initial_displacement, B);
    //Solve the system
    simulator.solve();
}
```

Bibliography

[1] Bai, R., Chen, K., and Joseph, D. D., 1992, "Lubricated pipelining: stability of core-annular flow. Part 5. Experiments and comparison with theory," J. Fluid Mech. **240** pp. 97–132.

[2] Beresnev, I. A., and Deng, W., 2010, "Theory of breakup of core fluids surrounded by a wetting annulus in sinusoidally constricted capillary channels,"Phys. Fluids **22** pp. 012105–012105-10.

[3] Blake, T. D., 2006, "The physics of moving wetting lines," J. Colloid Interface Sci. **299** pp. 1–13.

[4] Bretherton, F. P., 1961, "The motion of long bubbles in tubes," J. Fluid Mech. **10** pp. 166–188.

[5] Cox, B. G., 1962, "On driving a viscous fluid out of a tube," J. Fluid Mech. **14** pp. 81–96.

[6] Cox, R. G., 1986, "The dynamics of the spreading of liquids on a solid surface. Part 1. Viscous flow," J. Fluid Mech. **168** pp. 169–194.

[7] Dussan V., E. B., 1979, "On the spreading of liquids on solid surfaces: static and dynamic contact lines," Ann. Rev. Fluid Mech. **11** pp. 371–400.

[8] Dussan V., E. B., and Davis, S. H., 1974, "On the motion of a fluid-fluid interface along a solid surface," J. Fluid Mech. **65** pp. 71–95.

[9] Fairbrother, F., and Stubbs, A. E., 1935, "Studies in electroendosmosis. Part VI. The bubble-tube method of measurements," J. Chem. Soc. **1** pp. 527–529.

[10] Giavedoni, M. D., and Saita, F. A., 1997, "The axisymmetric and plane cases of a gas phase steadily displacing a Newtonian liquid - A simultaneous solution of the governing equations," Phys. Fluids **9** pp. 2420–2428.

[11] Goldsmith, H. L., and Mason, S. G., 1963, "The flow of suspensions through tubes," J. Colloid Sci. **18** pp. 237–261.

[12] Joseph, D. D., and Renardy, Y. Y., 1993, "Fundamentals of Two-Fluid Dynamics. II. Lubricated Transport, Drops and Miscible Liquids," New York: Springer-Verlag.

[13] Petitjeans, P., and Maxworthy, T., 1996, "Miscible displacements in capillary tubes. Part 1. Experiments," J. Fluid Mech. **326** pp. 37–56.

[14] Rodriguez, O. M. H., and Bannwart, A. C., 2008, "Stability Analysis of Core-Annular Flow and Neutral Stability Wave Number," AIChE Journal **54** pp. 20–31.

[15] Schulkes, R., 2008, "An introduction to Multiphase Pipe Flow."

[16] Schwartz, L. W., Princen, H. M., and Kiss, A. D., 1986, "On the motion of bubbles in capillary tubes," J. Fluid Mech. **172** pp. 259–275.

[17] Soares, E. J., Carvalho, M. S., and Souza Mendes, P. R., 2005, "Immiscible Liquid-Liquid Displacement in Capillary Tubes," Journal of Fluids Engineering, **127** pp. 24–31.

[18] Soares, E. J., and Thompson, R. L., 2009, "Flow regimes for the immiscible liquid-liquid displacement in capillary tubes with complete wetting of the displaced liquid," J. Fluid Mech. **641** pp. 63–84.

[19] Taylor, G. I., 1961, "Deposition of a viscous fluid on the wall of a tube," J. Fluid Mech. **10** pp. 161–163.